Oxygen Enriched Fuel Cell Propulsion in Regional Aircraft

Conceptual Design and Performance Assessment

Ângelo Gomes





Oxygen Enriched Fuel Cell Propulsion in Regional Aircraft

Conceptual Design and Performance Assessment

Thesis report

by

Ângelo Gomes

to obtain the degree of Master of Science at the Delft University of Technology to be defended publicly on October 20th, 2025 at 13:00 PM

Thesis committee:

Dr. ir. M. Pini TU Delft, chair
Dr. F. De Domenico TU Delft, committee
Dr. L. Lima Pereira TU Delft, committee

Supervisors:

F. Orefice TU Delft, supervisor
P. Balack DLR, supervisor

Place: Faculty of Aerospace Engineering, Delft

Project Duration: January, 2025 - October, 2025

Student number: 6061435

An electronic version of this thesis is available at http://repository.tudelft.nl/.



Preface

This thesis marks the end of my journey to obtain the Master of Science degree in Aerospace Engineering from the TU Delft. This report is the conclusion of all of the work done during this thesis in collaboration with DLR. Over this period I worked on the conceptual design of a fuel cell aircraft with the intent of analysing the effects of oxygen enrichemnt in its operation.

Firstly, I would like to thank everyone at DLR for their help and support while I was there for my internship and thesis. It was a fantastic experience to be in such an environment where everyone is included in discussions of the work done in the institute and a place where students and researchers interact as equals. I'm especially thankful to my supervisors at DLR, Philip Balack and Simon Müller, for helping me formulate the thesis, navigate this topic, and contact many experts. I want to extend this mention to Benjamin Fröhler for giving me the initial opportunity to do my internship at DLR.

To my TU Delft supervisor, Francesco Orefice, thank you for your commitment during the thesis and the quality of your supervision, even though you have just started supervising students. I'm glad to have been one of the first.

Thank you also to the many friends, both in Delft and at DLR, who made this whole time a lot more enjoyable.

Por último, um muito obrigado à minha mãe, irmão e namorada, por desde o início me incentivarem a seguir esta longa e difícil tarefa, acreditarem em mim e por me darem suporte sempre que fosse preciso, independentemente da distância. A vossa ajuda foi fundamental para conseguir completar esta jornada.

Ângelo Gomes Hamburg, October 2025

Abstract

The aviation sector is making several efforts to reduce its climate impact as the demand for air travel is expected to rise. These efforts include the development of novel propulsion systems that would reduce the emissions produced by aircraft. Proton exchange membrane fuel cells are considered a promising system for reducing emissions. However, their integration into an aircraft brings many challenges. Fuel cells have a significantly lower power density than conventional internal combustion engines. Their low operating temperature results in heavier heat exchange systems and increased drag, and substantially increases the system complexity due to the auxiliary system required and hydrogen storage.

One way to improve fuel cell performance is to operate it with oxygen enriched air. This thesis evaluates the impact of such an operation at aircraft level. This is achieved by performing the preliminary design of a regional aircraft where a developed fuel cell propulsion system model is implemented. This model includes the fuel cell stack and several balance-of-plant components assuming the state-of-the-art technology. The modelling allowed for the system's sizing and simulation under different flight scenarios and varying levels of oxygen percentage of the air supplied to the fuel cell. The integration and sizing of the oxygen tanks used to increase the oxygen percentage were conducted while considering regulations and the required oxygen content.

Results show that implementing a fuel cell propulsion system significantly increases the aircraft's maximum take-off mass (MTOM) compared to a conventional regional aircraft. The oxygen percentage variation showed that a reduction in MTOM is possible, reaching a maximum of 4%. This reduction resulted from a significant improvement in fuel cell propulsion system mass, with a maximum reduction of 45% while using pure oxygen, with the cruise part of the flight limiting any further improvements. Although MTOM was reduced, the downsizing of the fuel cell system resulted in a higher hydrogen consumption, increasing the required hydrogen mass by up to 20%. The reduction in fuel cell system mass is opposed by the added mass of oxygen and its tank system. Several sensitivity analyses showed that design choices can affect the system mass. Although that is verified, the effect of oxygen enrichment does not change, and the same trends are verified. The possibility of future improvements in fuel cell power density was also evaluated, where it was verified that such an improvement results in no reduction of MTOM with higher oxygen percentages. Under the conditions of the selected propulsion architecture, design choices and technology level, oxygen enriched fuel cell air supply operation is considered to have no positive impact on aircraft level performance.

Contents

Pr	eface	ì
Al	stract	ii
Li	st of Figures	iv
Li	st of Tables	vi
No	menclature	1
1	Introduction 1.1 Motivation	5 5 8
2	2.3 Oxygen Benefits and Drawbacks	9 16 24 28
3	3.1 Aircraft Sizing Workflow. 3.2 Modelling	30 31 49 54 54
4	4.1 Baseline	56 56 57 70
5 R4	5.1 Conclusion	79 79 80 89
17(ICI CIICCS	U)

List of Figures

1.1	Evolution and Future CO_2 Emissions [5]	5
1.2	Change in radiative forcing (left) and change in temperature (right) for lower and higher flight	
	altitudes for several emissions [6]	6
1.3	Volumetric and gravimetric density comparison between hydrogen and kerosene [11]	7
1.4	Comparison of climate impact between synfuel and hydrogen with respect to kerosene [8]	7
2.1	Fuel cell polarisation curve with voltage loss sources [10]	11
2.2	Fuel cell efficiency and percent of max power as a function of current density [10]	12
2.3	Pressure effect on polarization curve [32]	13
2.4	Temperature effect on polarization curve [32]	14
2.5	Cathode and anode humidity effect on polarisation curve [32]	15
2.6	Air excess ratio effect on polarization curve [34]	16
2.7	Oxygen percentage effect on polarization curve [16]	16
2.8	Example of fuel cell system architecture including fuel cell stack and balance of plant [31]	17
2.9	Dependency of aircraft energy usage with tank gravimetric efficiency for regional, transcontinental	
	and intercontinental aircraft [10]	18
2.10	Scheme of pressurisation system by warm gas return [48]	19
	Geometry of pod integrated tank concept [49]	20
	Proposed hydrogen tank configurations in the fuselage. Red areas are the tanks. [10]	20
	Cooling methods for PEMFC depending on power level [52]	21
	Heat exchanger ram air duct system [58]	22
2.15	Heat exchanger air side performance [65]	22
2.16	Annular and scoop inlet concepts [67]	23
	Compressor map [69]	24
2.18	Oxygen percentage effect on fuel cell performance [18]	25
2.19	Effect of operating pressure on dynamic response of fuel cell [36]	26
3.1	Aircraft design workflow	31
3.2	Model comparison with data from Schröder et al. [31]	36
3.3	Heat exchanger topology	37
3.4	Heat exchanger geometry definitions of tubes, top, and fins, bottom	38
3.5	Model comparison with data from Hao et al. [108]	42
3.6	Model comparison with data from Hao et al. [108]	43
3.7	Linear regressions for compressor with data from Celeroton [109], Fischer [110], ROTREX [111],	
	and Sprintex [112]	43
3.8	Linear regressions for filter with data from Freudenberg [114]	44
3.9	Linear regressions for humidifier with data from fumatech [115]	45
	Linear regressions for humidifier pressure drop with data from fumatech [115]	45
	Fuselage cross section with oxygen tank placement	49
	XDSM of first optimisation where each point is sized independently	50
	XDSM of second optimisation where stack size is fixed by the worst case of the first optimisation .	52
3.14	System sizing results comparison	53
4.1	Power supply source for the flight mission segments	56
4.2	MTOM breakdown for ambient air fuel cell operation	57
4.3	Isometric view of 21% oxygen aircraft	57
4.4	Percentage change in MTOM for varying oxygen percentages used in take-off and climb	58
4.5	Isometric view of 50% oxygen aircraft	58
4.6	Percentage change in fuel cell system mass for varying oxygen percentages used in take-off and climb	59

List of Figures

4.7 4.8	Power required at different flight phases for varying oxygen percentages used in take-off and climb Mass of the aircraft during the design mission for varying oxygen percentages used in take-off and	61
	climb	62
4.9	Aerodynamic efficiency of the aircraft at the sizing points for varying oxygen percentages used in take-off and climb	62
4.10	Side view of aircraft configurations, 21% oxygen at the top and 50% oxygen at the bottom	63
4.11	Design power factor of the three sizing points for varying oxygen percentages used in take-off and	
	climb	64
	Polarisation curves for varying oxygen percentages and representation of operating point at top-of-climb	65
	Optimum operating pressure for the varying oxygen percentages used in take-off and climb Efficiency of system with and without compressor power at a current density of $0.7A/cm^2$ for varying	66
4.15	operating pressures	67
	take-off and climb	68
	Change in hydrogen and oxygen mass for varying oxygen percentages used in take-off and climb	69
4.17	Efficiency of fuel cell system at cruise and top-of-climb for varying oxygen percentages used in	60
1 10	take-off and climb	69
4.10	take-off and climb	70
4 19	Percentage change in MTOM, fuel cell system mass and hydrogen mass for varying fuel cell areas at	70
1.17	an oxygen percentage of 21% at take-off and climb	71
4.20	Percentage change in MTOM and fuel cell system mass for varying fuel cell areas and oxygen	
	percentages used at take-off and climb	72
4.21	Percentage change in hydrogen mass and change in oxygen mass for varying fuel cell areas and	
	oxygen percentages used at take-off and climb	73
4.23	Percentage change in MTOM and fuel cell system mass for varying heat exchanger widths and oxygen	
	percentages used at take-off and climb	75
4.24	Percentage change in hydrogen mass and change in oxygen mass for varying heat exchanger widths	75
1 26	and oxygen percentages used at take-off and climb	75
	Percentage change in MTOM and fuel cell system mass for varying cruise altitudes and oxygen percentages used at take-off and climb	77
4.27	Percentage change in hydrogen mass and change in oxygen mass for varying cruise altitudes and oxygen percentages used at take-off and climb	78

2.1	Fuel cell technology comparison based on [23, 22, 24, 27, 29]	10
2.2	Comparison of hydrogen storage technologies [42]	18
2.3	Flammability limits as percentage by volume of air, adapted from [82, 79]	28
3.1	Bounds of variables that are fitted	34
3.2	Fuel cell model parameter values	35
3.3	Approximate mean temperatures on a two-fluid heat exchanger's hot- and cold-fluid sides [102]	39
3.4	Heat exchanger and intercooler design [103, 107]	41
3.5	Air side correlations validation	41
3.6	Heat exchanger geometry from Hao et al. [108] used for validation	42
3.7	Power train components power density and efficiency [117]	48
3.8	Aircraft TLARs	55
4.1	Mass breakdown of fuel cell system for one pod and sizing point for stack for varying oxygen percentages used in take-off and climb	60
4.2	Drag area, in m^2 , at cruise of most relevant components for varying oxygen percentages used in take-off and climb	63
4.3	Power density $[kW/kg]$ of fuel cell stack and complete system	64
4.4	Number of cells and stacks required at oxygen percentage for top-of-climb initial optimisation	66
4.5	Mass breakdown for one pod and DPFs of fuel cell system for varying fuel cell areas at an oxygen	
	percentage of 21% at take-off and climb	71
4.6	Mass breakdown for one pod and DPFs of fuel cell system for varying heat exchanger widths at an	
	oxygen percentage of 21% at take-off and climb	74
4.7	Mass breakdown for one pod and DPFs of fuel cell system for varying flight levels at an oxygen	77
	percentage of 21% at take-off and climb	77

Nomenclature

Abbreviations

Abbreviation	Definition
CcH ₂	Cryo Compressed Hydrogen
CR	Cruise
DLR	Deutsches Zentrum für Luft-und Raumfahrt
DPF	Design Power Factor
EASA	European Union Aviation Safety Agency
FAA	Federal Aviation Administration
HT-PEMFC	High Temperature Proton Exchange Membrane Fuel Cell
ISA	International Standard Atmosphere
LH_2	Liquid Hydrogen
LO_2	Liquid Oxygen
LT-PEMFC	Low Temperature Proton Exchange Membrane Fuel Cell
MTOM	Maximum Take-Off Mass
NTU	Number of Transfer Units
SAF	Sustainable Aviation Fuel
SOFC	Solid Oxide Fuel Cell
TheMa4HERA	Thermal Management for the Hybrid Electric Regional Aircraft
TLAR	Top Level Aircraft Requirement
TO	Take-Off
TOC	Top-of-Climb
TOFL	Take-Off Field Length
XDSM	Extended Design Structure Matrix

Symbols

Symbol	Definition	Unit
\overline{A}	Area	cm^2, m^2
A_0	Free Flow Area	m^2
ASR	Average Specific Resistance	$\Omega \ cm^2$
alt	Aircraft FLight Altitude	m
C	Molar Concentration	$mol\ m^{-3}$
C_{min}, C_{max}	Heat Capacity Rate	$J \ K^{-1} \ s^{-1}$
C_r	Heat Capacities Ratio	_
c_p	Specific Heat Capacity	$J \ K^{-1} \ kg^{-1}$
$\stackrel{\scriptscriptstyle{P}}{D}$	Diffusion Coefficient	$m^2 s^{-1}$
D_h	Hydraulic Diameter	m
D_{pipe}	Pipe Diameter	m
E^{pipe}	Fuel cell voltage	V
E_c	Activation Energy for Oxygen Reduction on Pt	$J \ mol^{-1}$
F	Faraday Constant	$A s^{-1}$
F_t	Thrust	N
f f	Fanning Friction Factor	_
f_{CCL}	Ionomer Fraction	_
HHV	Higher Heating Value	$J kg^{-1}$
H	Height	m
H_{vap}	Enthalpy of vaporisation	$kJ \ mol^{-1}$
h	Free Flow Height	
	Heat Transfer Coefficient	$m \ W m^{-2} K^{-1}$
$egin{array}{c} h_c \ i \end{array}$		$A cm^{-2}$
	Current Density	$A cm^{-2}$
i_0	Exchange Current Density	$A cm^{-2}$
i_{lim} .	Limit Current Density	A cm -
j	Colburn Factor	
k	Thermal Conductivity of Fin Material	$W m^{-1} K^{-1}$
L L / D	Length	m
L/D	Aerodynamic Efficiency of the Aircraft	_
l_{fin}	Fin Length	m
M	Molar Mass	$kg \ mol^{-1}$
Ma	Mach Number	_
m	Mass	kg
\dot{m}	Mass Flow	$kg \ s^{-1}$
ml	Fin Parameter	_
N	Number of components	_
NTU	Number of Transfer Units	_
Nu	Nusselt Number	_
n	Number of Electrons	_
P	Power	W
Pr	Prandtl Number	_
P_{req}	Power Required to Compensate for FC System Weight and Drag	N
p	Pressure	atm
p_{fin}	Fin Width	m
Q	Heat Flow	W
R	Ideal Gas Constant	$J \ mol^{-1} \ K^{-1}$
Re	Reynolds Number	_
S	Entropy of the Reaction	$J \ mol^{-1} \ K^{-1}$

Symbol	Definition	Unit
S_{pipe}	Yield Strength of Pipe	Pa
s_{fin}	Free Flow Fin Width	m
T	Temperature	K
t	Thickness	m
t_{TO}	Time for Take-off	s
UA	Heat Transfer Capacity	$W K^{-1}$
V	Volume	m^3
v	Velocity	$m\ s^{-1}$
W	Width	m
W_{total}	Total Propulsion System Weight	N
X_{O_2}	Oxygen Mole Fraction	−, %
α	Cathode Transfer Coefficient	_
β	Pressure Ration	_
γ	Specific Heat Ratio of Air	_
γ_p	Pressure Dependency Coefficient	_
Δ	Variation	_
δ	Thickness	cm
ϵ	Heat Transfer Effectiveness	_
η_g	Gravimetric Efficiency	-, %
$\eta_{act}, \eta_{ohm}, \eta_{conc}$	Activation, Ohmic, Concentration Losses	V
η_V	Voltage Efficiency	-, %
$ heta_{HE}$	Heat Exchanger Inclination Angle	0
λ	Water Content	_
λ_{O_2}	Oxygen Stoichiometric Ration	_
μ	Dynamic Viscosity	$Pa\ s$
ξ	Friction Factor	_
σ	Proton Conductivity	$\Omega^{-1}~cm^{-1}$
ρ	Density	$kg~m^{-3}$
$ ho_{cable}$	Linear Density	$kg \ m^{-1}$
$ ho_{eergy}$	Energy Density	$kW \ h \ kg^{-1}$
ρ_P	Power Density	$kW \ kg^{-1}$

Subscripts

Symbol	Definition
0	ambient conditions
air	
_	air
bp	bypass
CCL	cathode catalyst layer
Cable	power train cable
Conv	power train converter
c	cold
cell	singular fuel cell
comp	compressor
component	power train component
coolant	coolant
cr	crossover
design	values for design point
duct	duct where heat exchanger is placed
ed	fuel cell stack endplate
F	filter
FC	fuel cell
fin	heat exchanger fin
fuel	fuel
GB	power train gearbox
H	humidifier
HE	heat exchanger
H_2	hydrogen
h	hot
IC	intercooler
Inv	power train inverter
in	inlet
M	power train motor
m	mean value
max	maximum
mem	membrane
min	minimum
motor	electric motor
N_2	nitrogen
nz	nozzle
O_2	oxygen
out	outlet
primary	primary heat exchange surface
-	• •
pump ref	coolant pump reference conditions
•	
shaft	propeller shaft
stack	fuel cell stack
t	stagnation conditions
tank	tank
taxi	taxi in and out
tube	heat exchanger tube
VP	vapour cycle cooling system
wall	conditions at wall of fin

Introduction

1.1. Motivation

The current state of pollution is a driving factor in many industries, as it drives innovation to improve emissions and environmental quality. Aviation is not an exception, being one of the main contributors to emissions, requiring innovation to improve. Aviation emissions account for about 3.5% of the global net anthropogenic effective radiative forcing, where the CO_2 effect accounts for not even half of it [1]. Emissions from aviation include CO_2 , H_2O , NO, NO_2 , CO, a variety of hydrocarbons, sulfur oxides, soot, and other particles [2].

It might seem that the contribution of aircraft is not as significant as others, but aviation is the most unsustainable mode of transport available [3]. Besides that, being part of the transport sector, aviation is also part of the sector with the most significant growth and emissions. The aviation sector is expected to grow and expand due to globalisation, liberalisation of the air transport market, and low fares business models [4].

Figure 1.1 shows the expected increase in CO_2 emissions due to aviation expansion. It is clear that even with expected efficiency improvements at the historical rate of 2%, it would still result in a substantial increase in CO_2 emissions [5]. New technologies are necessary to reduce emissions significantly.

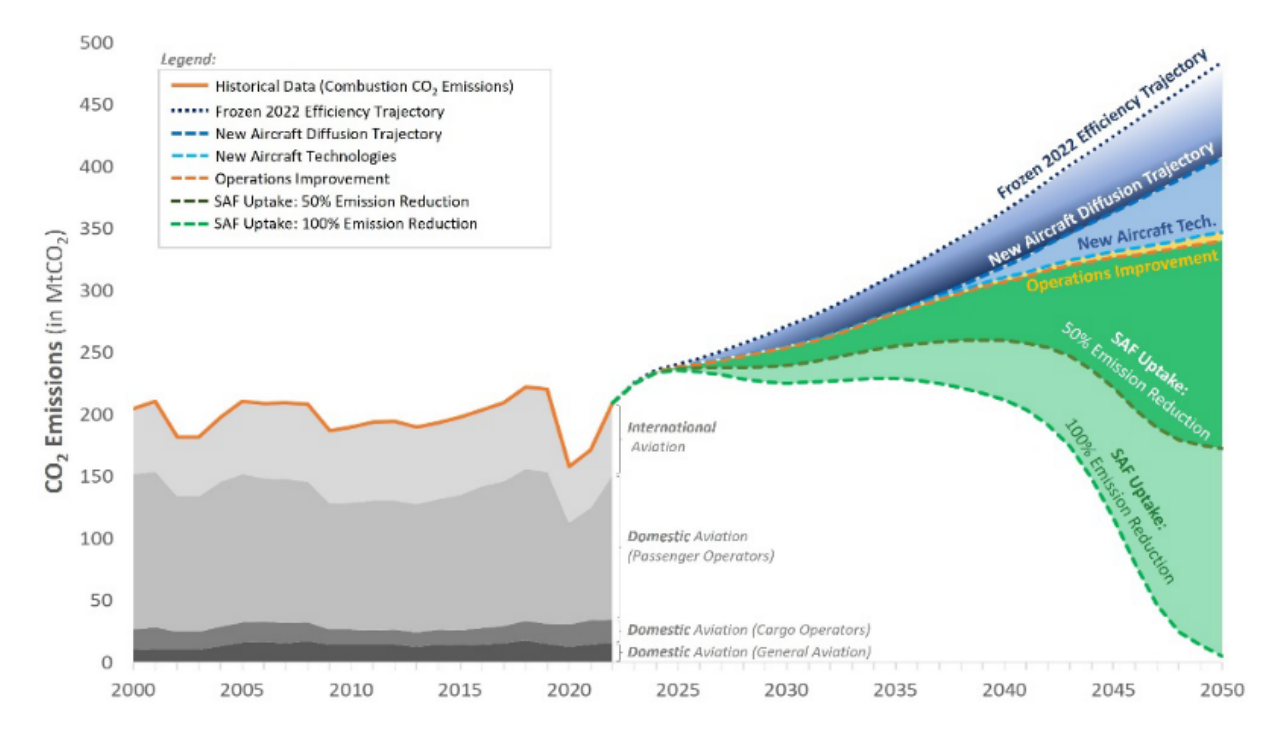


Figure 1.1: Evolution and Future CO_2 Emissions [5]

Besides that, the characteristics of aircraft emissions worsen the problem. Aircraft emit their exhaust products directly into the upper troposphere and lower stratosphere. For CO_2 emissions, this is not relevant, as CO_2 effects

1.1. Motivation 6

on the atmosphere are not altitude dependent, but for other types of emissions, significant changes in their behaviour stem from the change in altitude [2]. H_2O particles at aircraft flight altitudes can form contrails, ice crystals from the condensation of water vapour in the engine exhaust, resembling clouds. Contrails contribute to the warming effect of emissions but can be easily reduced if aircraft flight level changes, since ideal temperature and pressure conditions for their formation are not found at lower altitudes. The effects of NO_x emissions are also highly dependent on altitude since their effects are related to the chemical composition of the atmosphere and chemical reactions. The overall impact of altitude on climate change induced by aircraft emissions is presented in Figure 1.2. It can be seen that if the aircraft flies lower, even though the fuel consumption increases, due to lower aerodynamic efficiency, and the total emissions of all substances increase, the total radiative forcing, change in energy balance of the atmosphere, of the emissions reduces with only CO_2 effects contributing to the adverse impacts. This confirms that CO_2 is not altitude dependent; therefore, increased quantity emitted increases its effects.

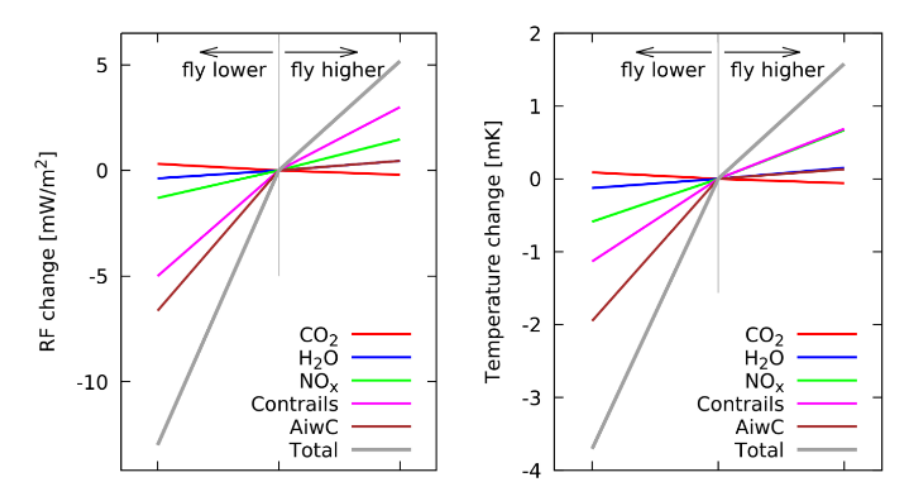


Figure 1.2: Change in radiative forcing (left) and change in temperature (right) for lower and higher flight altitudes for several emissions [6]

Several novel technologies have been introduced to improve aircraft climate impact. These are electric propulsion, Sustainable Aviation Fuel (SAF), and hydrogen fuel, for combustion or fuel cell propulsion. Each of these options has its pros and cons. SAF has already been used since no significant changes are required to the engine to operate with SAF. However, availability, production cost, and competition with food sources create a problem for its usage as the only substitution for kerosene [7]. Besides that, it also does not provide a suitable solution to non- CO_2 emissions [8].

As for electric propulsion, while it is the only zero-emissions source, in the case electricity is obtained without emissions, the low energy density of the batteries, with expected values of 500 - 600Wh/kg [9] that are several orders of magnitude lower than the ones shown in Figure 1.3 for hydrogen and kerosene, makes its use for long flights impossible. Besides that, it would require major reformulation of airport infrastructure for fast charging or battery exchange systems [8].

Using hydrogen as a fuel would also require significant changes in the airport infrastructure. The emissions resulting from its use depend on the application. For combustion, a lower reduction of emissions is expected since NO_x will be produced, while with a fuel cell, only H_2O is produced. Hydrogen has a higher gravimetric energy density than kerosene, but its volumetric energy density is much lower, as presented in Figure 1.3. Besides that, even to reach those values of hydrogen volumetric density, extreme conditions are required, for gaseous hydrogen, high pressures of up to 700 bar and for liquid hydrogen, temperatures below the liquid temperature of hydrogen, 2K. As a result, to store it in aircraft, heavy and complex tanks are required to reduce the volume required to store it, which withstand the high pressures and insulate the hydrogen from outside heat sources. These requirements reduce the tank gravimetric density, which is the ratio of hydrogen mass to hydrogen plus tank mass. Current developments indicate possible tank gravimetric efficiencies of 25% - 40% for liquid hydrogen, which are still below the tipping point proposed by Adler et al. [10] of 55%, over which hydrogen aircraft would perform better than kerosene ones. For kerosene, the tank's gravimetric efficiency is almost 100%, due to the tanks using the empty space of the wings, becoming integral tanks, where the wing itself is the tank. Besides that, the high volume required generates penalties due to increased aerodynamic drag or reduced passenger or cargo space. As a result, hydrogen is a better option

1.1. Motivation 7

for lower-range aircraft, mainly regional aircraft with ranges of about 500 nautical miles, where this penalty is less detrimental [8]. If, with the evolution of tank design, higher gravimetric densities are reached, hydrogen aircraft may become more energy efficient [10].

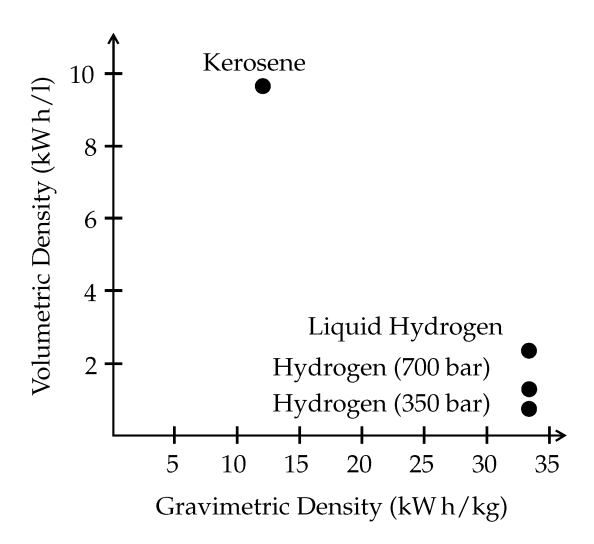
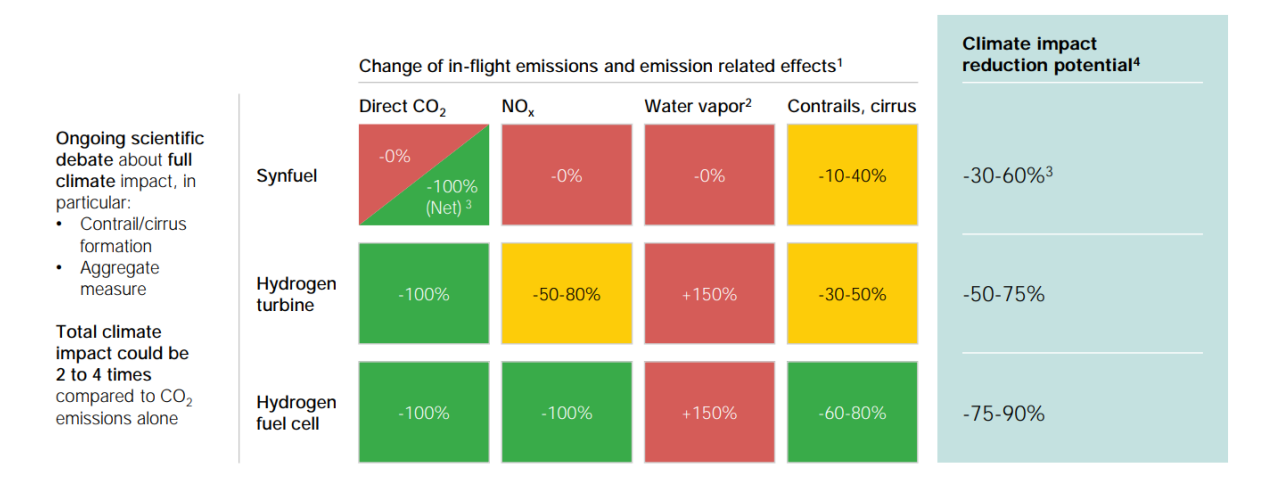


Figure 1.3: Volumetric and gravimetric density comparison between hydrogen and kerosene [11]

Figure 1.4 shows the possible reduction of emissions for each option, with synfuels representing SAF. Not to forget that for any of the solutions, the actual reduction in emissions depends on the sourcing of the fuel. For hydrogen to have the most significant effect in reducing emissions, it is essential that the most common current sources of hydrogen, coal and natural gas, are substituted by environmentally friendly ones [12]. With developments in water electrolysis with renewable electricity, it is possible to replace current hydrogen sources [7].

Compared to kerosene-powered aircraft, timeframe until 2100



- Assuming decarbonized production and transportation of fuels in 2050
- $\begin{array}{ll} 2. & 10 \text{ times lower climate impact than from CO}_2 \text{ emissions} \\ 3. & \text{Net CO}_2 \text{ neutral if produced with CO}_2 \text{ captured from the air} \\ \end{array}$
- Measured in CO₂ equivalent compared to full climate impact of kerosene-powered aviation

Figure 1.4: Comparison of climate impact between synfuel and hydrogen with respect to kerosene [8]

As the starting point of the development of fuel cell aircraft, the regional segment is crucial since the feasibility of implementing new technologies is higher [8]. Even though it only represents around 3% of total aviation emissions [7], it will serve as an opportunity to test the implementation of these enabling technologies to reduce emissions. It

could even develop into a replacement of the lower end of the short-range segment, reducing emissions even more [8], and with the understanding obtained, it could be used to scale up the technology for later use in larger aircraft.

An increase in the need for such aircraft in certain countries is already evident. In the Nordic countries, several commitments have been made to completely remove the usage of fossil fuels by 2030 in all domestic flights [13]. Norway has also committed to reducing emissions by 80% by 2040 in its domestic flights, which means that SAF would not be a solution anymore. Svensson et al. [14] have already done a study on the possibility of implementing fuel cell propulsion to fulfil all the Nordic domestic flight requirements, where it was concluded that such an aircraft could cover 97% of travel distances required.

Even for regional aircraft, it is expected that while a lower energy demand is possible, the cost per available seat kilometre and the take-off mass of the aircraft would increase [8]. Therefore, efforts should be made to evaluate any possible improvements to the efficiency and mass of such systems.

1.2. Research Objective

Since the fuel cell propulsion system increases the aircraft mass, efforts are made to reduce this system's mass. One of the main improvements currently being developed is the storage system. Where reducing tank mass and volume while keeping the same hydrogen storage conditions is desired. This type of change results in improvements at the auxiliary system level, but it does not improve the actual fuel cell efficiency. Improvements at the fuel cell level are another possibility to increase fuel cell propulsion efficiency. To do that, improvements to the materials used or the operating conditions under which the fuel cell runs are the options. At the material level, any improvement depends on significant research and breakthroughs. While for the operating conditions, its limits have been reached due to material limitations, working principles of the fuel cell, or the necessity of auxiliary components that reduce system efficiency.

One of the only operating parameters that has not been fully studied is the use of higher oxygen concentrations or even pure oxygen as the oxidant of fuel cells. The use of ambient air worsens the performance of a fuel cell, due to nonreacting nitrogen, and can degrade it faster, reducing its lifetime. Schumann et al. [15] report that a fuel cell system operating under pure oxygen instead of ambient air can have higher efficiencies while also providing other beneficial qualities to the aircraft. This study has several flaws that make it impossible to know if such a system would be better. First, the analysis is done for other applications that are not propulsion. Secondly, the methods used and how they were implemented are not disclosed. It is said that mathematical models in Matlab and experimental results were used, but no details are given. Finally, the mass of the systems, while calculated for the hydrogen supply part of the system, did not include the components of the oxidant supply, and was not used to analyse if a higher efficiency system with a higher mass would actually result in an overall improvement at the aircraft level. As this study was unclear on what assumptions were taken and what the effect would be on aircraft performance when considering system mass, a further analysis of this effect should be conducted. Besides that, several studies show that oxygen enrichment can significantly improve the efficiency of the system and reduce its mass [16, 17, 18]. Therefore, the following research objective is proposed:

Research Objective

The objective is to evaluate the effects of oxygen enrichment on the fuel cell propulsion system sizing and performance, and its impact at the aircraft level. This will be achieved through the development of models that are used to size and simulate the fuel cell system under different operating conditions.

Literature Study

This chapter presents the findings of a literature study on fuel cell propulsion systems and the effects of oxygen enrichment. The state of the art of fuel cells is discussed in Section 2.1. Then, the subsystems required to operate an aircraft's fuel cell propulsion system are presented in Section 2.2, followed by the study of the benefits and worries of oxygen enrichment in fuel cells in Section 2.3. Finally, the research questions are formulated and presented in Section 2.4.

2.1. State of the Art in Fuel Cells

The use of hydrogen as a fuel has long been studied as an alternative to reduce aviation emissions. One of the ways hydrogen can be used as an energy source is with fuel cells. There are several types of fuel cells, where the chemical energy of a fuel, with the help of an oxidant, is converted into electricity. Different reactants are the source of energy produced in the fuel cell, but usually, hydrogen, the fuel, and oxygen, the oxidant, are the choice.

In aviation, two main types of fuel cells have been investigated due to their higher state of development. One being the Low Temperature Proton Exchange Membrane Fuel Cell (LT-PEMFC) and the other the Solid Oxide Fuel Cell (SOFC) [19, 20]. Recently, a third alternative has also become a topic of interest, the High Temperature Proton Exchange Membrane Fuel Cell (HT-PEMFC) [21]. The main difference in how they function is related to what type of electrolyte membrane is used to transport ions. In a PEMFC, a polymer membrane serves as the electrolyte, whereas in a SOFC, a solid oxide membrane fulfils this role. As a result, the type of ions transported and their direction from cathode, oxygen side, to anode, hydrogen side, or from anode to cathode is different, as it will be detailed in this section. A single fuel cell does not provide the necessary power, requiring the connection of multiple fuel cells in series, which is called a fuel cell stack.

Fuel cells reactions occur at the cathode and anode, where the oxidation and reduction reactions occur. In the PEMFC, the reactions are, at the anode:

$$2H_2 \longrightarrow 4H^+ + 4e^-$$

And at the cathode:

$$O_2 + 4H^+ + 4e^- \longrightarrow 2H_2O$$

To complete the reactions, a membrane electrolyte assembly that transports the H^+ protons from the anode to the cathode is required. This membrane is an essential part of the fuel cell systems since its performance in the transport of ions is fundamental for the overall performance of the fuel cell. In the case of LT-PEMFC, it is necessary to control the water content in the membrane assembly since water molecules are responsible for transporting the H^+ protons. Therefore, it is necessary to control the exact water content in the membrane to prevent excess water, flooding, and lack of water, dry out [22]. Due to the possibility of the membrane drying, the LT-PEMFC has a temperature operation limit of about $100^{\circ}C$ [23]. Due to their relatively low operating temperature, LT-PEMFCs need bigger and heavier thermal management systems due to the low temperature rejection of heat. LT-PEMFCs are also much more prone to contamination due to carbon monoxide and other impurities of the membrane [10].

Even though their operation seems complex LT-PEMFC are still the most prominent choice for transport applications mainly due their low start up time and the fact that their power density, between $500 - 2500 mW/cm^2$, is the highest of every fuel cell [22].

To improve some of the downsides of the LT-PEMFC, the HT-PEMFC is seen as the next step. These fuel cells operate at a higher temperature $(100 - 200^{\circ}C \text{ [24]})$, reducing the cooling demand due to the higher temperature difference to ambient air. These cells also operate with membranes that are less sensitive to contamination, polybenz-imidazole membranes, which are doped with phosphoric acid, using no water, which makes it so that there is no need for water management systems [10, 25]. For now, they are still at a low development stage and have yet to surpass the performance of LT-PEMFC, but improvements are expected to lead to their more common use [26].

In the case of the SOFC, the reactions occurring are, in the anode:

$$2H_2 + 2O^{2-} \longrightarrow 2H_2O + 4e^-$$

And in the cathode:

$$O_2 + 4e^- \longrightarrow 2O^{2-}$$

In SOFCs, a solid oxide or ceramic electrolyte is used, transporting O^{2-} ions from the cathode to the anode, without any water management. Such fuel cells operate at temperatures between $600 - 1000^{\circ}C$, which improves the reaction rates of the fuel cell, enabling the use of simpler materials [10]. These high temperatures are simultaneously the advantages and disadvantages of SOFC, since the necessity to reach such temperatures results in high start-up times, material difficulties due to high temperature variation of the materials, and reduced life cycles and time [22, 27]. Even though their specific power is lower than LT-PEMFC, if the waste heat generated can be used to power other systems, their use can become more relevant [28].

In Table 2.1, an overview of characteristics for the three types of fuel cells is presented. Due to the current level of development, the high power density and quick start-up times, LT-PEMFCs are usually the fuel cells chosen for aircraft.

Fuel Cell	Operating Temperature ($^{\circ}C$)	Power Density (mW/cm^2)	Efficiency(%)	Advantages	Disadvantages
LT-PEMFC	10 – 100	500 - 2500	40 - 50	-Quick start-up time -High power density	-Thermal management system mass -Sensitive to fuel impurities -Water management system
HT-PEMFC	100 – 200	500 – 900	40 - 50	-Lower thermal management system mass - No water management -Less sensitive to impurities	-Low development level -Longer start-up times
SOFC	600 - 1000	250 - 500	50 - 60	-High efficiency -Increase in efficiency with residual heat usage	-Long start-up time -Short lifetime

Table 2.1: Fuel cell technology comparison based on [23, 22, 24, 27, 29]

2.1.1. Fuel Cell Performance

The theoretical voltage provided by a fuel cell can be described with the Nernst equation. With the variations of temperature and pressure taken into account, the theoretical potential of a fuel cell is presented in Equation 2.1.

$$E = E_{ref} + \frac{\Delta S}{2F} (T_{FC} - T_{FC,ref}) + \frac{RT_{FC}}{nF} \ln \left(p_{H_2}(p_{O_2}^{1/2}) \right)$$
 (2.1)

where E_0 is the standard-state reversible voltage, ΔS is the entropy of the reaction, F is the faraday constant, T_{FC} is the fuel cell temperature, with the subscript ref representing standard conditions and p_{H_2} and p_{O_2} are the fuel cell partial pressures of H_2 and O_2 , respectively.

These equations give the results for a theoretical operation. In reality, several processes reduce the cell voltage compared to the theoretical one. In Figure 2.1, a typical relation between cell voltage and current density, the polarisation curve, of a fuel cell is presented, where the three main mechanisms of voltage loss are presented.

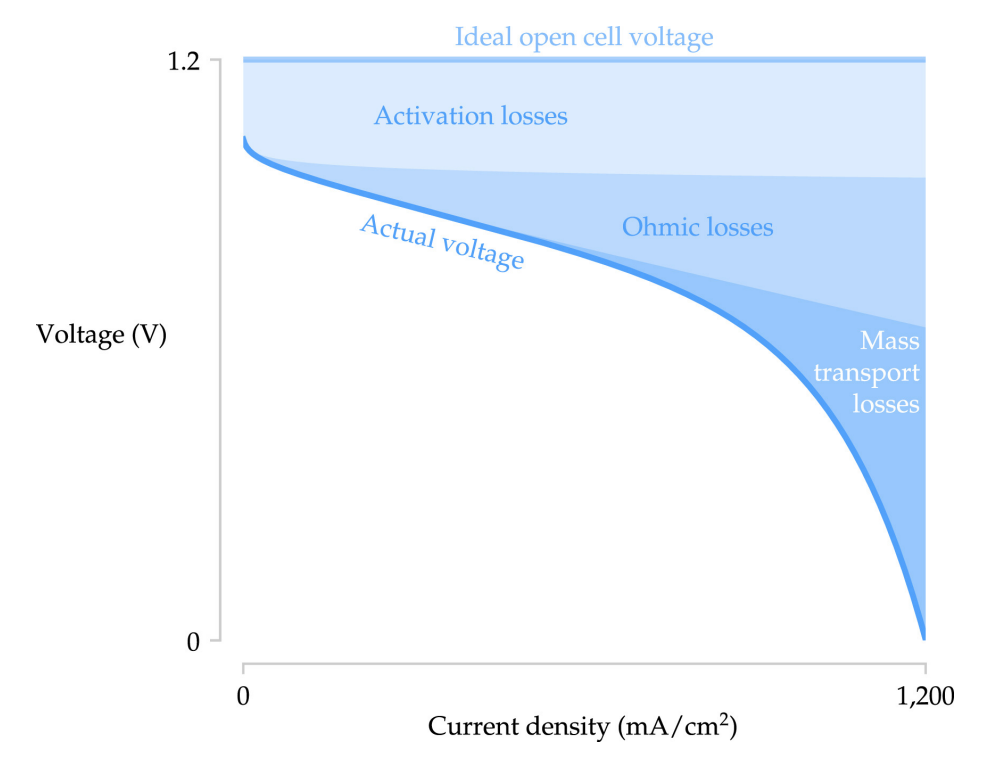


Figure 2.1: Fuel cell polarisation curve with voltage loss sources [10]

The first is the activation loss, which is related to the kinetics of the reaction and describes the extra voltage provided to the chemical reaction for it to occur. Such loss exists at both the anode and the cathode, but due to the slower rate of reaction of the oxygen reduction, the losses in the cathode are much higher than the ones at the anode. This extra voltage provided is therefore unavailable and does not contribute to the useful voltage. These losses are closely related to the exchange current density, i_0 , which is the equilibrium current of the reactions, representing the amount of electrons flowing at zero current density. If only the cathode reaction is considered, since the kinetics of reaction are significantly slower for the oxygen reduction than for the hydrogen oxidation [22], i_0 is the exchange current density of the cathode only. A higher exchange current density is desired because it represents a higher activity that generates more current, and because if the desired current is lower than the exchange current, it will be supplied with no losses associated. In conclusion, a cathode with a larger exchange current will have a smaller voltage loss than one with a smaller exchange current [30, 10].

The second loss results from internal resistances found in the fuel cell. They are called ohmic losses since they follow Ohm's law and therefore have a linear relation with the current density, as seen in Figure 2.1. These resistances come from both the protons flowing through the membrane and the flow of electrons through the wiring. Both resistances are combined in a factor, the ASR, area specific resistance.

The ASR of the cell is mainly dominated by the proton resistance since the electron resistance tends to be much smaller [22]. It is also highly dependent on material choice and thickness. In the case of a LT-PEMFC, as explained in Section 2.1.2, the water content and temperature of the membrane are also a fundamental aspect of this loss mechanism.

The last loss mechanism is the mass transport loss or concentration losses, since it results from a reduction in concentration due to insufficient mass transport. At high currents, the reactants at both the cathode and anode are being consumed rapidly. As a result, their partial pressure and concentration at the electrodes are reduced, and if the reactants are not replaced rapidly, the fuel cell performance drastically decreases. This limitation is mainly determined by the rate at which reactants are supplied through the channels or the rate at which they can diffuse through the electrodes. So it can also be a material driven loss. This loss describes the maximum current the fuel cell can operate at because it represents the maximum rate at which reactants can be supplied [10]. Above this current, the limiting current i_L , the fuel cell starves.

The modelling of the fuel cell can then consider all of the losses presented through either experimental fitting or more detailed models of each specific loss mechanism.

Besides this difference, there are studies where only the steady-state performance of the fuel cell is analysed [31, 32, 33, 34], which are the majority of studies, while in others the transient or dynamic performance is also a case of study [35, 36].

For the work to be done in this thesis, it was decided that a steady-state modelling of the fuel cell would be the best approach. This is due to several reasons. Firstly, studying the dynamic response of a fuel cell is more important in applications where the power demanded from the fuel cell varies a lot in time, such as in automotive applications [36]. While changes in required power on an aircraft are expected, they do not happen with the same frequency as those in automotive applications. When such variations exist, a battery can provide such peak power requirements. Besides that, the level of complexity required from DLR for this study was of a simpler and low computational power model that could be used to size the systems of a fuel cell propulsion unit while taking into account power demands and conditions of specific flight points. Therefore, this model will be used in conceptual aircraft design where the dynamics are not required.

Lastly, while it does not motivate the choice, the effects of oxygen enrichment in fuel cell dynamic response and performance seem to be all positive, as it will be detailed in Section 2.3.1, so modelling them would create a positive point to transition to higher oxygen content usage.

The efficiency of the fuel cell follows the polarisation curve, as seen in Figure 2.2. At the same time, its specific power, the ratio between power at a certain current and maximum power, has a different behaviour. As the current increases, efficiency reduces, as the voltage does, but the specific power increases, up to a maximum, after which it decreases. This effect has some implications for aircraft implementation. In an aircraft, the same power could be obtained by a more efficient fuel cell operating at lower currents, by using a higher number of fuel cell stacks, resulting in a higher mass of the fuel cells but a lower mass of fuel. Or it could be provided by a lower efficiency system with higher specific power at higher currents, resulting in a lower mass for the fuel cell stacks but a higher mass of fuel required. The optimum point in terms of total mass is a point between the two extremes.

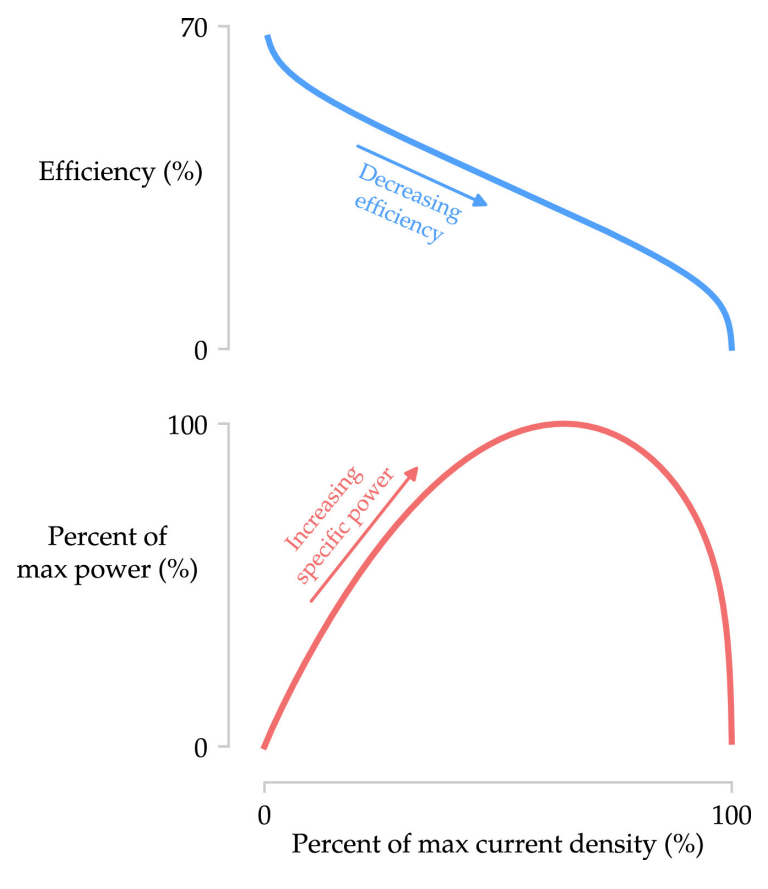


Figure 2.2: Fuel cell efficiency and percent of max power as a function of current density [10]

2.1.2. Influence of Parameters on Fuel Cell Performance

The performance of a fuel cell strongly depends on parameters like temperature, pressure, relative humidity, air excess ratio, and oxygen concentration. The optimal values of these parameters are the subject of many studies, as it is not a trivial or straightforward process to determine them [31].

Pressure

The effect that the pressure of the fuel cell has on its performance can be explained mostly by the variation of the partial pressure and concentration of oxygen with respect to the total pressure.

Fuel cells operating at a higher total pressure have a higher oxygen partial pressure and concentration at the fuel cell reaction interface. This has many beneficial effects on the fuel. Firstly, it will aid in the kinetics of the reaction, since a higher concentration of reactants helps the reaction take place faster [30], which can be seen as an increase in i_0 . Lastly, with an increase in oxygen concentration in the electrode, at high currents, when the reactant depletion is high, the replenishing of reactants will be faster, allowing for operation at higher currents with lower losses, resulting in a higher i_L . Besides the improvements in the irreversible losses of the fuel cell, a higher pressure also improves the maximum voltage obtained in theory. This is because, as shown in Equation 2.1, the term where the pressure of the reactants is taken into account will be higher with higher pressures. The effect of pressure on the fuel cell performance has been shown in several studies on the operating conditions of fuel cells [37, 32, 31], an example of this effect is presented in Figure 2.3.

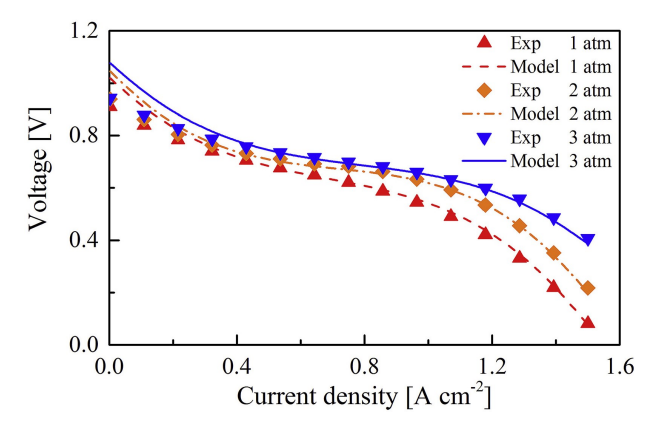


Figure 2.3: Pressure effect on polarization curve [32]

Even if, when looking at the fuel cell performance, the increase in pressure results in a higher efficiency and power output, it is important to notice that there are also adverse effects of increasing pressure. This is the case when looking at the overall systems required to provide the desired operating conditions for the fuel cell. To keep the pressure at the desired level even at high altitudes, a compressor is required, since the performance of the fuel cell would diminish at lower pressures [30]. The necessity for the compressor adds a weight and a power penalty. While the weight is usually low compared to other components of the system, the power the compressor requires to keep the operating pressures of the fuel cell is not. It can reach about 20% to 25% of the total fuel cell power [38]. It is then clear that increasing the pressure as much as possible is not always the best option; there is a need to do a trade-off to obtain the optimum overall performance of the system.

Temperature

Temperature has many effects on the performance of the fuel cell that result in opposite effects on fuel cell efficiency. In the theoretical voltage of a fuel cell and in the equations for the voltage losses, an increase in temperature results in a lower voltage and therefore a lower efficiency. However, just like for pressure, there are effects of increasing the temperature that also influence parameters that drive irreversible voltage losses.

A higher temperature is related to higher particle agitation, increasing the likelihood of a reaction occurring and therefore a higher rate of reaction, which, like for the pressure, will reduce the activation losses in the fuel cell [22].

With respect to the activation losses there is also the possibility for the temperature increase to increase losses, this occurs at high current densities due to the high activation overvoltages required at these currents [22]. At higher temperatures, gases can also contain more water vapour, reducing the possibility of flooding the fuel cell [39]. An increase in temperature also has a positive effect on proton conductivity of the membrane and diffusivity of reactants, reducing ohmic and concentration losses, respectively. The improvements in fuel cell performance with temperature can be seen in Figure 2.4.

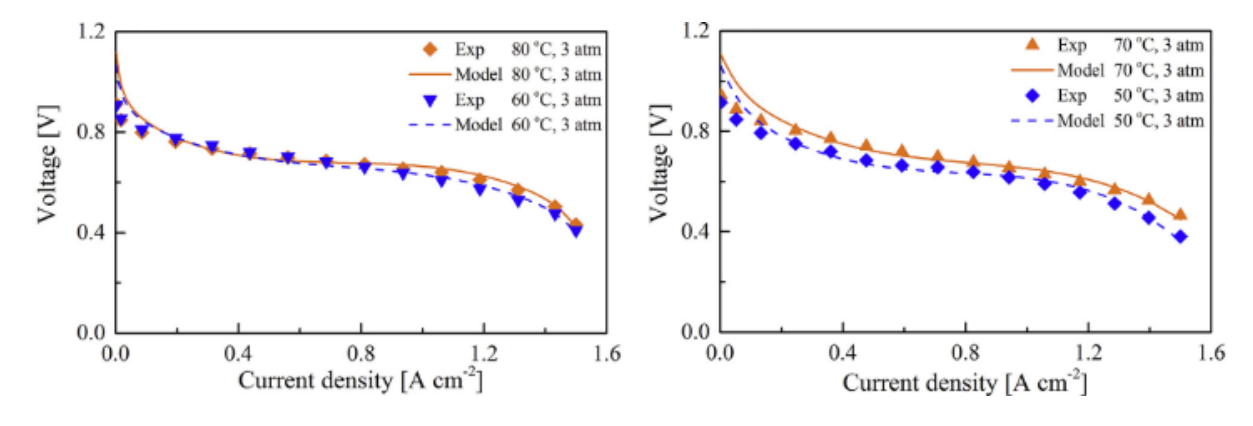


Figure 2.4: Temperature effect on polarization curve [32]

Another adverse effect of increasing the temperature arises from the possibility of drying out the membrane. This can happen if the temperature of the fuel cell is too high and the water production is slower than the rate at which it evaporates. Therefore, it is important also to increase humidity at higher temperatures [37], up until the limit is reached, where water humidity is at its maximum and increasing the temperature is no longer feasible.

When it comes to the effects of temperature on the overall system performance, an increase in temperature results in higher efficiency. With higher temperatures, the heat generated from the fuel cell is easier to dissipate in the heat exchanger, reducing its mass [40].

Relative Humidity

Some of the effects of relative humidity on fuel cell performance have already been discussed in the previous sections. It is due to the working principle of a LT-PEMFC and its materials that water content is such an important aspect. Usually, LT-PEMFC membranes are made of Nafion, and their conductivity increases with relative humidity [22], improving performance of the fuel cell, Figure 2.5. The operation of the membrane eventually has its limits, already detailed previously, where at low and high water content, dry out and flooding can occur, respectively.

These requirements make the existence of a humidifier for the cathode necessary. This is because at the anode side only pure hydrogen is used, and the recirculation of the hydrogen introduces water in the anode [41].

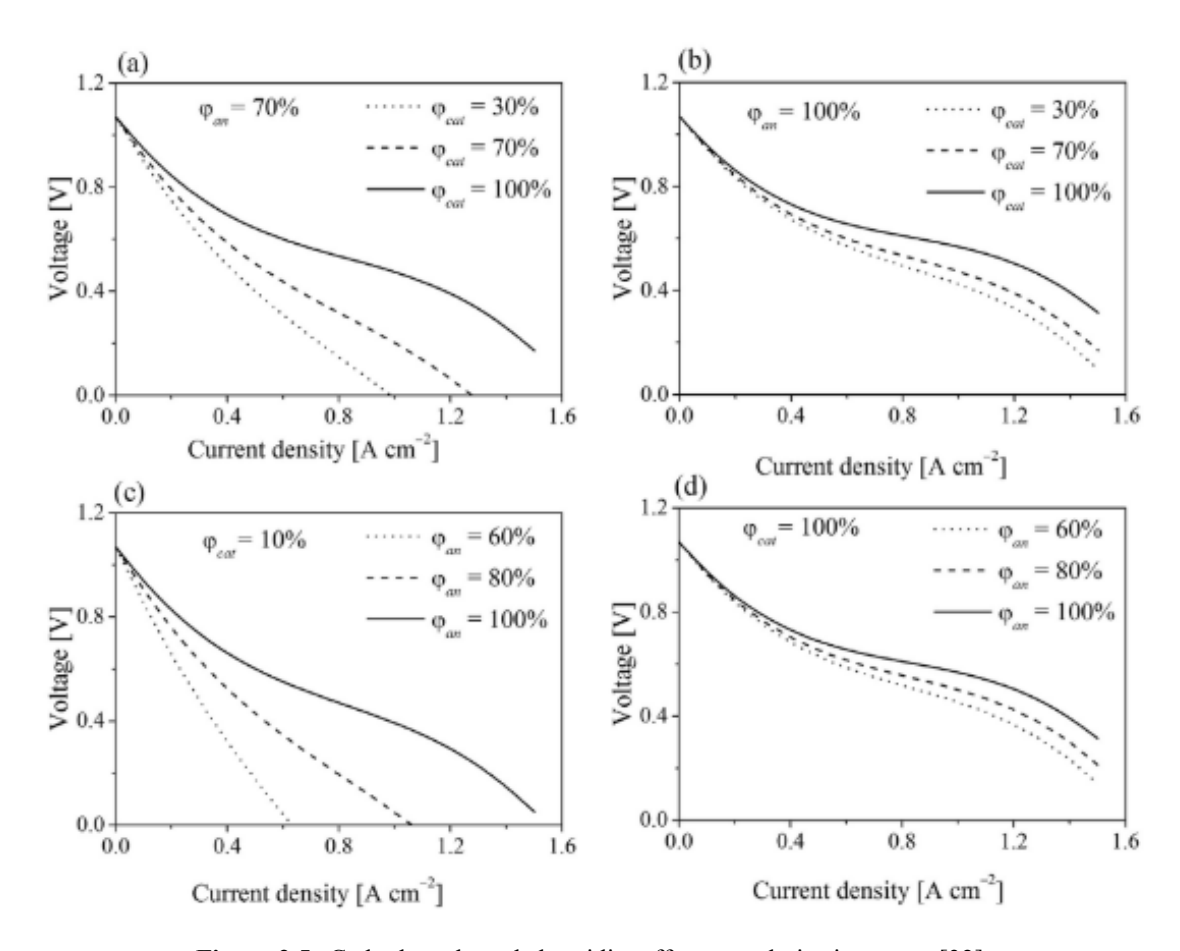


Figure 2.5: Cathode and anode humidity effect on polarisation curve [32]

Air Excess Ratio

The hydrogen depletion along the fuel cell channels is less of a problem since only hydrogen is available to react in its side of the fuel cell, the anode. On the cathode side, since air is supplied, at the end of the fuel cells, there is a lower concentration of oxygen, increasing the losses of the fuel cell and reducing its performance. As a result, an excess of air with respect to the stoichiometric value is necessary to react with the hydrogen supplied on the anode. Therefore, a higher air excess ratio or air stoichiometric ratio results in higher fuel cell voltages [34, 31, 30], Figure 2.6. The necessity of exceeding air causes issues associated with the required power to pressurise the airflow. The need to pressurise more air and consume more power can invalidate the gain obtained from a higher air excess ratio and decrease performance [31].

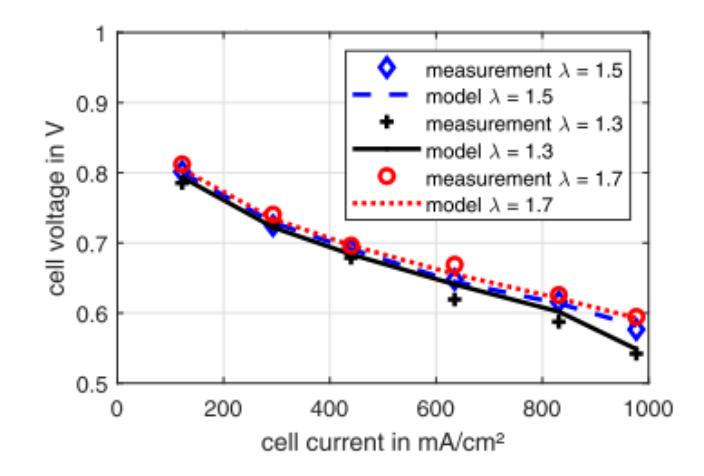


Figure 2.6: Air excess ratio effect on polarization curve [34]

Oxygen Percentage

The supply of different oxygen percentages in the oxidant flow of the fuel cell can significantly change its power output and performance. As mentioned, the pressure effects are mostly associated with the increased oxygen partial pressure and concentration, which can be achieved by increasing total pressure or by increasing the oxygen percentage in the mass flow. Therefore, the effects are similar to the ones obtained for an increase in pressure, with both an increase in theoretical voltage due to a higher partial pressure and a reduction of the irreversible losses. In the case of the activation losses, a higher oxygen percentage increases the kinetics of the reaction at the cathode, which is the limiting reaction of the fuel cell, and results in lower activation losses. Besides that, it will also affect the mass transport losses, since with a higher concentration of oxygen, the starvation of the fuel cell occurs at a higher current density [17]. Another improvement of oxygen enrichment is that it allows for higher operating temperatures, reducing the losses, mainly the activation and ohmic losses, even more. The final result of all these effects is shown in Figure 2.7, where the polarisation curve for different oxygen percentages is shown.

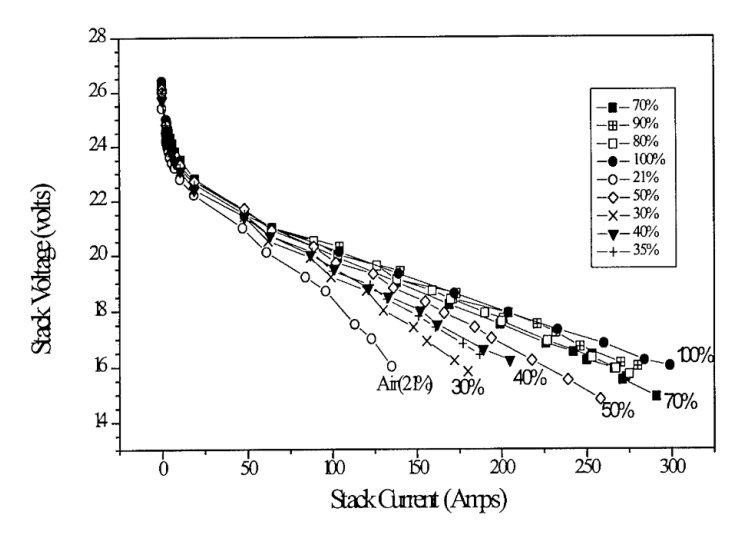


Figure 2.7: Oxygen percentage effect on polarization curve [16]

2.2. Balance Of Plant

To integrate a fuel cell as a source of power in an aircraft and keep the operating conditions under which it works controlled, there is a need for several extra components that comprise the Balance-of-Plant (BoP) of the fuel cell. The BoP is composed of 3 main groups: the hydrogen storage, the heat management, and the air supply.

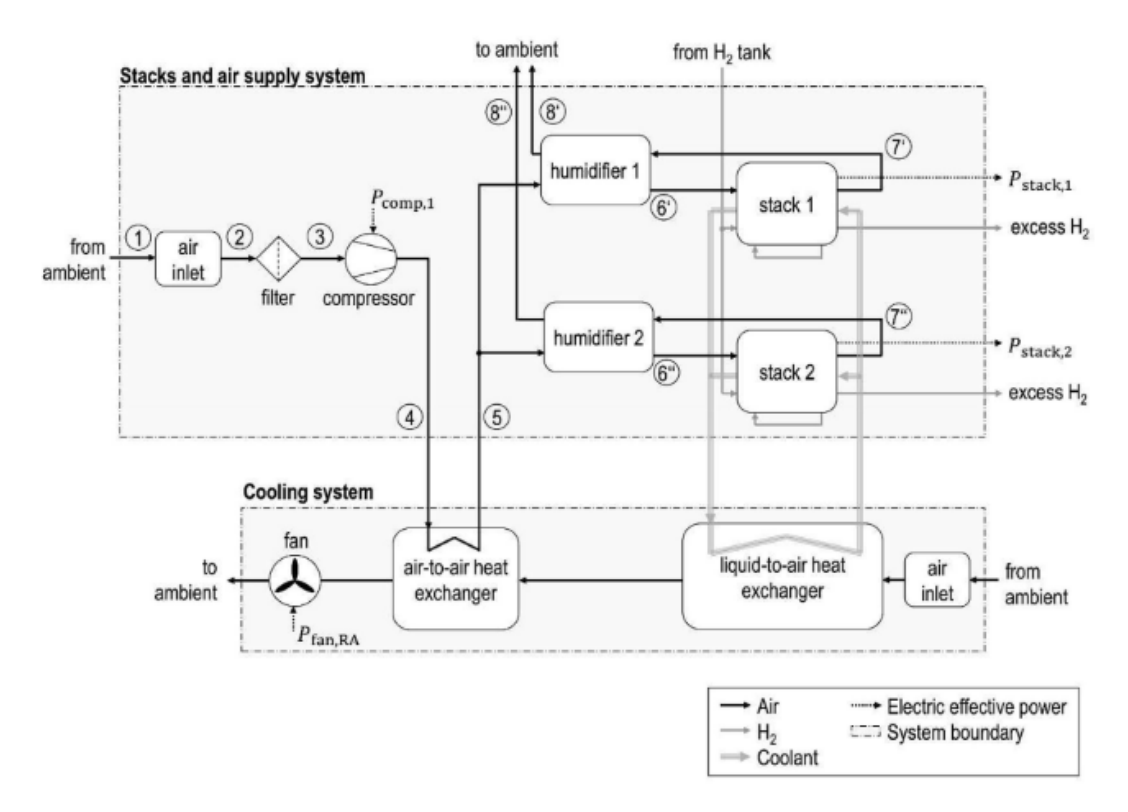


Figure 2.8: Example of fuel cell system architecture including fuel cell stack and balance of plant [31]

2.2.1. Hydrogen Storage and Distribution

To provide the reactants to the fuel cell, a hydrogen supply is also necessary, as it is not readily available in the atmosphere as oxygen is. Hydrogen as an energy supply has certain qualities and some downsides. It has much higher specific energy, the energy per unit mass of the fuel, than kerosene, which is about four times higher, which is good in an aircraft since the same amount of energy can be provided by a much lighter fuel. However, it also has a much lower energy density, the energy per unit volume of the fuel. Because of this, it is necessary to use systems that improve the hydrogen energy density. Such systems are usually heavy, negating some of the benefits of their introduction. Hydrogen embrittlement and permeation, due to the small size of hydrogen molecules, are also driving factors for the high masses of the tanks [10], reducing energy density. Measures in terms of material choice need to be taken with these factors in mind, which can drive price and weight up.

An essential characteristic of a tank is the gravimetric efficiency, Equation 2.2.

$$\eta_g = \frac{m_{fuel}}{m_{fuel} + m_{tank}} \tag{2.2}$$

Where m_{fuel} is the mass of fuel inside the tank and m_{tank} is the tank mass required to store that fuel. The gravimetric density can be given as a decimal or as a percentage.

There are several storage means studied for hydrogen in an aircraft. In Table 2.2, several options are presented with some relevant values for their evaluation. These include the gravimetric efficiency, the volumetric density, the operating conditions of the storage and its relation to the fuel cell operating conditions, the kinetics of supply, and its safety and maturity level.

From the table, three main options seem currently viable due to their maturity level: compressed H_2 (CH₂), liquid H_2 (LH₂) and cryo compressed H_2 (CcH₂). The high pressures in compressed H_2 tanks increase the tank mass to much resulting in a lower gravimetric density while also providing low safety levels due to possibility of high pressure leaks and explosions [42]. Liquid H_2 relies on storing hydrogen at or below its liquid temperature. The main drawback of liquid H_2 is the boil-off that occurs when heat transfer from outside the tank vaporises the liquid hydrogen, increasing pressure inside the tank. This is a problem because these tanks are not designed for high pressures. As a result, these tanks require well insulated walls and even venting systems that also result in a lower

gravimetric density. In this case, the decrease is not as significant as the one for compressed hydrogen. Due to better gravimetric and volumetric density, while also being safer due to low operating pressures, liquid hydrogen is the preferred option. Lastly, there is cryo-compressed H_2 , a hybrid of both methods as it combines high pressure with low temperature. Since it is designed for high pressure, boil-off is not as much of a problem [43], but cryo-compressed tanks still have the same safety issues as the compressed ones due to high pressures. Their design is therefore a balance between increasing pressure to increase volumetric density, but not so much that the gravimetric density reduces to a point where no overall improvement is reached [44].

Technology	$n_g[wt\%]$	$n_v[MJ/L]$	$T[^{\circ}C]; p[bar]$	$\Delta T[^{\circ}C]; \Delta p[bar]$	$Q[kJ/kg_{H_2}]$	Kinetics	Safety	Maturity level
CH ₂	5.7	5.6	20; 700	35; -699	/	fast	low	high
LH_2	7.5	6.4	-253; 1.5	313; 0	/	fast	medium	high
CcH_2	7 to 10	6.1 to 5.9	-207 to -195; 350 to 700	267 to 255; -349 to -699	/	fast	low	high
	5 to 6	4	-233 to -193; 300	293 to 253; -299				
MOFs	4.50 to 5.25	2 to 6	-196; 80	256; -79	7	fast	medium	low
LT MH ($LaNi_5, LaNi_{4.8}Al_{0.2}$)	1.36 to 1.43	1.4 to 1.6	25; 5	-5; -4	1.5E+04 to 1.7E+04	moderate	high	low
HT MH (Mg, Mg_2Ni)	3.8 to 4.8	2.2 to 3.0	25; 5	-290; -4	3.8E+04 to 6.4E+04	slow	high	low
$MBH (CoB - LiBH_4)$	8	9.3	25; 1	-290; 0	2.7E+04	slow	high	low
LOHC (H0 NEC-H12 NEC)	4.1	4.3	25; 1	-210; 0	2.7E+04	fast	high	very low
Chemical (NH ₂)	8	9	25: 10	-390: 0	3 1E+04	moderate	medium	very low

Table 2.2: Comparison of hydrogen storage technologies [42]

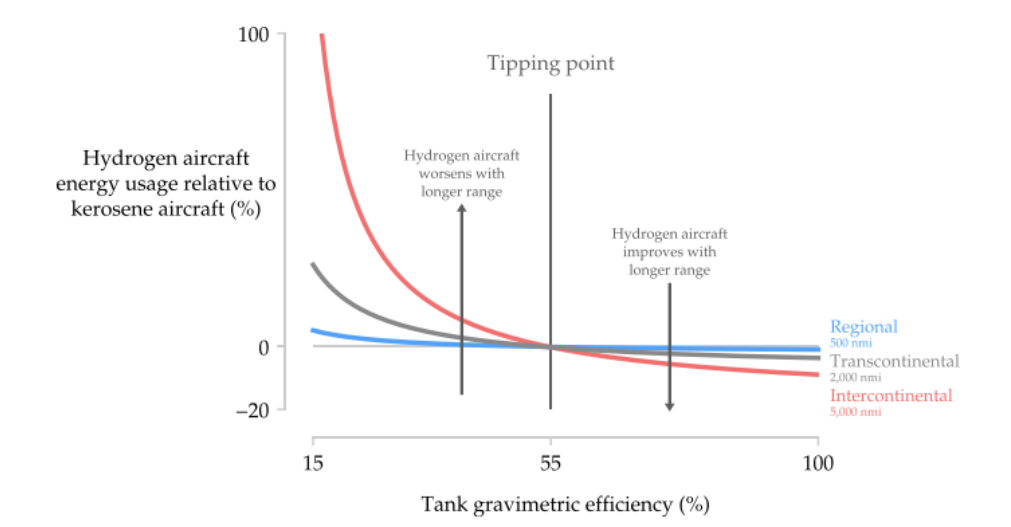


Figure 2.9: Dependency of aircraft energy usage with tank gravimetric efficiency for regional, transcontinental and intercontinental aircraft [10]

From this comparison, liquid hydrogen storage seems to be the best option because of its safety and comparable performance with cryo-compressed. Besides that, the values provided by Massaro et al. [42] are low estimations of what could be possible with liquid hydrogen. Some predict that LH₂ tanks can reach much higher gravimetric efficiencies from 30% to much more optimistic values of 90% [10]. While the upper limits are still not yet completely understood, it is still clear that liquid H_2 currently has a much higher potential than other storage options. At the moment, the lower gravimetric efficiencies of hydrogen storage are the most significant limiting factor when compared to kerosene aircraft, and that is why, at the moment, many researchers say that hydrogen aircraft will only be beneficial for short- to medium-range aircraft [10]. In Figure 2.9, the necessary tank gravimetric efficiency improvements are clear, as at around a gravimetric efficiency of 55%, a hydrogen aircraft would have a lower energy use than its kerosene counterpart.

Insulation of LH₂ tanks can also be accomplished with different manufacturing choices. The most developed is spray-on foam insulation, and the upcoming development is the use of vacuum-insulated tanks. Ultimately, a combination of both is possible [10]. The necessary thickness of the insulation is directly related to the boil-off effect, because the dormancy time requirement of the tanks, which is the time they need to ensure safety and operation under the allowable conditions while not in use, depends on the heat transfer through the walls. Therefore, a higher

dormancy time requires better insulation to prevent a boil-off rate that would exceed the maximum pressure, leading to the venting of some hydrogen [45]. The tank walls will also require the structural component that withstands the pressure loads. The thickness and weight of it depend on the maximum allowed pressure in the tank, the outside tank pressure, the material properties, and the radius of the shell [46].

The boil-off in a LH₂ tank has already been mentioned as an undesired effect that would increase pressure inside the tank to a value above its operating limit. The opposite can happen when, as LH₂ is drawn from the tank, the pressure inside the tank eventually reduces, because the increase in pressure due to boil-off can not compensate for this decrease [47]. As a result, the operating pressure of the tank will end up being below a critical value, which may be set due to the operating pressure of the fuel cell or of the pump providing hydrogen to the fuel cell. This effect would reduce the pressure at which hydrogen could be supplied to the fuel cell, reducing its efficiency. To supply the required heat to the tank, a battery could be used together with a heating component. Still, two main disadvantages exist: it consumes additional electric energy of the already very limited supply, and a defect at the heater or the cables running through the vacuum space both lead to extremely high repair costs [48]. A better option would be to use a heating coil that would discharge some of the heat provided to hydrogen back to the inside of the tank, as shown in Figure 2.10. This system would be cheaper and easier to repair [48].

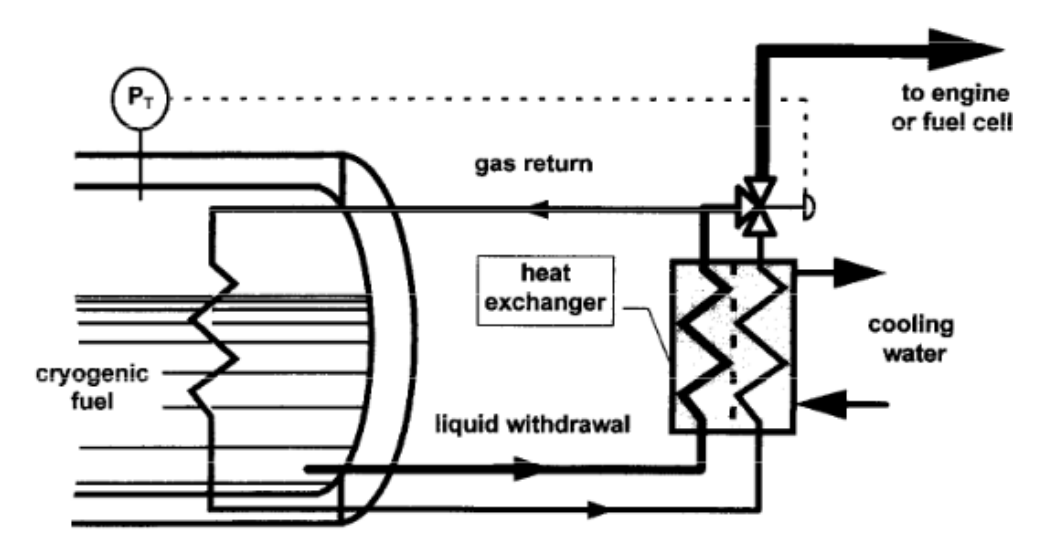


Figure 2.10: Scheme of pressurisation system by warm gas return [48]

Besides the limitations already specified, another problem with hydrogen tanks is their integration in the aircraft. Contrary to kerosene hydrogen tanks, when integrated into the wing frame, the result is a much lower gravimetric efficiency [13]. This is because liquid hydrogen tanks require the highest volume to external area ratio, since the lower the area, the lower the heat transfer, and therefore the tank can be made lighter [42]. As a result, different tank positions have been evaluated, each with different drawbacks. Wing pods increase aerodynamic drag but also provide the bending moment relief that kerosene in the wings would. Tanks integrated in the fuselage result in either an increase in fuselage length or a reduction in passenger or cargo capacity.

The wing pod configuration results in a higher fuel consumption and brings clearance issues at take-off into consideration [49]. An example of such a configuration is presented in Figure 2.11.

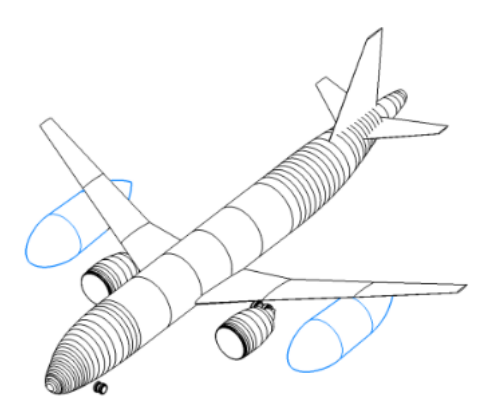


Figure 2.11: Geometry of pod integrated tank concept [49]

For the fuselage integrated tanks, the position may take different configurations. Some examples are presented in Figure 2.12. In the first configuration, the tank in the rear part of the fuselage results in stability and trim problems due to the change in the centre of mass during flight. The middle one, where there is both a tank in the front and the rear parts of the fuselage, would not have the same stability and trim issues. Still, for narrowbody aircraft, it would require a cutout in the tank in order for pilots to go through, which could turn out not to be viable due to its low fuselage diameter [10]. Out of these first two options, Onorato et al. [46] concluded that in terms of performance, the configuration with an aft and forward tank does have a better performance. Even though more tanks result in a lower tank gravimetric density, the benefits of higher trim performance outweigh it. The last possibility is to place the tanks above the fuselage with an extra fairing to smooth the aircraft's shape. While this approach results in several safety benefits, it also increases the fuel burn compared to an inside the fuselage tank, due to the added drag of the extra wet area [10, 49].



Figure 2.12: Proposed hydrogen tank configurations in the fuselage. Red areas are the tanks. [10]

Even if the configuration with one aft and forward tank is not used, there is a need for at least two tanks. This is a result of regulations. Both EASA and FAA require some redundancy, ensuring that a single failure, in this case a tank failure, will not result in total fuel supply failure. Ensuring that the supply of each engine is independent of the supply to any other engine [50, 51].

Another distinction can be made in the tank integration. This is the difference between integral and non-integral tanks. In the former, the tank walls form the fuselage itself, making the tank heavier since it would have to endure the fuselage loads, reducing gravimetric efficiency. However, the overall empty weight of the aircraft can be reduced. This effect makes comparing integral and non-integral tanks, which fit inside the fuselage, difficult [10]. Since many other aspects of fuselage design need to be taken into account when implementing integral tanks, only non-integral tanks will be considered.

2.2.2. Heat Management System

When under operation, a fuel cell produces heat from resistances, latent heat of water, or irreversibilities. This heat needs to be dissipated, since if this were not the case, the fuel cell would be heating and its performance would degrade, even leading to damage to the fuel cell. With LT-PEMFC, the heat is generated at relatively low temperatures with respect to ambient temperatures, which makes the required heat exchanger bigger and heavier.

For the choice of cooling system, several options are analysed and used for fuel cells. In Figure 2.13, the most common options for fuel cell cooling systems are presented.

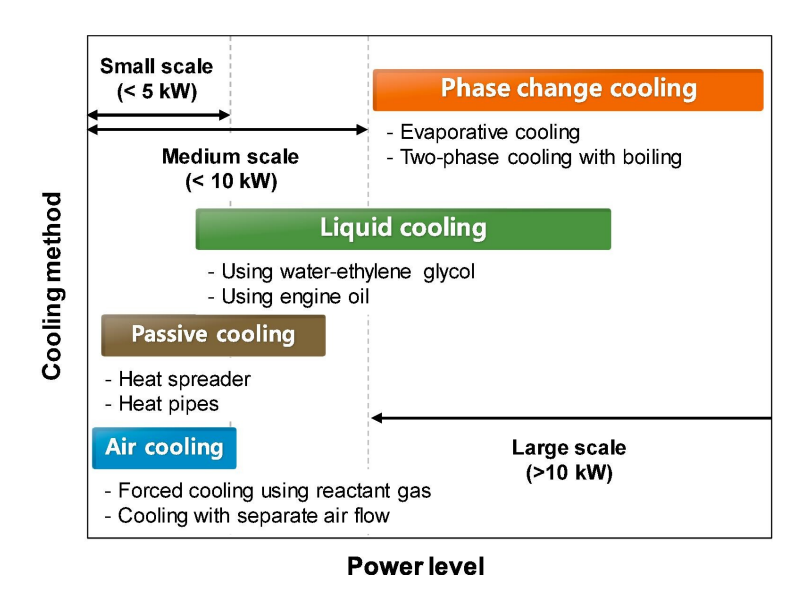


Figure 2.13: Cooling methods for PEMFC depending on power level [52]

Air cooling is usually used for systems with lower power levels, consisting of air passing through the cathode or cooling plates between the cells. For passive cooling, the heat is dissipated via conduction, natural convection, or radiation [53]. These systems have the lack of extra components that would increase system mass as their best feature. This type of cooling becomes unsustainable once the required heat dissipation becomes so high that the cooling air flow and heat transfer area required become too high [54]. At this point, liquid cooling or phase change cooling, where a separate radiator is used, is required.

In the liquid cooling systems, a coolant flows through cooling channels in the fuel cell, absorbing heat that is then pumped to a heat exchanger where the heat is dissipated into ambient airflow [54]. In these systems, to maintain a low temperature gradient inside the fuel cell, the difference between coolant inlet and outlet temperature at the fuel cell is kept at a low value of around 10K [55, 56]. In a liquid cooling system, a pump is also required to maintain the coolant circulating at the desired pressure. The coolant used in most applications of liquid cooling in fuel cells is a mixture of deionised water due to its high specific heat and therefore high heat absorption capacity, and an antifreeze liquid such as ethylene glycol, usually in a proportion of 50/50 [57, 58].

The last option for cooling the fuel cell is the phase cooling systems, which have emerged recently and propose an increase in heat dissipation. Phase change cooling uses the latent heat of the coolant to remove heat from the fuel cell. Two main options arise from this concept. Evaporative cooling, where liquid water is added to the cathode side, removes heat from it when evaporating and also humidifies the cell [54]. The other option would be to use a system similar to water cooling, where the coolant changes phase from liquid to vapour and vice versa throughout the system [59], two-phase cooling with boiling, making use of the latent heat of the coolant to absorb and remove the waste heat of the fuel cell. Therefore, in the evaporative and two-phase cooling with boiling, the temperature of the fuel cell must be higher than the boiling temperature of the coolant [60].

Even though these systems have been studied and have shown possible improvements in system mass and drag, certain problems keep them from being the common option. In evaporative cooling, there is the need to redesign heat exchangers because aluminium is not an option, as it contaminates the system, and high efficiencies of water separation are required to have the evaporative cooling be a better option than liquid cooling [54]. In the case of the two-phase cooling system, the worry comes from the fact that it operates really well under uniform temperatures, which is not the case for a LT-PEMFC. Besides that, if at any point in the heat exchangers the coolant reaches the complete vapour form, it reduces its heat transfer significantly, worsening the heat dissipation [61]. Lastly, further developments in both technologies are required before they can be implemented as better and suitable options [54].

Ram Air Duct

To reject the waste heat generated by the fuel cell with a liquid cooling system, a heat exchanger is required. In the implementation of heat exchangers for fuel cell cooling, several studies have incorporated the heat exchanger within a ram air duct [55, 40, 58], as shown in Figure 2.14. Through the ram air duct, the air initially suffers a compression in a diffuser, where the air reduces its velocity and increases its pressure. This is done so that the pressure drop over

the heat exchanger is minimised. Then the air passes through the heat exchanger, where its temperature increases. Lastly, the air is expanded through a nozzle to ambient pressure, increasing its velocity. Due to the differential in velocity to ambient air, some thrust is produced [62].

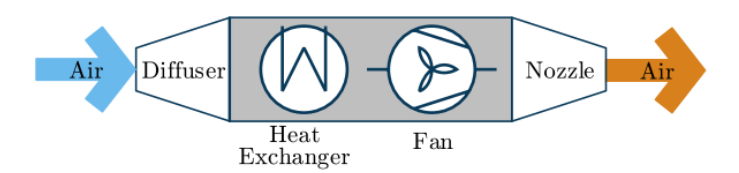


Figure 2.14: Heat exchanger ram air duct system [58]

The implementation of the ram air duct is done since the use of large heat exchangers can create a substantial increase in the aircraft's drag, degrading its performance [62, 40]. This is known as the Meredith effect and is used in piston engine aircraft [63]. The improvements from this effect can negate some of the cooling drag or even create some net thrust [62, 40]. While some studies neglect this effect either by stating that it would not have a significant effect on extra drag or by stating that the drag generated would be compensated by the extra thrust [40], in the work done in this thesis, the extra drag and thrust produced due to the heat exchanger will be taken into account.

The heat exchanger is a tube or plate and fin heat exchanger with counterflow. These heat exchangers are indicated for fuel cells in aircraft applications due to their compact design, efficient heat transfer, and modular capabilities that improve their adaptability to stringent space requirements [64]. On the coolant side, tubes are used since the coolants are usually liquids with high thermal conductivity and density. In contrast, on the air side, several geometries are used to increase the heat transfer area to compensate for the lower thermal conductivity and density of air. Figure 2.15 shows an analysis of the performance of several air side geometries, concluding that the one with the better conjugated performance is the offset strip-fin, and therefore that geometry is used in the present study.

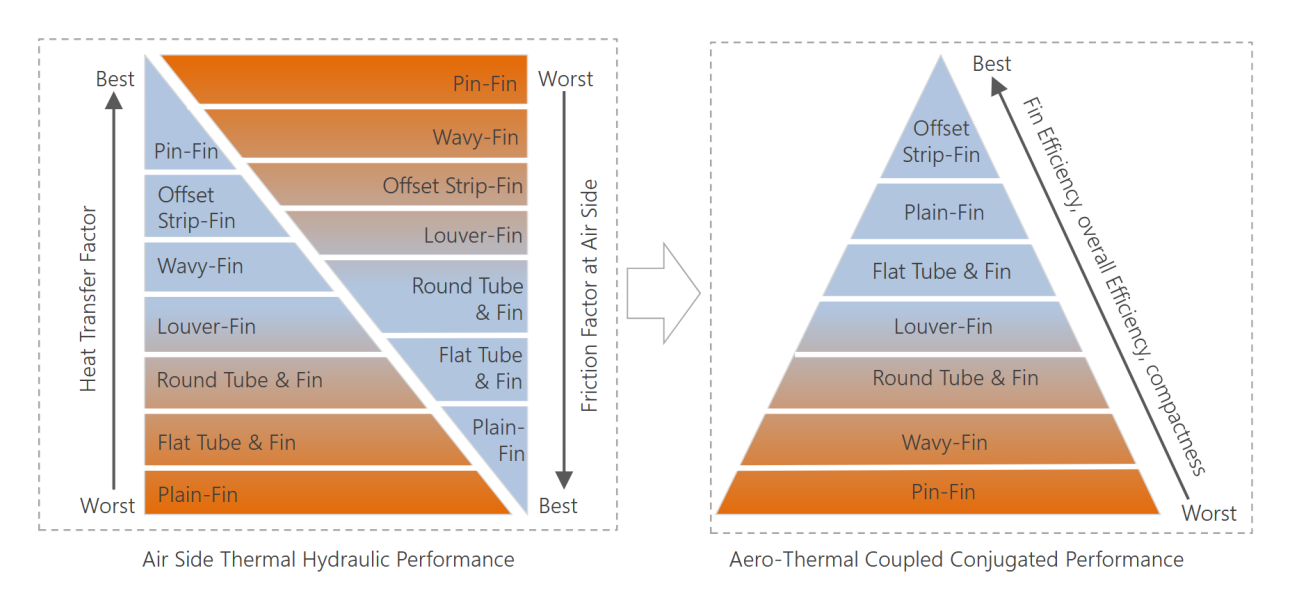
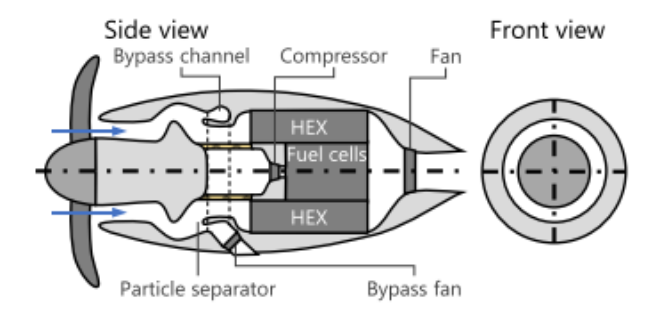


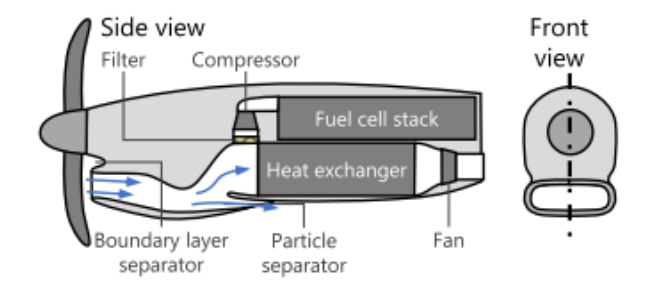
Figure 2.15: Heat exchanger air side performance [65]

A problem that originates from the heat exchanger size is the possible increase of the nacelle housing the fuel cell system's frontal area. With respect to this, studies have been conducted on the possibility of tilting the heat exchanger such that its frontal area is kept while reducing its effect on nacelle size and keeping the pressure drop over it low [62]. A limit of around 70° was found to be the point over which the pressure drop becomes too significant due to the inclination of the heat exchanger [66].

The air supply design is also a topic of interest since its design will affect what extra penalties will be introduced to the aircraft's performance. In a propeller driven aircraft with fuel cells, two main design concepts obtain the best performance. The scoop inlet and the annular inlet, Figure 2.16, with the scoop inlet having the best performance.



Annular inlet concept



Scoop inlet concept

Figure 2.16: Annular and scoop inlet concepts [67]

A variation of the scoop inlet is also possible, where a movable lip is used. This configuration provides better performance in total pressure ratio but increases system complexity, cost, and mass [67].

Lastly, there is also the option to add a fan to the ram air duct system to provide sufficient air flow at low speeds on ground operations.

2.2.3. Air Supply System

In the projected use of fuel cells in aircraft, the oxidant is to be provided by ingesting ambient air to the fuel cell cathode side.

The air required to operate the fuel cell can be provided by the same inlet that provides air for the thermal management system, as shown in Figure 2.16. The air needs to be at a certain temperature, pressure, and humidity to ensure the fuel cell operates under optimal conditions, which makes necessary the use of several components. These are the air filter, compressor, intercooler, and humidifier.

The air filter is responsible for filtering impurities in the air that cause damage to or contaminate the fuel cell. Fuel cells in general and even more specifically LT-PEMFC can significantly reduce their performance due to contamination [10]. The air filter is a passive system requiring no additional power to work. Its contribution to the increase in power consumption comes from its weight and the pressure drop of the air flowing through it, with both being relatively small.

The compressor becomes essential mainly at high altitudes since the ambient pressure will be much lower than the desired operating pressure. The compressor is a substantial component of the system regarding power demand. This is mostly due to the power required to pressurise air, since the weight of the compressor does not contribute significantly to an increase in system mass; that would require more thrust and therefore power from the fuel cell to compensate for. In most aircraft fuel cell applications, the choice of compressor tends to be the centrifugal compressor because they are compact, lightweight and efficient [38, 68]. These compressors also have their operating limits that need to be considered when choosing and using the models. These limits encompass the surge limit at low mass flows and high pressure ratios since stall may occur and create reverse flow, damaging the compressor. The choke limit, at high flow rates and low pressure ratios, depends on the geometry of the compressor, since when air reaches the speed of sound, it can not be further accelerated. The speed limit at high pressure ratios and flow rates due to structural

considerations [68]. A typical compressor map that relates pressure ratio with corrected mass flow is presented in Figure 2.17, where the limits are shown.

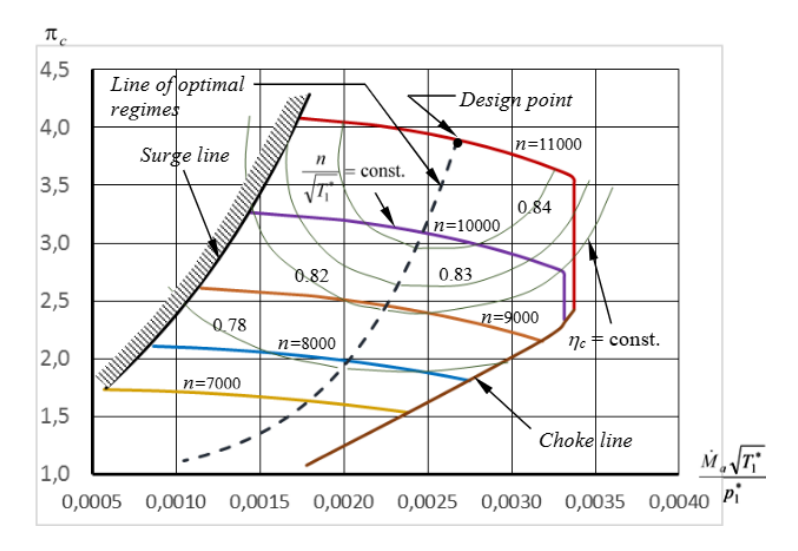


Figure 2.17: Compressor map [69]

After compression, the air reaches temperatures that are above the operating limits of both the fuel cell and humidifier. To prevent any damage and ensure the system is working correctly, the air must be cooled down to the desired fuel cell temperature. To do this, the same options as the ones provided for the main heat exchanger are valid. Since the required heat dissipation is lower, an air-to-air cooling may suffice, as the one used in Figure 2.8, but since a liquid cooling system is already in place, using it to also do this heat exchange would be advantageous to reduce system mass, since the heat capacity of the liquid coolant is much higher than that of air. Liquid cooled intercoolers are also already used in many fuel cell systems [68, 55].

Lastly, before entering the fuel cell, the air must be humidified to the desired level of humidity. To do this, two options are available; one uses a passive humidifier that uses exhaust air to humidify the air coming in [68, 31], as presented in Figure 2.8. While the other option is to separate water from the exhaust gas with a condenser and reintroduce it in the fuel cell air inlet [38]. With the latter being of interest if a turbine was to be used to recover some energy from the high pressure air of the fuel cell, since it would make the air suitable for a turbine by preventing frost formation on the turbine [31]. Since it would add complexity and weight to the systems, and it is not yet sure if such a system would improve efficiency, the simpler, passive humidifier will be used.

2.3. Oxygen Benefits and Drawbacks

The use of fuel cells in aircraft is hindered by their high mass, and consequently low power densities, which are lower than the power densities of conventional turboprop engines [70]. Therefore, efforts should be made to improve fuel cell systems. As already detailed, H_2 tank optimisation seems to be the approach with substantial room for improvement. Nonetheless, other options are also viable. One possibility might arise from using oxygen enriched air or even pure oxygen in the fuel cell. This section will highlight the benefits and drawbacks of this architecture.

2.3.1. Fuel Cell

The fuel cell performance by itself, not considering any other subsystems, improves with the increase of oxygen percentage in the air supplied to the cathode, since it will result in higher voltages and current densities. The reasons for this improvement were detailed in Section 2.1, where it was explained that higher oxygen percentages improve fuel cell performance by increasing the reversible voltage and reducing all irreversible losses.

Such improvements increase the efficiency of the fuel cell by a significant margin, with St-Pierre [17] concluding that an increase of 10% from 53% to 63% is possible, when pure oxygen is used, with a fuel cell mass reduction of about 20%. These values are just an estimation as the increase depends on the operating current density, as can be seen in Figure 2.18, where for different current densities the deviations between different oxygen percentages performance changes. The increase in efficiency would result in a significantly lower mass and size of the fuel cell.

Besides that, the amount of H_2 needed would reduce, resulting in a lower tank mass as well. In Figure 2.18, the voltage, efficiency, and power increase with air oxygen percentages are presented.

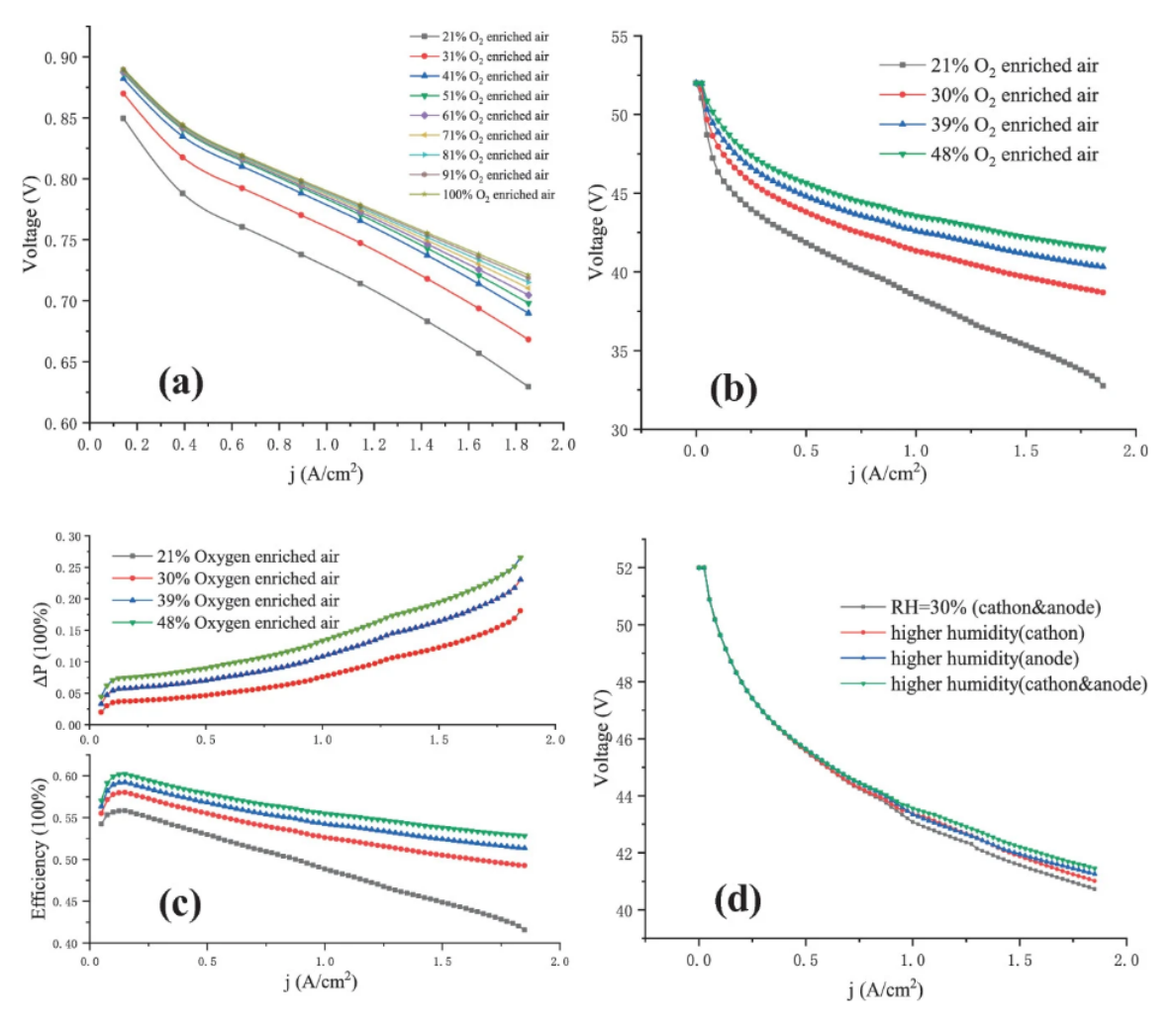


Figure 2.18: Oxygen percentage effect on fuel cell performance [18]

Besides the increased efficiency for the same current density, oxygen enrichment also allows the fuel cell to operate at much higher current densities for the same voltage. In such cases, the mass of the fuel cell can be reduced much more, by up to 50% [16]. In this case, the mass reduction is much more substantial, but no increase in efficiency is obtained.

One last important effect of the increase in oxygen concentration is the dynamic response of the fuel cell. Even though it will not be analysed in depth in this thesis, it is important to evaluate the effects of changing oxygen concentration on the dynamic response of the fuel cell. This is to ensure that no worsening of the dynamic response exists. Yan et al. [36] found that the dynamic response of a fuel cell under different conditions seems to follow the same behaviour as the steady-state response. Therefore, it is confirmed that higher oxygen concentration would improve the dynamic response of the fuel cell. This effect was not evaluated directly by increasing oxygen content; instead, it was done by increasing the operating pressure, which would have the same effect as increasing oxygen concentration. The results of such a study are shown in Figure 2.19, where it can be seen that a higher air excess ratio, or air stoichiometric ratio, provides a faster response.

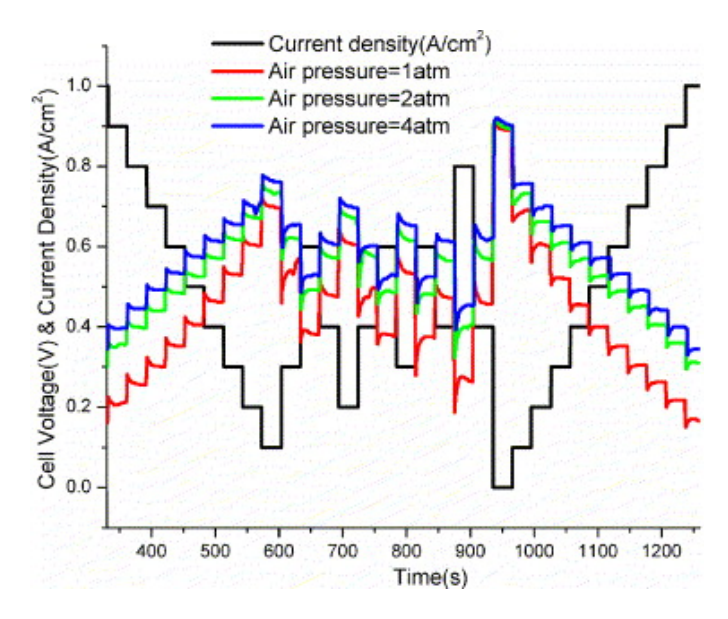


Figure 2.19: Effect of operating pressure on dynamic response of fuel cell [36]

2.3.2. Balance Of Plant Effect

In an aircraft, the rest of the components that ensure the correct functioning of the fuel cell have a significant effect on the overall system power consumption and mass. Therefore, these should also be analysed to ensure the feasibility of oxygen enriched operations. Throughout this section, the distinction between a pure oxygen operated fuel cell and an enriched air, namely a flow with a higher concentration of oxygen, operated fuel cell will be made. This is because different requirements apply to each of the cases.

Oxygen Storage and Distribution

Firstly, the new components that would be added to the BoP will be introduced. With the need for a higher concentration of oxygen, a system that would provide it is needed. For that, several options are possible.

Air separation membranes are already used in aircraft for tank inerting systems that reduce oxygen concentration in the kerosene tanks to reduce the flammability risk [71, 72]. These systems could increase oxygen concentration in the air supplied to the fuel cell by using the oxygen enriched air that they generate. The problem with these systems is that the required mass flow for a fuel cell is higher than the one provided by the systems in current use. This is because O_2 and N_2 are molecules of similar size and weight, which makes these systems have a worse performance. Besides that, to obtain the desired separation, operating conditions of several bars above ambient pressure are required [73]. As a result, to provide enough mass flow, big, heavy, and power demanding systems would be necessary.

Other options are the ones used in oxygen production plants. These are, among others, cryogenic air separation, swing adsorption-based systems, and mixed ionic–electronic conducting ceramic-based membranes [74]. These options are also unsuitable for an aircraft, as they are once again big, heavy, and power demanding, based on extreme operating temperatures and pressures.

The last possible option would be to have oxygen tanks supplying either the extra oxygen to enrich the air or the totality of pure oxygen. For such tanks, the same options available for the hydrogen tanks exist, with the liquid O_2 being once again the best due to its higher gravimetric density. Besides that, the volume of oxygen, and therefore tank volume, required would only be half of that for hydrogen since only one molecule of oxygen is required for each two of hydrogen. This is important because configurations that would not be viable for hydrogen tank placement can be feasible for oxygen tank placement. Oxygen tanks would also be possibly lighter since the liquid temperature of oxygen is higher than that of hydrogen, 90K and 20K, respectively. Besides that, the enthalpy of vaporisation of oxygen is higher than that of hydrogen, $\Delta H_{vap,H_2} = 0.90kJ/mol$ and $\Delta H_{vap,O_2} = 6.82kJ/mol$ [75]. This also lowers the boil-off, as more energy is needed to vaporise oxygen. Some estimations of the volumetric and gravimetric density of liquid O_2 tanks result in a tank that is smaller in volume and lighter [76] for the same stoichiometric required quantities of H_2 and O_2 . Besides that, the fact that the oxygen molecule is bigger also has benefits. Since, in comparison with hydrogen, permeation would not be a problem, no fuel would be lost through that process. Unfortunately, the same worries apply concerning embrittlement, since oxygen, mainly at the low temperatures of

LO₂, may also reduce the stress resistance of materials [77]. Therefore, the same meticulous material choice must be made for oxygen tanks.

Some more negative aspects of oxygen usage also exist because the mass of oxygen required is 8 times higher than the amount of hydrogen mass required, since per one molecule of oxygen, two molecules of hydrogen are needed, and the molar mass of oxygen is about 16 times higher than the molar mass of hydrogen, 16/2 = 8. This is the main detriment of a system that would use pure oxygen.

One important aspect of liquid oxygen tanks is that certified tanks are already available for aircraft use, as they were developed to supply oxygen for crew and passengers [78].

Air Supply System

Next, the air supply system changes will be explained. In a pure oxygen operation with the oxygen being supplied by the tank, there would be no need for the air supply system of the fuel cell. This means no air filter, compressor, intercooler, or humidifier, since a loop configuration would also be used on the oxygen side, as on the hydrogen side, providing the required humidification to the cathode. The air filter and the humidifier result in a slight reduction in mass, which would not be significant, but the removal of the compressor results in a different outcome. As stated previously, the compressor power can reach around 25% of the fuel cell power at cruise altitudes. A significant reduction in fuel cell mass would be possible if it were not needed, since the extra power would not need to be supplied. Even if oxygen enriched air is used, where the ambient air would be supplied with pure oxygen to increase oxygen concentration, the compressor requirement would be lower. Due to the addition of pure oxygen at the desired pressure, the necessary compression of the air for it to have the desired operating pressure at the fuel cell would also be lower since the tank would store oxygen at pressures higher than ambient at high altitudes.

Heat Management System

Lastly, the thermal management system will be revised. The same ram air duct configuration would still be necessary to release the waste heat generated by the fuel cell. However, some major improvements would also be possible, mainly in the size of the heat exchanger.

As specified before, the fuel cell under higher oxygen concentrations is more efficient and will generate less waste heat. Besides that, there is the possibility of operating the fuel cell at a higher temperature. Both of these factors would contribute to a smaller heat exchanger. Partially due to less heat waste demand and partially due to the higher temperature difference to the ambient air if the fuel cell operating temperature is higher. This is an important aspect because the thermal management system is one of the biggest, if not the biggest, contributor to the overall fuel cell system mass [56].

2.3.3. Lifetime and Cost

Now that all the BoP components have been described, other considerations should also be provided.

The lifetime of a system is very relevant for its use, as it has several economic implications. This is relevant for the oxygen enrichment analyses because the higher oxygen concentration seems to have a negative effect on a fuel cell's lifetime. For example, platinum, which is used as a catalyst, is not stable at high potentials and can electrochemically or chemically oxidise, something that an increase in oxygen concentration accelerates [17]. Besides that, the carbon used to support the catalyst may also suffer increased oxidation from the rise in oxygen. It will also increase the concentration of radicals that can degrade the membrane and diffuse through it, increasing mass transfer losses.

Knowing if the higher concentration of oxygen will result in an overall reduction of the lifetime of a fuel cell is difficult because it also represents an improvement in some of the problems associated with using air. It is the contamination due to the nitrogen content in the air. Nitrogen can diffuse through the membrane and contaminate the system. This effect is a known problem in fuel cells with a loop in the hydrogen side because it creates the need to purge the loop to remove the nitrogen contaminant [31, 68, 10]. Due to this purge, there is a loss of hydrogen, which during a flight mission may account for up to 3% of the total hydrogen consumption.

With all these different effects playing a role, it is hard to know if oxygen enrichment will improve or deteriorate the longevity of a fuel cell. As it is not seen as fundamental for this thesis to analyse such factors, these considerations of cost and lifetime will not be taken into account in the work performed.

2.3.4. Risks

The implementation of the whole system surrounding the fuel cell has some inherent risks already described, mainly due to the tanks used. One aspect that has yet to be mentioned is the risk of hydrogen combustion. This risk comes

2.4. Research Question 28

from the flammability limits of hydrogen, which are much broader than the ones for kerosene, as presented in Table 2.3. When changing from kerosene to hydrogen, the limits go from 0.7%-5% to 4%-75%. Also, when exposed to air with enriched oxygen content, the flammability limits of hydrogen become even bigger, with the upper flammability limit reaching 94%. This is important because the flammability limits represent the range of mixture fractions that will burn when provided with an ignition source. Therefore, with an increase in this range, when oxygen concentration is increased, the risk of burning occurring is higher. Besides that, the ignition energy necessary for hydrogen is really low [79]. Together, both of these characteristics make the flammability risk of hydrogen high. Another characteristic of fuels is the autoignition temperature, the temperature at which fuels can autoignite without any external ignition source. This is a positive point for hydrogen because its autoignition temperature is about $560^{\circ}C$ [80], which is high, even more when comparing to kerosene, which has an autoignition temperature of $210^{\circ}C$ [81].

If oxygen enrichment is used, the increased flammability risk is something to consider, mainly the placement of tanks. Most likely, placing H_2 and O_2 tanks far from each other is the best option to prevent the risks that leaks may bring.

Fuel-Oxidizer	Lower Flammability Limit	Upper Flammability Limit
Kerosene-Air	0.7%	5%
H_2 -Air	4%	75%
$H_2 - O_2$	4%	94%

Table 2.3: Flammability limits as percentage by volume of air, adapted from [82, 79]

2.4. Research Question

From the literature review presented, it is clear that a gap is present in oxygen-enriched fuel cell systems. Much research has been conducted to understand the influence of operating conditions and their optimisation on the fuel cell level [31, 32, 37, 34, 30]. And, to implement such knowledge in an aircraft, studies have been performed concerning fuel cell propulsion in aircraft [21, 83] and to the influence of aircraft operating conditions on fuel cell performance and sizing [68, 56, 42]. The result of such studies is that, for now, it is still not possible to obtain a performance that could compete with current kerosene-powered propulsion systems. However, improvements in fuel cell performance have been proven with the use of oxygen enrichment [84, 17]. Schumann et al. [15] concluded that oxygen enriched fuel cell systems could be more efficient than those supplied with ambient air when used as the aircraft power provider. Even though that is the case, no information on the effects of implementing such a system on the aircraft and its performance was provided. In conclusion, no study on the combination of an oxygen enriched fuel cell and its integration in an aircraft has been done, while also considering the variations of mass of the system.

Therefore, with the literature study presented, the following research question is proposed to be answered:

Research Question

What are the effects of a propulsion system based on oxygen enriched fuel cells on the design and performance of the overall aircraft and subsystems, including their masses and power requirements?

To answer this question, several possibilities will be taken into account. As explained before, the weight of oxygen required to do a full mission with pure oxygen operation is very high. So, it might be so much of a penalty that the improvements in other components cannot compensate for it. For that reason, different possibilities will be studied. The use of oxygen enrichment only in high power segments of flight, such as take-off and climb, will also be one of them. This is seen as a possibility due to the sizing of the systems. The aircraft systems need to be sized for the most demanding segments of flight, and if in more power demanding segments, efficiency can be improved, the sizing segment of flight might become the one with lower demand, cruise. This would reduce size and weight, reducing the penalty of using an oversized system for the longest flight segment.

Another question that must be answered revolves around placing the extra tanks needed for oxygen storage. Both safety, operation, and performance should be considered in its placement.

Lastly, with the work done, it will be possible to quantify the improvements in each subsystem of the BoP for each oxygen enrichment case, from reductions in mass to power demand.

2.4. Research Question 29

It will be of interest to analyse the effects of the drag and thrust generated by the cooling system, and if it results in an overall positive or negative contribution.

Research Sub-Questions

- What is the most efficient oxygen enrichment scenario, pure oxygen operation or partial oxygen enrichment?
- \bullet What is the best position of the H_2 and O_2 tanks taking into account the safety concerns and performance of the aircraft?
- What are the effects of oxygen enrichment on the mass and power requirements of each subsystem?
- What are the effects of flight altitude on an aircraft with oxygen enrichment?

Methodology

This chapter provides the methodology used to create the aircraft designs studied in this report. In Section 3.1, the workflow used to implement all the tools required for the aircraft sizing is presented. In Section 3.2, the models used to size the fuel cell propulsion system and how they are implemented are described, as the main addition of this thesis to the workflow. The validation of such methods is provided following their description to ensure the fidelity of such implementation. Lastly, the designed aircraft will be described in Section 3.5, where the Top Level Aircraft Requirements (TLARS) and the design parameters will be provided.

3.1. Aircraft Sizing Workflow

The workflow base was provided by DLR and was initially created for the clean aviation TheMa4HERA project [85]. This workflow was then altered to fit the needs of the current study, with the implementation of a tool that sizes a fuel cell propulsion system and creates an engine map for the use of other tools. In addition to the tool developed for this thesis, other tools in the workflow were developed at DLR and provided for use in this study. Two different levels of fidelity are used. Level 0 (L0) methods, which are based on statistical or empirical design rules, allow for the exploration of the design space at a low computational cost. And Level 1 (L1) tools that focus on specific disciplines and are based on simplified physics models [86].

The tools provided by DLR are the following:

- Overall Aircraft Design: openAD is a tool that completes the conceptual aircraft design based on handbook methods, being a L0 tool [87].
- Aircraft Mission Calculation: AMC calculates the mission fuel consumption by solving the equations of motion at each time step with the help of the aerodynamic polars and the engine maps. It performs both the calculations for the design and the reserve mission. The results of this tool are used to estimate the power required for the climb by comparing the climb time obtained with the desired target [88, 89].
- Low Speed Performance: LSperfo performs a time-step calculation of the take-off by solving the equations of motion; the result of this analysis, the take-off field length, is used to adjust the take-off power in order to meet the take-off field length requirement [90].
- Liquid Hydrogen Tank: With the fuel mass calculated by AMC, the LH₂ tanks are sized using geometric definitions and values provided by DLR.

The workflow starts with an input file that contains the required inputs for openAD and all other tools. After all tools are run, the results of each tool are synthesised to create a new openAD input from the updated values of the higher fidelity methods, such as the mission fuel mass, the take-off field length, and the volume and mass of the tanks. With that, the power requirements, fuselage geometry, and component masses, among others, are adjusted.

Once convergence is reached, the final output with the result of every tool's last run is obtained for further analysis and data processing. The visual representation of this workflow is presented in Figure 3.1.

The contribution of this thesis to the workflow comes in the form of creating a tool that sizes and simulates the performance of a fuel cell propulsion system and is capable of performing such a procedure for varying oxygen percentages in the oxidant mass flow. Besides that, the placement and sizing of additional oxygen tanks were also added to the workflow. The description of how both of these sizing procedures are performed will be detailed in the

following section. Finally, the last addition performed in this thesis to the workflow is the synthesis of all of the tools' data to update the inputs for a new iteration.

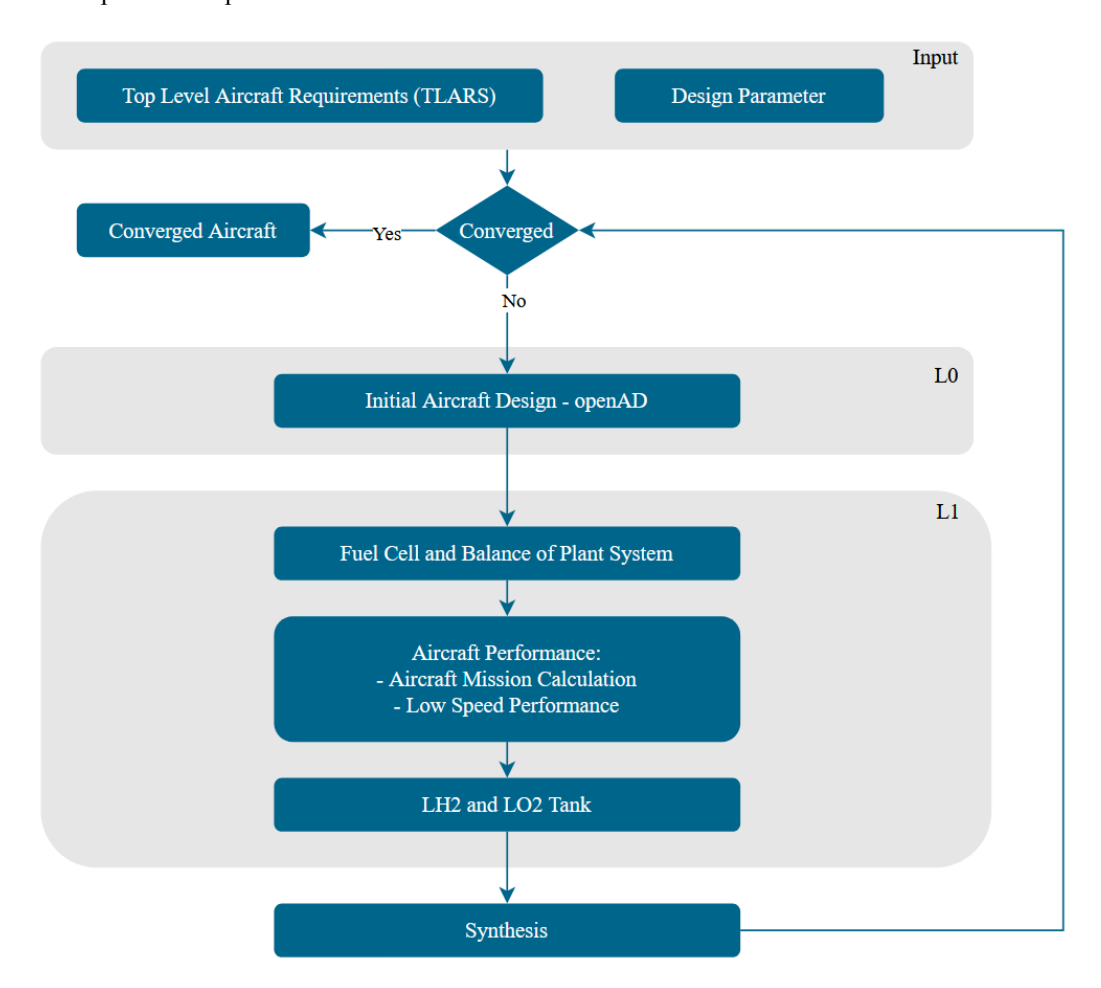


Figure 3.1: Aircraft design workflow

3.2. Modelling

3.2.1. Fuel Cell

The fuel cell modelling is a crucial part of the study as it is required to capture the influence of temperature, pressure and oxygen concentration on the fuel cell performance.

The Nernst equation gives the ideal open circuit voltage of the fuel cell, Equation 2.1 [22], with the subtraction of an additional factor, E_{cr} , which accounts for the open circuit voltage loss due to hydrogen cross-over from anode to cathode without reacting [91], resulting in the following equation

$$E = E_{ref} + \frac{\Delta S}{2F} (T_{FC} - T_{FC,ref}) + \frac{RT_{FC}}{2F} \ln \left(p_{H_2}(p_{O_2}^{1/2}) \right) - E_{cr}$$
 (3.1)

There are several irreversible losses in a fuel cell as explained in Section 2.1.1. While accounting for these losses, the same variation in temperature, pressure, and oxygen content should be present in the model.

For the activation losses Equation 3.2 is used, which is based on [22].

$$\eta_{act} = \frac{RT_{FC}}{4\alpha F} \ln\left(\frac{i}{i_0}\right) \tag{3.2}$$

where α is the cathode transfer coefficient and i_0 is the exchange current density, which is calculated from a reference value $i_{0,ref}$ with Equation 3.3 [39].

$$i_0 = i_{0,ref} \left(\frac{p_{O_2}}{p_{O_2,ref}}\right)^{\gamma_p} e^{\frac{-E_c}{RT_{FC}}(1 - \frac{T_{FC}}{T_{FC,ref}})}$$
 (3.3)

where the subscript ref represents reference conditions and E_c is the activation energy of the cathode reaction.

The ohmic losses are accounted for with an equation that obeys Ohm's law, Equation 3.4. Although there are ionic and electronic resistances, only ionic charge transport resistances are considered as they dominate [22].

$$\eta_{ohm} = iASR \tag{3.4}$$

$$ASR = \left(\frac{\delta_{mem}}{\sigma_{mem}} + \frac{\delta_{CCL}}{f_{CCL}^{0.15}\sigma_{CCL}}\right)$$
(3.5)

where ASR, the average specific resistance is obtained from Equation 3.5 [92], δ is the thickness of the layer, k is the conductivity, and f is the ionomer fraction. The subscripts mem and CCL represent the membrane and the cathode catalyst layer, respectively.

To obtain the conductivities of the membrane and CCL, the same equation applies, Equation 3.6.

$$\sigma = (0.005139\lambda - 0.00326)e^{\left(1268\left(\frac{1}{303} - \frac{1}{T_{FC}}\right)\right)}$$
(3.6)

where λ is the water content in the component, which will be assumed to be 14 since the fuel cell is considered to operate under the assumption that the membrane is in vapour-equilibrated conditions [93]. Therefore, there is no liquid water in the membrane; this assumption will have further effects in the modelling of the system.

Lastly the concentration losses are modelled with Equation 3.7 [22].

$$\eta_{conc} = \left(1 + \frac{1}{\alpha}\right) \frac{RT_{FC}}{4F} \ln\left(\frac{i_{lim}}{i_{lim} - 1}\right)$$
(3.7)

where α is the cathode transfer coefficient and i_{lim} is the limiting current, which is calculated from a reference value and conditions, Equation 3.8. It is taken as proportional to the diffusivity and oxygen concentration in the cathode, following the same approach as in [22]. Here, the water content in the membrane could also affect the diffusivity of the reactants, but since it is assumed that such a value does not change during the fuel cell operation, such an effect is not introduced.

$$i_{lim} = i_{lim,ref} \frac{C_{O_2}}{C_{O_2,ref}} \frac{D_{O_2}}{D_{O_2,ref}}$$
(3.8)

Where C is the concentration in the fuel cell channel and D is the diffusivity of the reactant.

The concentration and diffusivity are obtained from Equation 3.9 and the Chapman–Enskog formula [94], Equation 3.10.

$$C_{O_2} = \frac{p_{FC} X_{O_2}}{R T_{FC}} \tag{3.9}$$

$$D_{O_2} = D_{O_2,ref} \left(\frac{T_{FC}}{T_{FC,ref}}\right)^{(3/2)} \frac{p_{FC,ref}}{p_{FC}}$$
(3.10)

With all the losses accounted for, the cell voltage is calculated.

$$E_{cell} = E - \eta_{act} - \eta_{ohm} - \eta_{conc} - E_{cr}$$
(3.11)

Once the voltage of the fuel cell is determined, the amount of power produced by a stack of fuel cells is calculated with Equation 3.12.

$$P_{FC} = iA_{cell}E_{cell}N_{cell} (3.12)$$

where A_{cell} is the active cell area and N_{cell} is the number of cells in a stack.

The voltage efficiency of the fuel cell is defined as

$$\eta_V = \frac{P_{FC}}{\dot{m}_{H_2} H H V_{H_2}} \tag{3.13}$$

where HHV_{H_2} is the higher heating value of hydrogen and \dot{m}_{H_2} is the mass flow of hydrogen supplied. The mass flow of hydrogen is computed with the following equation

$$\dot{m}_{H_2} = \frac{N_{cell} i A_{cell}}{2F} M_{H2} \tag{3.14}$$

where M_{H_2} is the molar mass of hydrogen. The mass flow of oxygen can be computed similarly with

$$\dot{m}_{O_2} = \frac{N_{cell} i A_{cell}}{4F} M_{O_2} \lambda_{O_2} \tag{3.15}$$

where λ_{O_2} is the oxygen stoichiometric ratio, the amount of oxygen to be supplied with respect to the stoichiometric one. A value of 1.7 minimises compressor power consumption while keeping an optimal fuel cell performance [31]. As explained in Section 2.1.2, the necessity of using a higher amount of oxygen than necessary comes from the use of ambient air in the cathode; therefore, a correction is applied to this factor such that it linearly reduces to 1.05 when pure oxygen is being used,

$$\lambda_{O_2} = 1.05 + \frac{1 - X_{O_2}}{1 - 0.21} (1.7 - 1.05). \tag{3.16}$$

A reduction of the stoichiometric ratio to 1 would not be feasible because there is always a need for some air flow to remove the produced water.

Since the fuel cell does not always operate with pure oxygen, the nitrogen mass flow rate also needs to be computed. This is done using the percentage of oxygen in the air, X_{O_2} , and the molar mass of nitrogen, M_{N_2} ,

$$\dot{m}_{N_2} = \dot{m}_{O_2} \frac{1 - X_{O_2}}{X_{O_2}} \frac{M_{N_2}}{M_{O_2}} \tag{3.17}$$

One last point to consider is that if the desired oxygen percentage is above the one in atmospheric composition, there needs to be a distinction between the flow of oxygen from the tank and that from ambient air. For that, the following equations are used,

$$\dot{m}_{O_{2,air}} = \dot{m}_{O_2} \frac{0.21(1 - X_{O_2})}{(1 - 0.21)X_{O_2}} \tag{3.18}$$

$$\dot{m}_{O_{2,tank}} = \dot{m}_{O_2} - \dot{m}_{O_{2,air}} \tag{3.19}$$

Finally, the mass flow of ambient air is the following

$$m_{air} = \dot{m}_{O_{2,air}} + \dot{m}_{N_2}. (3.20)$$

With the power of a stack and its efficiency, the waste heat to be dissipated is calculated.

$$Q = P_{FC}(\frac{1}{\eta_V} - 1) \tag{3.21}$$

Since the systems are to be analysed in an aircraft integration context, their weight and volume should be considered. In the case of the fuel cells, not only their characteristics should be accounted for, but also the weight and volume of the endplates that comprise a fuel cell stack. For this, the analysis performed by Schröder et al. [95] is

used, where the mass and volume of the stacks are calculated as follows,

$$m_{stack} = m_{cell} N_{cell} + m_{stack,ep} N_{stack} (3.22)$$

$$V_{stack} = V_{cell} N_{cell} + V_{stack,ep} N_{stack}$$
(3.23)

where the mass of the cell is $m_{cell} = 0.072kg$, the mass of the endplates of a stack are $m_{stack,ep} = 9.139kg$ and their respective volumes are $V_{cell} = 0.068L$ and $V_{stack,ep} = 7.143L$. The required number of cells for a certain power is computed by rearranging Equation 3.12,

$$N_{cell} = \frac{P_{FC}}{iA_{cell}E_{cell}}. (3.24)$$

The number of stacks necessary for the fuel cells required is calculated by assuming a maximum value of 455 cells per stack [95], rounding the number up to the nearest integer,

$$N_{stack} = ceil\left(\frac{N_{cell}}{455}\right). {(3.25)}$$

Parametrization and Validation

As shown in the model described for the fuel cell, its performance depends on many parameters, some known or defined and others fitted to some reference data. To fit these parameters, data from the thermodynamics institute at DLR was provided for a Hydrogenics HD4 stack. For this fitting, the least squares method was implemented by a Python package that would compute the minimum of the least squares function [96]. The bounds for the fitted variables and their respective references are given in Table 3.1.

Variable	Unit	Lower Bound	Upper Bound	Ref. for Bounds
$i_{0,ref}$	A/cm^2	$1 \cdot 10^{-8}$	$1 \cdot 10^{-1}$	[94], [97], [98]
$i_{lim,ref}$	A/cm^2	1	100	[31]
α	-	0.1	0.5	[97], [22]
δ_{ccl}	cm	0.0005	0.0015	[56], [94]
γ	_	0.5	1.5	[99], [100]

Table 3.1: Bounds of variables that are fitted

The final values used for the fitted parameters are presented in Table 3.2, together with the values used for the variables that are not fitted. The fuel cell active area, A_{FC} , defines the power density of the fuel cell, the ratio of power provided to mass, since a higher fuel cell active area results in higher power density of the fuel cell stack. Equation 3.12 shows that fewer cells are required to provide the same power if the fuel cell area increases. The chosen value of $250cm^2$ results in a maximum power density of about 2kW/kg, a representative value of state-of-the-art fuel cells. The data and the model are compared in Figure 3.2. It is important to notice that not all data points were used to calibrate the model, as certain conditions, such as drying of the fuel cell, are encountered in the data, and the described model cannot predict such behaviour. This is evident at higher temperatures in the data provided, since in those values, no further improvement of the fuel cell voltage is present, resulting in a levelling off of the curve, which is the result of membrane drying.

Table 3.2: Fuel cell model parameter values

Variable	Value	Unit
A_{cell}	250 [31]	cm^2
E_0	1.23	V
E_{cr}	0.2 [91]	V
E_c	66000	$Jmol^{-1}$
F	96485	$kgmol^{-1}$
f_{CCL}	0.15 [101]	_
HVV_{H_2}	$1.418 \cdot 10^{8}$	Jkg^{-1}
R	8.314	$Jmol^{-1}k^{-1}$
ΔS	-163	$Jmol^{-1}k^{-1}$
$i_{0,ref}$	$5.4805 \cdot 10^{-05}$	A/cm^2
$i_{lim,ref}$	1.3162	A/cm^2
α	0.1915	_
δ_{ccl}	$5.5\cdot10^{-4}$	cm
γ	1.448	_
$p_{FC,ref}$	101325	Pa
$T_{FC,ref}$	298.15	K
$X_{O_2,ref}$	0.21	_
$C_{O_2,ref}$	$\frac{p_{FC,0}X_{O_2}}{RT_{FC,0}}$	$mol\cdot m^{-3}$
$D_{O_2,ref}$	$2.06 \cdot 10^{-5}$	m^2s^{-1}

Figure 3.2 shows that the model used in the present study can depict the performance of a fuel cell under several different conditions. For high temperatures, the model would not provide the same results as the experimental data used, since in the described model, the effects of phenomena such as the drying or flooding of the fuel cell are not predicted.

Since the proposed model would not predict such phenomena, the temperature at which the fuel cell is operated is kept constant, as any optimisation with such a variable would likely result in an unrealistic result. As a result, a constant operating temperature of $80^{\circ}C$ is used based on several studies [68, 21, 42].

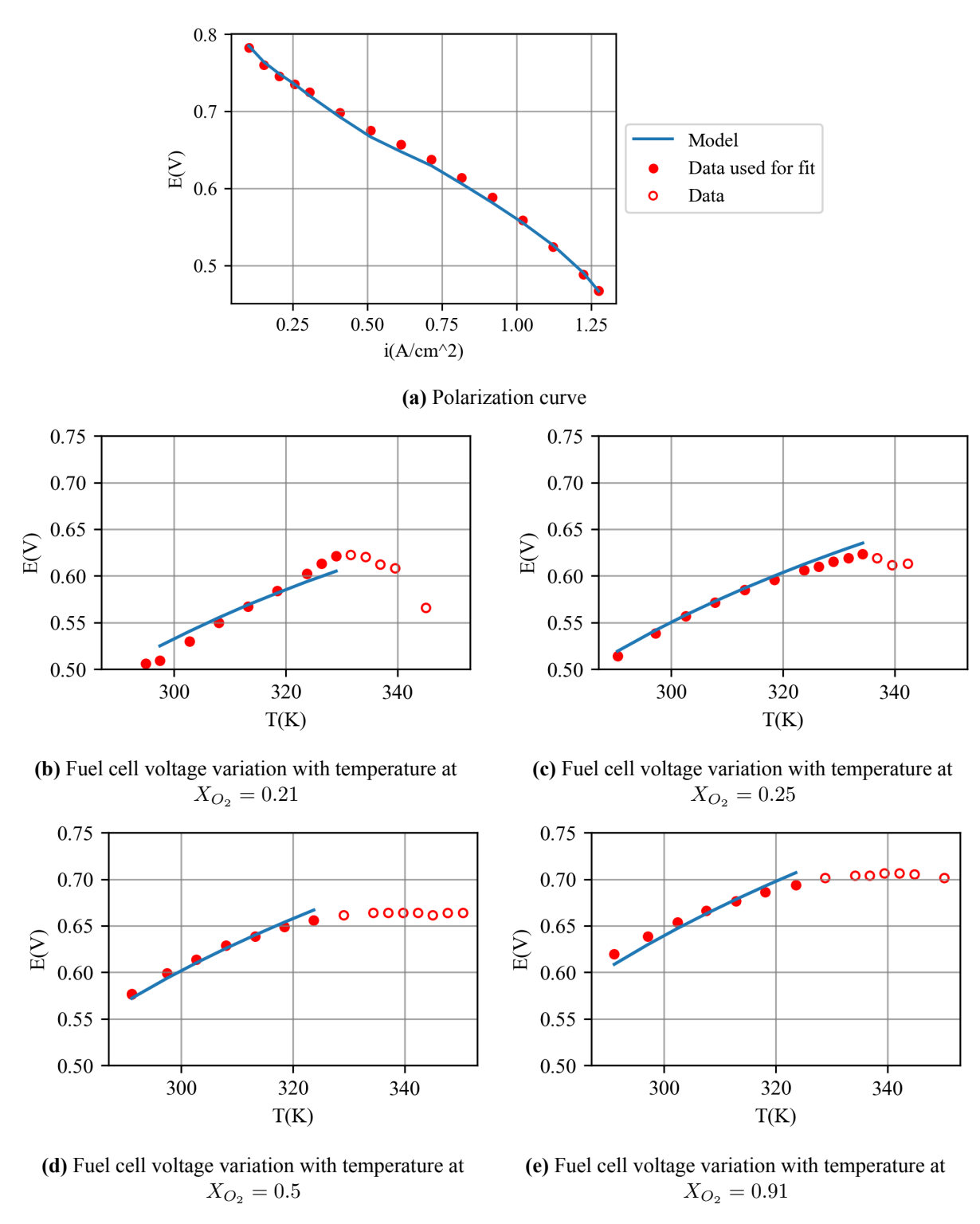


Figure 3.2: Model comparison with data from Schröder et al. [31]

3.2.2. Heat Exchanger

$\epsilon-NTU$ Method

For the heat exchanger model the $\epsilon-NTU$ method in [102] is implemented since it is the most widely used method in heat exchanger design, which is based on the effectiveness of heat transfer, ϵ , and the number of transfer units, NTU.

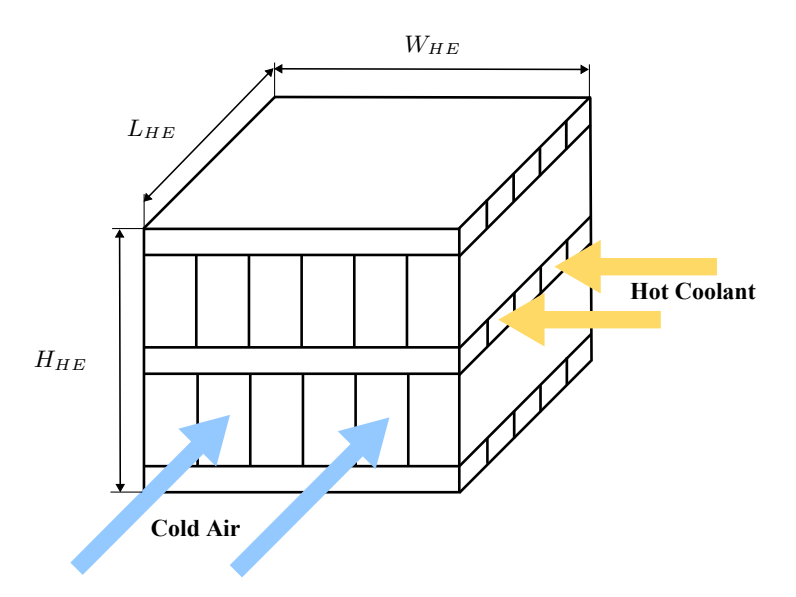


Figure 3.3: Heat exchanger topology

The effectiveness is the ratio of heat transfer between the two fluids to the maximum possible heat transfer,

$$\epsilon = \frac{Q}{Q_{max}} \tag{3.26}$$

where the maximum heat transfer is obtained from the minimum heat capacity and maximum temperature difference between the two fluids,

$$Q_{max} = C_{min}(T_{h.in} - T_{c.in}) (3.27)$$

$$C_{min} = min(\dot{m}_{air}c_{p,air}; \dot{m}_{coolant}c_{p,coolant})$$
(3.28)

Usually, the minimum heat capacity is on the air side due to its lower specific heat capacity, which is more than three times lower than that of the coolant used.

While the maximum heat is known, the actual transferred heat depends on the effectiveness, which is a function of the NTU and the heat capacities ratio, $C_r = \frac{C_{min}}{C_{max}}$, Equation 3.29 [102].

$$\epsilon = f(NTU, C_r) \tag{3.29}$$

The NTU depends on both the fluid properties and the geometry of the heat exchanger. Its relation with the effectiveness depends on the heat exchanger's topology. Being that the topology analysed in this work is of an unmixed cross-flow single-pass heat exchanger, Figure 3.3, the following relation applies

$$\epsilon = 1 - exp\left(\frac{1}{C_r}NTU^{0.22}(exp(-C_rNTU^{0.78}) - 1)\right)$$
(3.30)

Geometry

To implement the $\epsilon-NTU$ method, the heat exchanger's geometry is required to compute values used in the method, such as heat transfer and free flow areas. The type of heat exchanger used is the offset fin strip type on the air side with flat tubes on the coolant side for reasons detailed in Section 2.2. The geometry of each side of the heat exchanger and the geometric parameters that define them can be seen in Figure 3.4.

All the parameters besides the length of the heat exchanger will be fixed, with the length of the heat exchanger resulting from a sizing procedure.

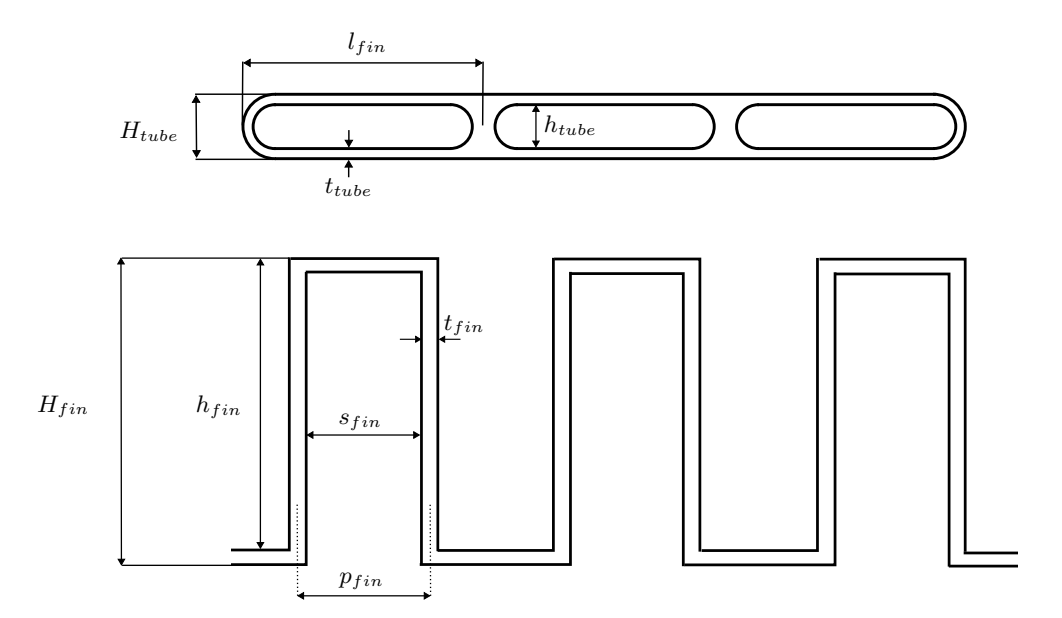


Figure 3.4: Heat exchanger geometry definitions of tubes, top, and fins, bottom

The heat transfer area of the air side is defined from [102] as

$$A_{fin} = 2h_{fin}l_{fin} + 2h_{fin}t_{fin} + s_{fin}t_{fin}$$

$$\tag{3.31}$$

$$A_{primary} = 2s_{fin}l_{fin} (3.32)$$

With the total heat transfer area being

$$A_{air} = N_{fins}(A_{primary} + \eta_{fin}A_{fin})$$
(3.33)

where N_{fins} is the total number of fins, to be calculated with Equation 3.43, and η_{fin} is the fin efficiency, which for an offset fin can be calculated with the following equations [102]

$$\eta_{fin} = \frac{tanh(ml)}{ml} \tag{3.34}$$

$$ml = \left(\frac{2h_{c,air}}{k_{fin}t_{fin}}\left(1 + \frac{t_{fin}}{l_{fin}}\right)\right)^{0.5} \left(\frac{H_{fin}}{2} - t_{fin}\right)$$
(3.35)

where $h_{c,air}$ is the air side heat transfer coefficient and k_{fin} is the thermal conductivity of the fin material, in the case of the chosen material, aluminium, a value of 190W/m.K is used.

The total heat transfer area of the coolant side is made up of only the primary surface, as no fins are present, and is calculated with

$$A_{coolant} = p_{fin}(\pi h_{tubes} + 2(l_{fin} - H_{tubes}))N_{tubes}N_{finsperpassage}N_{offsets}$$
(3.36)

where $N_{offsets}$ is a positive integer for the number of fin offsets in the heat exchanger since for this design the width of a tube is the same as the length of a fin, $N_{finperpassage}$ is a positive integer for the number of fins per air passage and N_{tubes} is a positive integer for the number of tube sections in the direction of the heat exchanger height.

Another area value that will be useful later on the method is the free flow area of both fluid sides. Such values are computed with the following equations,

$$A_{0,air} = s_{fin} h_{fin} N_{airpassages} N_{finperpassage}$$
(3.37)

$$A_{0,coolant} = (h_{tubes}(l_{fin} - H_{tubes}) + \pi \frac{h_{tubes}^2}{4}) N_{offsets} N_{tubes}$$
(3.38)

The number of fins, fins per passage, air passages and tube sections are calculated assuming that at both ends of the heat exchanger there is an air section. For a certain heat exchanger height (H_{HE}) , width (W_{HE}) and length (L_{HE}) the following equations apply,

$$N_{airpassages} = 1 + \frac{H_{HE} - H_{fin}}{H_{tubes} + H_{fin}}$$
(3.39)

$$N_{finperpassage} = \frac{W_{HE}}{p_{fin}} \tag{3.40}$$

$$N_{tubes} = N_{airpassages} - 1 (3.41)$$

$$N_{offsets} = \frac{L_{HE}}{l_{fin}} \tag{3.42}$$

$$N_{fins} = N_{airpassages} N_{finperpassage} N_{offsets}$$
(3.43)

To complete the implementation of the method, the properties of the fluids are also required. For the air side, the correlation for the Colburn and friction factors from [103] are used,

$$j_{air} = 0.6522Re_{air}^{-0.5403}(s_{fin}/h_{fin})^{-0.1541}(t_{fin}/l_{fin})^{0.1499}(t_{fin}/s_{fin})^{-0.0678}$$

$$(1 + 5.26910^{-5}Re_{air}^{1.34}(s_{fin}/h_{fin})^{0.504}(t_{fin}/l_{fin})^{0.456}(t_{fin}/s_{fin})^{-1.055})^{0.1}$$
(3.44)

$$f_{air} = 9.6243 Re_{air}^{-0.7422} (s_{fin}/h_{fin})^{-0.1856} (t_{fin}/l_{fin})^{0.3053} (t_{fin}/s_{fin})^{-0.2659}$$

$$(1 + 7.66910^{-8} Re_{air}^{4.429} (s_{fin}/h_{fin})^{0.920} (t_{fin}/l_{fin})^{3.767} (t_{fin}/s_{fin})^{0.236})^{0.1}$$
(3.45)

where the Reynolds number is computed by using the mass flow of the fluid,

$$Re = \frac{\dot{m}D_h}{A_0\mu} \tag{3.46}$$

where \dot{m} is the mass flow, D_h is the hydraulic diameter, A_0 is the free flow area and μ is the dynamic viscosity. This Reynolds number definition applies to both the air and the coolant side. For each side, the hydraulic diameter is defined as

$$D_{h,air} = \frac{4s_{fin}h_{fin}l_{fin}}{2(s_{fin}l_{fin} + h_{fin}\cdot l_{fin} + h_{fin}\cdot t_{fin}) + s_{fin}t_{fin}}$$
(3.47)

$$D_{h,coolant} = \frac{4(h_{tubes}(l_{fin} - H_{tubes}) + \pi h_{tubes}^2/4)}{(\pi h_{tubes} + 2(l_{fin} - H_{tubes})}$$
(3.48)

The dynamic viscosity, μ , heat capacity, c_p , and thermal conductivity, k, are taken for average temperature values of the fluids in the heat exchanger. The average temperature of the fluids is calculated with the method from Shah et al. [102] for cross-flow heat exchangers. The process is presented in Table 3.3, for a general hot and cold fluid, subscript h and c, respectively, since, depending on the application of the model, for the main heat exchanger or for the intercooler, the correct set of equations should be used. The subscripts in, out and m are for the inlet, outlet and average conditions, respectively.

Table 3.3: Approximate mean temperatures on a two-fluid heat exchanger's hot- and cold-fluid sides [102]

$$C_{max} \text{ Hot Fluid, } C_{min} \text{ Cold Fluid} \qquad C_{max} \text{ Cold Fluid, } C_{min} \text{ Hot Fluid} \qquad \\ C_{r} < 0.5 \text{ Case} \qquad \\ T_{h,m} = \frac{T_{h,in} + T_{h,out}}{2} \qquad \qquad T_{c,m} = \frac{T_{c,in} + T_{c,out}}{2} \qquad \\ \Delta T_{lm} = \frac{(T_{h,m} - T_{c,out}) - (T_{h,m} - T_{c,in})}{\ln\left(\frac{T_{h,m} - T_{c,o}}{T_{h,m} - T_{c,in}}\right)} \qquad \Delta T_{lm} = \frac{(T_{h,in} - T_{c,m}) - (T_{h,out} - T_{c,m})}{\ln\left(\frac{T_{h,in} - T_{c,m}}{T_{h,out} - T_{c,m}}\right)} \qquad \\ C_{r} \ge 0.5 \text{ Case} \qquad \\ T_{h,m} = \frac{T_{h,in} + T_{h,out}}{2} \qquad \qquad T_{c,m} = \frac{T_{c,in} + T_{c,out}}{2}$$

With the mean temperatures, the fluid properties are obtained from the tool Cantera [104] for the air properties and from the Coolprop database [105] for the coolant.

With the fluid properties, the Prandtl number is computed [102]

$$Pr = \frac{C_p \mu}{k} \tag{3.49}$$

Once the Colburn factor and the Prandtl number are obtained, the Nusselt number of the air can be computed with the following equation [102]

$$Nu_{air} = jRePr^{1/3} (3.50)$$

For the coolant side, the set of equations found in *VDI heat atlas* [106] is used to compute the coolant Nusselt number. For the case the where $Re_{coolant} < 2300$ the following equations are used

$$Nu_2 = 1.615(RePrD_h/W_{HE})^{1/3} (3.51)$$

$$Nu_3 = \left(\frac{2}{1 + 22.2Pr}\right)^{1/6} (RePrD_h/W_{HE})^{1/2}$$
(3.52)

$$Nu = (3.66^{3} + 0.7^{3} + (Nu_{2} - 0.7)^{3} + Nu_{3}^{3})^{1/3}$$
(3.53)

And for the case where $Re_{coolant} > 10^4$ the Nusselt number is

$$Nu_{coolant} = \frac{(\xi/8)RePr}{1 + 12.7\sqrt{\xi/8}(Pr^{2/3} - 1)} \left(1 + (D_h/W_{HE})^{2/3}\right)$$
(3.54)

where

$$\xi = (1.8\log_{10}Re - 1.5)^{-2} \tag{3.55}$$

On both laminar and turbulent cases, a factor is applied to account for the variation of temperature-dependent properties, as is the case for the thermodynamic properties of the coolant. This factor considers the Prandtl number at the wall temperature, which, following Schröder et al. [95] approach, is defined as

$$T_{wall} = \frac{\frac{T_{coolant,in} + T_{coolant,out}}{2} + \frac{T_{air,in} + T_{air,out}}{2}}{2}$$
(3.56)

The factor applied is $\left(\frac{Pr}{Pr_{wall}}\right)^{0.11}$ [106].

Once the Nusselt numbers are obtained, the heat transfer coefficient of either the air or the coolant is calculated with the following equation

$$h_c = \frac{Nuk}{D_h} \tag{3.57}$$

With the thermodynamic properties and the heat transfer area of both the fluids, the heat transfer capacity of the heat exchanger, UA, is calculated with

$$\frac{1}{UA} = \frac{1}{h_{c,air}A_{air}} + \frac{1}{h_{c,coolant}A_{coolant}}$$
(3.58)

The previous equation assumes that the aluminium's resistance is negligible due to its high thermal conductivity. Finally, the number of transfer units is calculated

$$NTU = \frac{UA}{C_{min}} \tag{3.59}$$

Once the outlet conditions are known, the pressure drop over the heat exchanger is calculated. For this purpose, only the friction component of the pressure drop is accounted for, since the pressure variations at the inlet and outlet of the heat exchanger partially compensate for each other. This approach is in accordance with Shah et al. [102], that suggested that frictional pressure drop dominates. The equation used to calculate the pressure drop is the following

$$\Delta p_{HE} = 2 \frac{L_{HE} f_{air} \mu_{air}^2 Re_{air}^2}{D_{h,air}^3 \rho_{air}}$$
 (3.60)

The mass of the heat exchanger can be directly calculated from the geometric variables defined as well as the volume of the coolant side, which will be used to obtain the total coolant mass required to maintain the system operational.

The heat exchanger air side design was chosen from the list used by Raj M. Manglik et al. [103] to develop the used correlations. From the several heat exchangers provided, the geometry presented in Table 3.4 was picked due to being a good combination of compactness, or heat transfer area per volume, while not resulting in a high pressure drop due to that same compactness.

Table 3.4: Heat exchanger and in	tercooler design [103, 107]
----------------------------------	-----------------------------

Variable	Value(mm)
t_{fin}	0.102
h_{fin}	6.239
S_{fin}	1.522
l_{fin}	3.188
h_{tubes}	1.6
t_{tubes}	0.2

Validation

To validate the heat exchanger modelling, the air side correlations were verified with data from the software EchTerm by Greth [GRETh . 2025]. The data was obtained through Scoccimarro [55] study, since access to the Echterm software was not possible. The values used for the verification and the results are presented in Table 3.5.

Table 3.5: Air side correlations validation

Variable	Value	Results	EchTerm	Model
$\overline{t_{fin}}$	0.1mm	h_c	$336.3Wm^{-2}K^{-1}$	$345.7Wm^{-2}K^{-1}$
h_{fin}	2.3mm	Δp	794.9Pa	830.3Pa
s_{fin}	1.16mm			
l_{fin}	3.1mm			
L_{HE}	2.2cm			
v_{air}	$27.11ms^{-1}$			
T_{air}	$20^{\circ}C$			
p_{air}	1bar			

The results obtained with the implemented model are within 5% of the values obtained with EchTerm, which is within an acceptable range.

After the smaller verification of the air side correlations, the whole heat exchanger model is validated with the work of Hao et al. [108]. In this study, the data obtained from an experimental setup of a heat exchanger are used to validate the implementation of a model. The heat exchanger used has offset fin strips on both the coolant, in this case water, and the air side, and therefore is not the same as the one used for this thesis. Nevertheless, this validation is reasonable due to a lack of available validation data for this type of heat exchangers and since the air side is the

limiting factor of the heat exchange. For the water side geometry, the values from Hao et al. [108] are adjusted to allow for their implementation in the developed model. The values used are presented in Table 3.6.

Variable	Value(mm)
t_{fin}	0.2
h_{fin}	9.3
s_{fin}	1.8
l_{fin}	4.0
h_{tubes}	2.8

 t_{tubes} N_{tubes}

 L_{HE}

 $N_{airpassages}$

0.1

13

14

140

 Table 3.6: Heat exchanger geometry from Hao et al. [108] used for validation

The first comparison is made with the numerical model used by Hao et al. [108]. In Figure 3.5, the results of both numerical models are presented. The thermal resistance, $R_{thermal}$, measures the inlet temperature difference between air and water per unit of heat transferred. The results obtained with the model of this thesis are substantially higher than the ones from Hao et al. [108], increasing the higher the mass flow of air. Such a result was expected since, as mentioned previously, the water side geometry differs, with it being worse at heat transfer when fins are not used, since the fins increase turbulence in the flow, which improves heat transfer. Therefore, a lower heat transfer for the same difference in inlet temperatures is expected. Even though the values do not match, the heat transfer behaviour with respect to the mass flow of air is similar. When analysing the pressure drop, the values obtained are much more similar to the ones from Hao et al. [108]. This is expected since the correlations used for the air side are the same in both models. The differences may stem from the method used to compute the air properties, since no information is given on that matter.

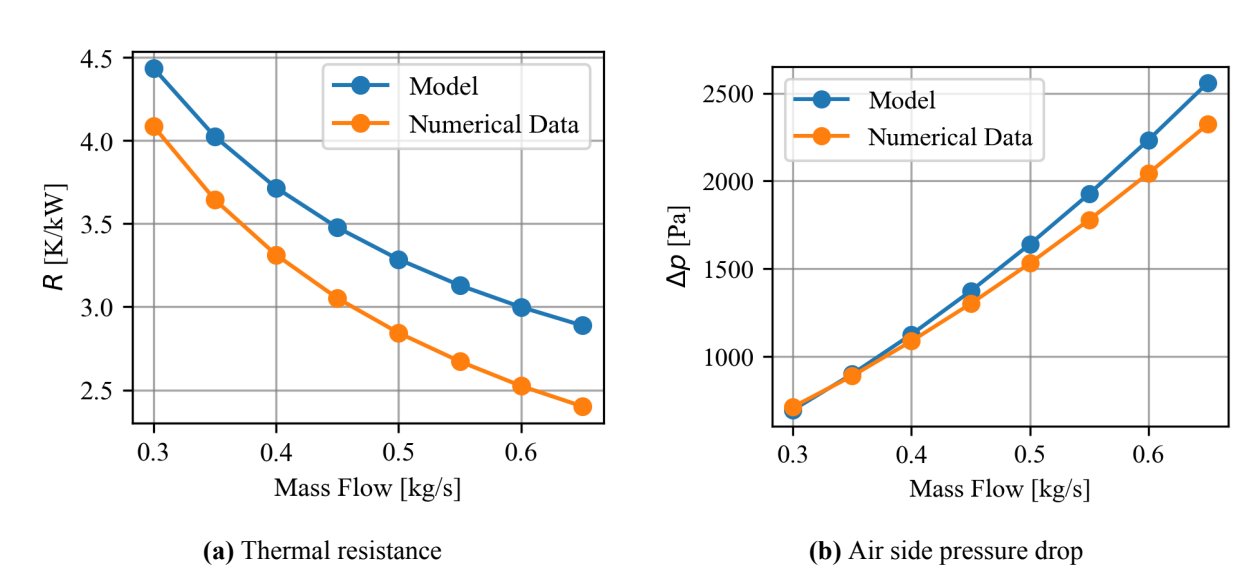


Figure 3.5: Model comparison with data from Hao et al. [108]

The experimental data is presented in Figure 3.6. From the heat transfer plot, it is clear that the discrepancy between the experimental and numerical data from Hao et al. [108] remains. The model used in this thesis results in a lower heat transfer for the same conditions due to the already presented reasons. In the case of the pressure drop, a much higher, unexpected difference is present. In this case, the numerical data from Hao et al. [108] was not provided. Still, the same or even worse deviation is expected, since from the previous comparison, the pressure drop

from the present model was higher. There is no clear reason for this difference, with Scoccimarro [55] speculating that the test section dimensions and wall interaction with the fluid might be the origin of such a difference. Besides that, it could also be possible that the separation of the flow at the test section, which the numerical models would not predict, would lead to the present differences.

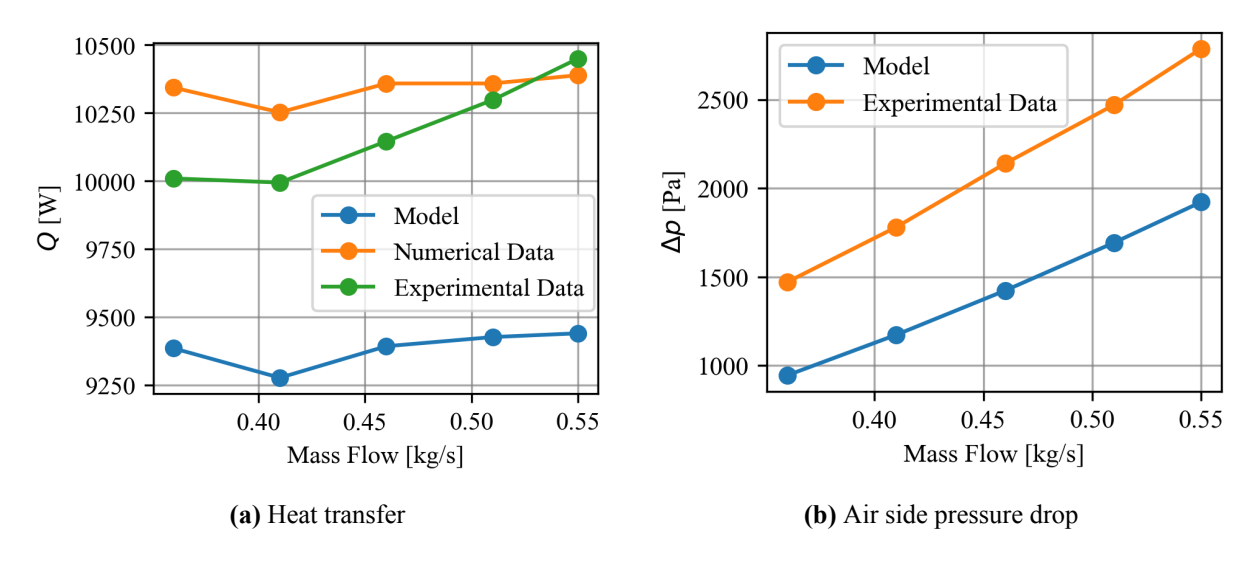


Figure 3.6: Model comparison with data from Hao et al. [108]

3.2.3. Compressor

The compressor model is based on a linear regression obtained from available compressor data by Celeroton [109], Fischer [110], ROTREX [111], and Sprintex [112], which relates the compressor power to its mass and volume. The results are shown in Figure 3.7.

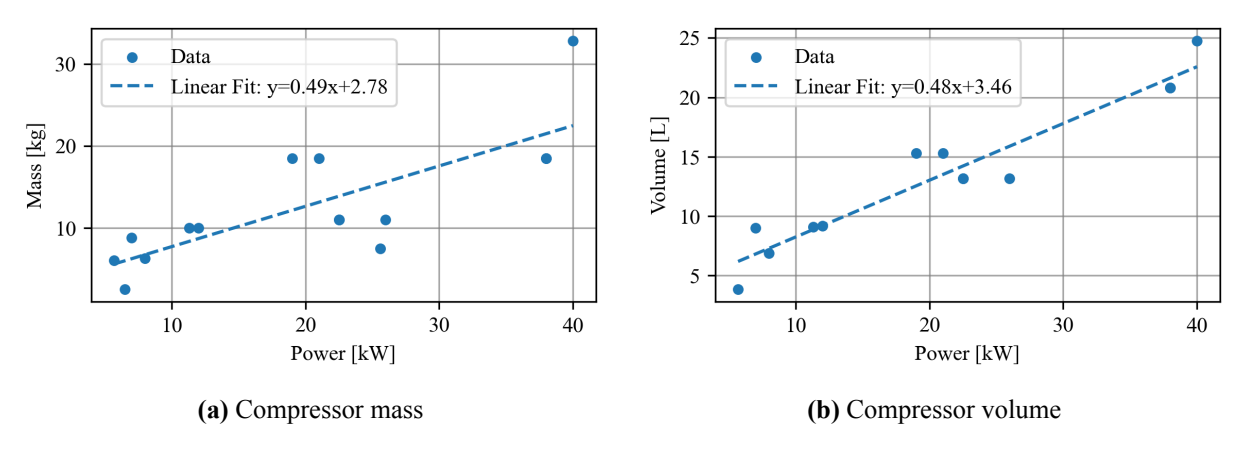


Figure 3.7: Linear regressions for compressor with data from Celeroton [109], Fischer [110], ROTREX [111], and Sprintex [112]

Its power needs to be calculated to obtain the compressor's mass and volume. This is done with equation Equation 3.61.

$$P_{comp} = \frac{\dot{m}_{air,FC}\bar{c}_{p,air}}{\eta_{comp,motor}} (T_{t,comp,out} - T_{t,comp,in})$$
(3.61)

where $m_{air,FC}$ is the mass flow of air that goes to the fuel cell, $\overline{c}_{p,air}$ is the average specific heat capacity of air, $\eta_{comp,motor}$ is the electric motor efficiency which takes a constant value of 0.98, $T_{t,comp,in}$ is the inlet temperature of the compressor, that is defined from inlet properties and ambient conditions and $T_{t,comp,out}$ is the outlet temperature of the compressor.

The outlet temperature of the compressor depends on the operating pressure of the fuel cell and on the pressure drop of the air supply path. As a result, its value is calculated with the following equation

$$T_{t,comp,out} = T_{t,comp,in} (1 + \frac{1}{\eta_{is}} (\beta^{(\gamma-1)/\gamma-1}))$$
 (3.62)

where η_{is} is the isentropic efficiency of the compressor, assumed to be 0.80, β is the pressure ratio, and γ is the specific heat ratio. The pressure ratio needs to take into account all pressure losses of the air supply path, being defined as follows,

$$\beta = \frac{p_{FC} + \Delta p_{IC} + \Delta p_H}{p_{t.comp.in} - \Delta p_F} \tag{3.63}$$

where p_{FC} is the operating pressure of the fuel cell, Δp is the pressure drop over each component, with IC, H and F standing for intercooler, humidifier and filter, respectively, and $p_{t,comp,in}$ is the inlet pressure.

One last detail of the model is that the specific heat capacity of air is taken as an average over the range of inlet and outlet temperatures, since, due to the large difference between these two values, the specific heat capacity varies significantly. It is calculated with

$$\overline{c}_{p,air} = \frac{1}{T_{t,comp,out} - T_{t,comp,in}} \int_{T_{t,comp,in}}^{T_{t,comp,out}} c_{p,air}(T) dT$$
(3.64)

3.2.4. Filter

The filter is a crucial part of the system as it ensures all other components can operate under ideal conditions with no contamination. To model such a component, several filter products were used to create a relation that outputs the filter volume from the air mass flow in standard litres per minute (SLPM) that needs to be filtered. The same could not be achieved for its mass, since in the product data sheets, there was no information on the mass of the filters. Therefore, the mass of the filter is estimated using the equation found in the thesis by Vroom [113],

$$m_F = 6 \cdot \dot{m}_{air,FC} \tag{3.65}$$

Another fundamental result of the filter performance is the pressure drop over it. If the same approach for obtaining a linear regression with product data were used for the pressure drop, the resulting pressure drop would be in the range of $20000 \sim 30000 Pa$. That is because in the application of this study, each pod will require an air mass flow of around 0.5kg/s, which equates to $5 \cdot 10^5 SPLM$, which, when extrapolated to the data in Figure 3.8, results in the previously given values of pressure drop. Since the pressure drop over the filter is more a concern of the length of the filter and the flow speed over it, it will be assumed that an arrangement where the pressure drop could be kept small is used. Therefore, 600Pa is used as the pressure drop over the filter to size the system.

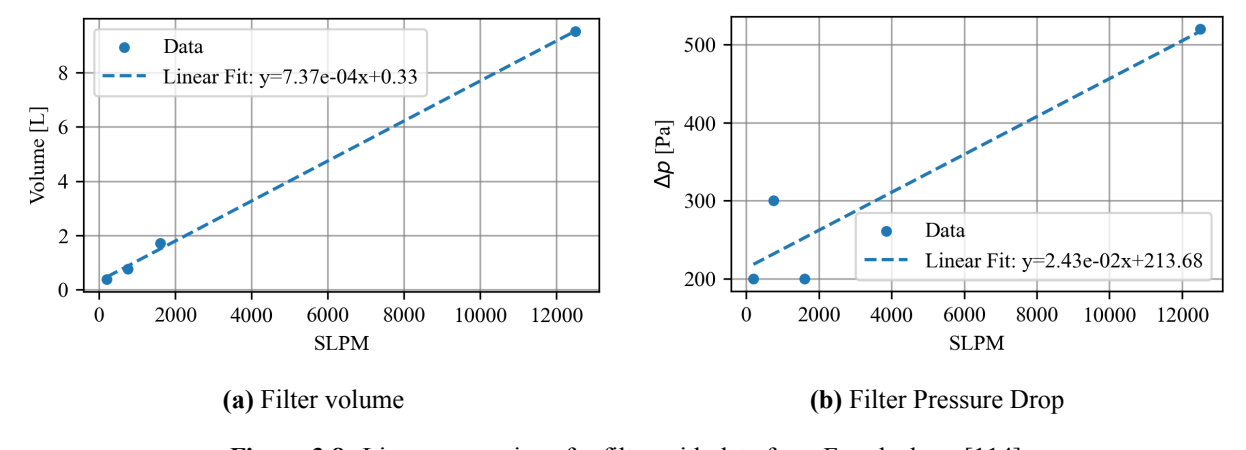


Figure 3.8: Linear regressions for filter with data from Freudenberg [114]

3.2.5. Humidifier

In the humidifier case, a very similar approach to the one taken for the filter is used. In this case, data for both volume and weight are available and are then used to obtain the equations required, shown in Figure 3.9. Once again, the resulting equations are with respect to the SLPM of air.

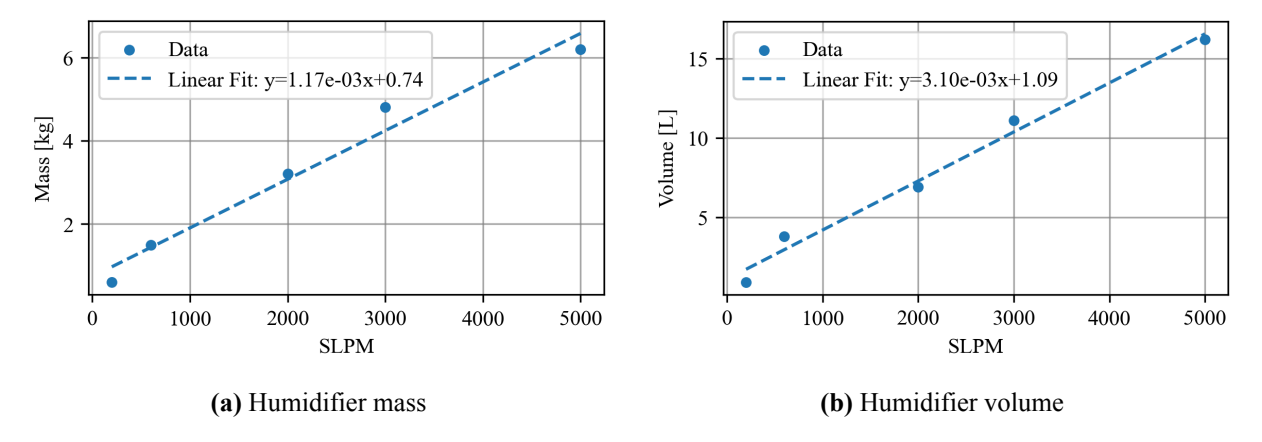


Figure 3.9: Linear regressions for humidifier with data from fumatech [115]

Just as it happened for the filter, the pressure drop would also be extremely high in the humidifier if the same linear regression method were used. In this case, from the data in Figure 3.10, a pressure drop of around 600kPa would be achieved. Therefore, a pressure drop of 8000Pa for the humidifier will be assumed.

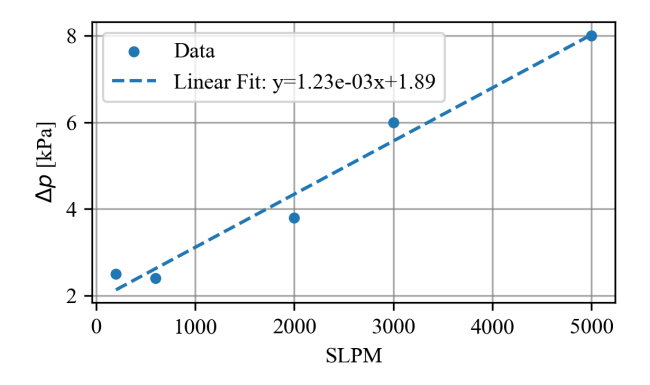


Figure 3.10: Linear regressions for humidifier pressure drop with data from fumatech [115]

3.2.6. Air Duct

The air duct comprises the inlet, heat exchanger and nozzle. In terms of geometry, the inlet and nozzle will not be analysed or sized in detail, and the tool openAD already estimates the nacelle mass. To calculate the conditions at the inlet, under the advice of DLR researchers, it is assumed that the propeller does not influence the speed of the ambient air entering the inlet, as it is difficult to accurately predict the influence that the propeller has on the flow for every flight phase. Therefore, the total pressure and temperature at the inlet are calculated with the following equations

$$T_{t,0} = T_0 \left(1 + \frac{(k-1)}{2} M a_0^2\right)^{(\gamma/(\gamma-1))}$$
(3.66)

$$p_{t,0} = p_0 \left(1 + \frac{(k-1)}{2} M a_0^2\right)^{(\gamma/(\gamma-1))}$$
(3.67)

where the subscript 0 represents ambient conditions.

It is assumed that there are no losses at the inlet and diffuser [116], and therefore the total ambient conditions are the ones used at the heat exchanger and compressor inlets.

The height and width of the duct where the heat exchanger will be placed are also user defined and together with the inclination angle of the heat exchanger are used to compute the actual height of the heat exchanger with the following equation

$$H_{HE} = \frac{H_{duct}}{\cos \theta_{HE}} \tag{3.68}$$

Such inclination has been proved to increase the heat transfer and pressure drop. Since no method was found to model such an increase in pressure drop, it is not accounted for.

After the heat exchanger, the air flow is expanded back to ambient pressure, $p_{nz,out} = p_0$ since the flow is always under subsonic conditions. As a result, the mass flow of air results from the pressure and temperature variation over the heat exchanger and the nozzle area. In this study, the nozzle is assumed to be a variable area nozzle such that the flow expands perfectly for a particular mass flow.

The conditions after the heat exchanger are known from the results of its model, and with that, the speed of the flow at the nozzle is calculated, assuming a nozzle total pressure ratio of 0.99 [116], with the following equations

$$p_{t,nz,out} = 0.99(p_{t,0} - \Delta p_{HE}) \tag{3.69}$$

$$Ma_{nz,out} = \sqrt{\frac{2}{\gamma - 1} \left(\left(\frac{p_{t,nz,out}}{p_{nz,out}} \right)^{\frac{\gamma - 1}{\gamma}} - 1 \right)}$$
 (3.70)

$$v_{nz.out} = Ma_{nz.out} \sqrt{\gamma RT_{nz.out}}$$
(3.71)

where $T_{nz,out}$ is the static air temperature at the nozzle outlet and is calculated with Equation 3.66, where the total temperature is the one at the exit of the heat exchanger.

Finally, the area of the nozzle and, consequently, the thrust of the heat exchanger air flow is calculated with the following equations

$$A_{nz,out} = \frac{\dot{m}_{air,HE}}{\rho_{nz,out} v_{nz,out}}$$
(3.72)

$$F_t = \dot{m}_{air,HE}(v_{nz,out} - v_0) - (\dot{m}_{air,FC} + \dot{m}_{O_2,tank})v_0$$
(3.73)

Besides the contribution of the air duct flow, there is also the contribution of the air and possible tank oxygen flow that goes through the fuel cell. This part of the momentum loss calculation assumes that the fuel cell flow is dispensed with no velocity.

3.2.7. Coolant Loop

The last part of the modelled system is the components related to the coolant transport and storage. A pump is required to keep the coolant flowing. The required power of this pump is not evaluated as it represents a very low percentage of the total power produced by the fuel cell [113, 95], not even reaching 0.5% of the total power. The power this pump and other low power components is accounted for as a fixed percentage increment in the required power of the fuel cell of 1% [56].

For the mass and volume of the coolant pump, manufacturer data provided by Schröder et al. [95] is used, and a linear scaling of this baseline design is used

$$m_{pump} = m_{pump,base} \frac{\dot{m}_{coolant}}{\dot{m}_{coolant,base}}$$
(3.74)

$$V_{pump} = V_{pump,base} \frac{\dot{m}_{coolant}}{\dot{m}_{coolant,base}}$$
(3.75)

where $\dot{m}_{coolant,base} = 5kg/s$ is the baseline coolant mass flow, $m_{pump,base} = 3.4kg$ is the baseline pump mass and $V_{pump,base} = 7.7L$ is the baseline pump volume.

The mass flow of the coolant is calculated with the waste heat from the fuel cell and assuming that the temperature variation of the coolant in the fuel cell, $\Delta T_{coolant,FC}$, is of 10K, where its exit temperature is the operating temperature of the fuel cell. The mass flow of coolant is then calculated with

$$\dot{m}_{coolant} = \frac{Q}{c_{p,coolant} \Delta T_{coolant,FC}}$$
(3.76)

To flow to and from the different components, pipes are required. The pipe area is 20% of the free flow area of the coolant in the heat exchanger. With its area, the diameter of the pipe is calculated

$$D_{pipe} = \sqrt{\frac{4A_{pipe}}{\pi}} \tag{3.77}$$

To calculate the mass of the pipe a thickness of 2mm is assumed unless a verification with Barlow's formula results in a required thickness of more than 2mm. This verification is done with the following equation

$$t_{req} = \frac{\frac{p_{pipe}D_{pipe}}{2S_{pipe}}}{1 - \frac{p_{pipe}}{S_{pipe}}}$$
(3.78)

where p_{pipe} is the internal pressure of the pipe, S_{pipe} is the yield strength of the material and D_{pipe} is the pipe diameter. For this calculation, aluminium is used as the pipe material with a yield strength of 170MPa and the internal pressure of the pipe is 0.3MPa.

With the thickness and a specified length of the pipes, the mass of the pipes is calculated

$$m_{pipe} = L_{pipe}\pi((\frac{D_{pipe}}{2} + t_{pipe})^2 - \frac{D_{pipe}^2}{4})\rho_{al}$$
 (3.79)

where $L_{pipe}=3m$ is the pipe length and ρ_{al} is the aluminium density.

The last mass that needs to be accounted for is the mass of the coolant itself. For that, the total volume the coolant needs to occupy is calculated. The total volume comprises the liquid side of the heat exchanger and intercooler, the pipe, and the coolant channels of the fuel cells, with only the volume of the coolant channels yet to be defined. The value used for the coolant channel volume is 10% of the total stack volume, as DLR researchers indicated that this would be a reasonable estimate.

The mass of coolant in the systems is

$$m_{coolant} = (V_{coolant,HE} + V_{coolant,IC} + V_{pipe} + 0.1V_{stack})\rho_{coolant}$$
(3.80)

where $V_{pipe} = A_{pipe} L_{pipe}$.

3.2.8. Power Train

Since the power values provided to size the system are the shaft power required by the propeller, P_{shaft} , it is necessary to translate that power to the power that the fuel cells need to provide.

The components required for the power train, starting from the one connected to the propeller, are the gearbox, the motor, the inverter, the cables, and the converter. For each of the components, their mass, as well as the output power of the next component, is calculated with the following equations

$$m_{component} = \frac{P_{out,component}}{\rho_{P,component}}$$
(3.81)

$$P_{out,component+1} = \frac{P_{out,component}}{\eta_{component}}$$
(3.82)

where $\rho_{P,component}$ is the power density and $\eta_{component}$ is the efficiency.

The only exception to this set of equations is the cable mass, which is calculated with the linear mass density of the cable and its length, Equation 3.83. For each pod, an assumed length of 2 meters is used for the cables.

$$m_{cable} = L_{cable} \rho_{cable} \tag{3.83}$$

where ρ_{cable} is the linear density of the cables, with a value of 5kg/m

The specific power and efficiency of each component is given in Table 3.7.

Table 3.7: Power train components power density and efficiency [117]

	$\rho_P(kW/kg)$	η
Gearbox	17	0.995
Motor	17	0.98
Inverter	18	0.995
Converter	10	0.975

The power that the fuel cell needs to generate is the following

$$P_{FC} = \frac{P_{shaft}}{\eta_{GB}\eta_{M}\eta_{Inv}\eta_{Conv}\eta_{Cable}} + P_{offtakes} + P_{comp}$$
(3.84)

where $P_{offtakes}$ is the aircraft systems offtake power that the propulsion system also needs to provide as extra power.

3.2.9. Battery

Since the propeller's effect is not considered at the air duct inlet, at low speeds, the pressure drop over the heat exchanger would be greater than the increase in pressure from the flow speed. As a result, the air duct would not have flow. Since this is the case, there would be no heat dissipation at take-off. Therefore, to provide the required power at take-off, a battery is used until a Mach number of 0.2 is reached, from which the fuel cell is used, because at this point the passive air duct can function accordingly.

To size the battery, both power density and energy density are used, with the worst case scenario being the sizing criterion. Since the battery application is for a short-duration, high-power supply, the corresponding values for such a battery from [9] will be used. The following equation is used to obtain the battery mass

$$m_{battery} = max \left(\frac{2t_{TO}P_{battery} + Energy_{taxi}}{\rho_{energy} \cdot 3600}, \frac{P_{battery}}{\rho_{P,battery}} \right)$$
 (3.85)

where t_{TO} is the take-off time, $Energy_{taxi}$ is the energy required for taxi in and out, $\rho_{energy} = 180kWh/kg$ is the energy density, $\rho_{P,battery} = 5.4kW/kg$ is the power density and $P_{battery}$ is the power required from the battery. The power the battery needs to provide is the same as that of Equation 3.84.

If a battery is used, there is also the need for a cooling system to dissipate the waste heat it generates. In this case, a vapour cycle cooling system is required due to the low operating temperatures of batteries. A simple approach of using the power density to obtain the mass of this system is used. With equation Equation 3.21 and an efficiency of $\eta_{battery} = 0.95$, the waste heat of the battery is calculated. Together with a power density of $\rho_{P,VP} = 0.2kW/kg$ [118], the mass of this cooling system is obtained with the following equation

$$m_{VP} = \rho_{P,VP} Q_{battery} \tag{3.86}$$

3.2.10. Tanks

The liquid hydrogen tanks are modelled with a tool provided by DLR. With this model, an assumed gravimetric efficiency of 30% is used, and the placement of the tanks is behind the cabin, in the aircraft's tail section. When liquid oxygen tanks are needed, a simple approach of assuming a specific gravimetric and volumetric density is taken. The data available for such oxygen tanks is very limited. While several values can be found for medical applications, for mobile fuel cell applications, only one was found [76], where the gravimetric density is, $\eta_{gr,O_2}=0.786$ and the volumetric density is, $\rho_{tank,O_2}=661kg/m^3$, for a tank with aluminium walls and vacuum multi-layer insulation. These values already account for system integration components, such as valves.

With these values and the amount of liquid oxygen required for the mission of the aircraft, which is a result of the AMC tool, the mass and volume of the tank can be calculated with the following equations

$$m_{tank,O_2} = m_{O_2} \left(\frac{1}{\eta_{gr,O_2}} - 1 \right) \tag{3.87}$$

$$V_{tank,O_2} = \frac{m_{O_2}}{\rho_{tank,O_2}}$$
 (3.88)

The placement of the oxygen tanks was decided based on the availability of space, safety concerns and weight distribution. Since the hydrogen tanks are at the rear section of the aircraft and because the oxygen tanks would require much less volume, due to being used in shorter segments of flight and because the stoichiometric amount of molecules of oxygen is half of the hydrogen ones, they are placed in the cargo bay in front of the wing. As a result, there is also a substantial distance between hydrogen and oxygen tanks, preventing risk-inducing situations of their mixing outside the fuel cell. This placement also balances the distribution of weight in the aircraft.

With its placement decided, the geometry of the tanks was defined. In the same manner as any cryogenic liquid, a cylindrical tank is used. Since two tanks are required to comply with regulations, two tanks are placed side by side. Lastly, the maximum diameter of such tanks was calculated based on the cross-section of the fuselage used, presented in Figure 3.11. The diameter of the tanks was optimised to make use of the maximum area out of the available one. As a result, the diameter of each tank is $d_{tank} = 0.82m$.

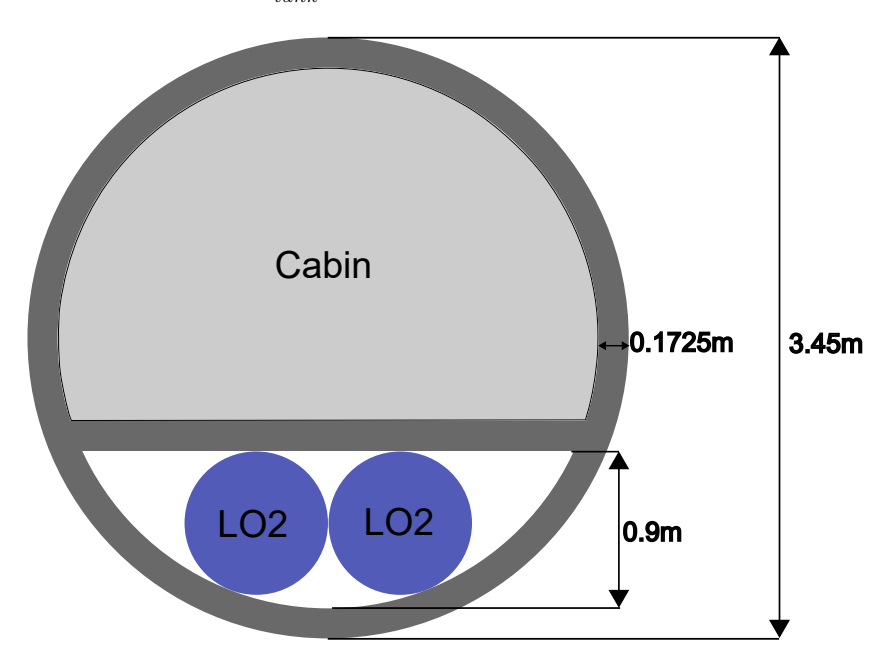


Figure 3.11: Fuselage cross section with oxygen tank placement

3.3. System Sizing

For the system sizing, three flight points will be evaluated. They are take-off at the second segment point, top-of-climb and cruise. Different Mach, altitude, power, aerodynamic efficiency, and ambient conditions apply for each point. At each design point, an optimisation is performed for the mass flow of air through the air duct, the fuel cell's operating pressure, and the design power factor. The design power factor is a value that relates the operating power of the fuel cell with respect to the maximum power that the fuel cell can produce. This value is fundamental since a high design power factor is the equivalent of a high operating current, resulting in a low fuel cell mass, but a high cooling power demand due to the lower efficiency of the fuel cell. Conversely, a low design power factor requires a higher fuel cell mass to provide the desired power, but at a higher efficiency and lower cooling power. The mass flow of air through the air duct is optimised since there is an optimum between improved cooling performance for high mass flows and low pressure drop for lower mass flows. Lastly, the operating pressure is optimised because its value affects the subsystems. A higher operating pressure improves fuel cell efficiency but requires a higher compressor

power and intercooler length. Therefore, it might happen that a higher operating pressure actually reduces the net fuel cell efficiency and increases the total mass of the system.

The optimisation is done for a singular objective function. This objective function is an equation that calculates the total power required from the propulsion unit to compensate for its own weight and drag. The following equation is used

 $P_{req} = \frac{W_{total}v_0}{\frac{L}{D}} - F_T v_0 \tag{3.89}$

where W_{total} is the total system weight and $\frac{L}{D}$ is the aerodynamic efficiency of the aircraft.

To understand how the sizing is done, the process will be explained with all the relevant methods implemented that use the presented models.

Firstly, the ambient conditions are calculated for the Mach and altitude of a specific point. After the compressor, intercooler and fuel cell models are implemented until a converged solution is reached. The convergence is necessary since the compressor power depends on the mass flow of air, resulting from the fuel cell analysis, which also accounts for the compressor power.

The implementation of the intercooler follows an iterative approach in which the intercooler's length is the result of such a process. In addition to the intercooler length, the required coolant temperature difference to reduce the air temperature is also an output of this system. This result is used to obtain the temperature to which the main heat exchanger needs to cool down the coolant.

Once the intercooler design is complete, the fuel cell is sized. For a specific design power factor and operating conditions, the number of singular fuel cells and stacks, the mass flows of reactants and the mass flow of coolant are calculated. With the mass flows of reactants coming from the tanks, be it H_2 or O_2 , it is assumed that heat dissipation could be achieved by boiling and heating the reactants to the fuel cell operating temperature, for hydrogen starting from a temperature of 20K and for oxygen starting from a temperature of 90K. The result is the inlet temperature of the coolant at the heat exchanger, which is lower than the operating temperature of the fuel cell due to the reactant cooling.

With the converged mass flow of air, the humidifier and the filter are sized. Followed by the sizing of the heat exchanger, which is done similarly to the intercooler, by iterating until the length at which the waste heat is dissipated is reached. In the end, the exit conditions of the mass flow of air through the heat exchanger are computed, and the resulting thrust is calculated.

This process is completed for each set of design variables until the optimum has been found. An XDSM of the optimisation is shown in Figure 3.12.

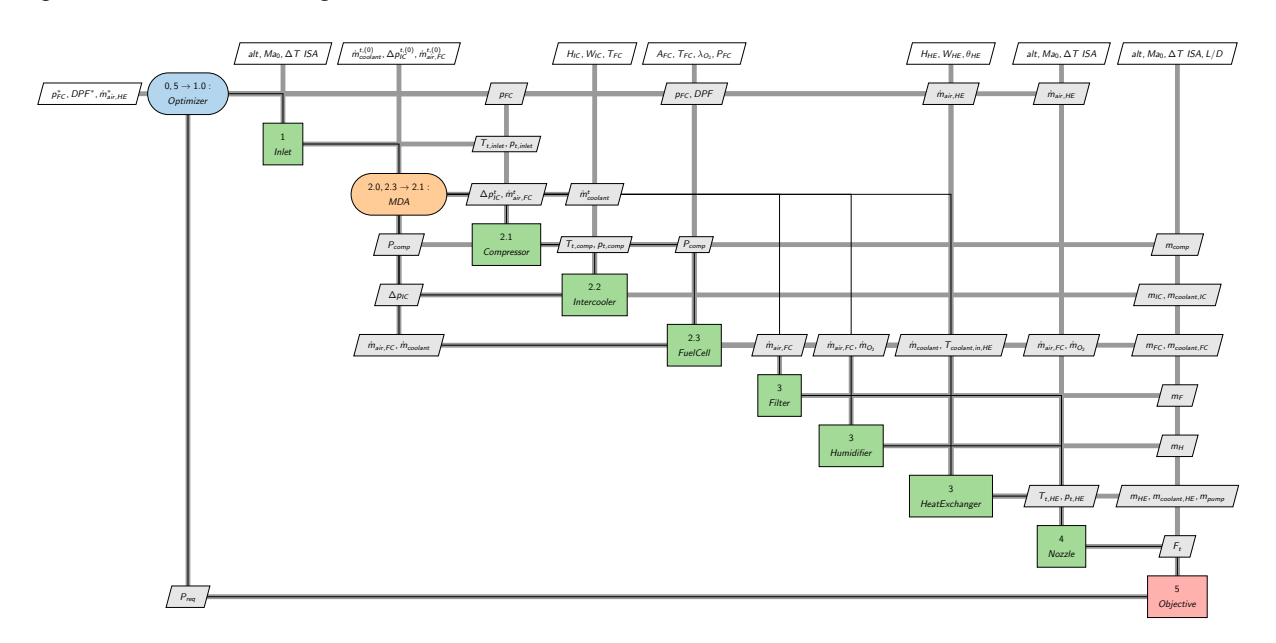


Figure 3.12: XDSM of first optimisation where each point is sized independently

The optimizer used is from the python Scipy [96] library, more specifically the differential evolution optimizer [119, 120, 121, 122]. The choice of this optimiser came as a result of the characteristics of the optimisation at hand. Several of the different methods used in the fuel cell system sizing have a non-differentiable discontinuous nature, such as the number of fuel cells or the length of the heat exchanger. Therefore, gradient-based optimisers could have difficulties dealing with such design spaces. The chosen optimiser is also capable of dealing with multiple variables. It is better implemented with fast objective functions, since it performs many function evaluations, as is the case with this sizing procedure, which takes less than 0.05s. The optimiser used is a stochastic global optimiser, and if not set up correctly, it could result in differing results each time it is run. To prevent such undesired effects, the options of the optimiser were tuned to a value that ensured reproducibility of the results.

The chosen optimiser does not require any initial guess but still requires bounds. The bounds of the DPF were set at 0.2 and 1 for the lower and upper bounds, respectively. The lower bound is not set at zero because for really low values of the DPF, the stack mass would increase rapidly, such that those points would not be part of the feasible domain when integrated in the aircraft. Therefore, the lower bound was increased to prevent an increase in design space and computational time. For the bounds of the operating pressure, the lower bound is set as the maximum between 1atm and the minimum operating pressure that would ensure the operating temperature of the fuel cell is met. This is because after the compressor, the temperature may not be the one set as the operating temperature if the operating pressure is too low. Therefore, the pressure ratio required to reach it would be higher than that needed to reach 1atm. The upper bound was set at 2atm, with both the lower and upper bounds of 1 and 2 atm being recommended by Schröder et al. [95]. The bounds of the mass flow of air are dynamically set, with Equation 3.90, by taking into account the power demand of the design point and a worst and best case scenario for the fuel cell efficiency of 30% and 65%, respectively. In every optimisation, the optimum mass flow is compared with the mass flow bounds to ensure that the bounds do not limit the solution.

$$\dot{m} = \frac{P(\frac{1}{\eta_V} - 1)}{c_{p,air}\Delta T_{air}} \tag{3.90}$$

Since this optimisation will be performed for 3 flight points, the worst case scenario out of the three would be picked. If the worst value for each subsystem were picked, some systems would be unnecessarily oversized. This is because the main component of the system, the fuel cell stack, defines the conditions for every other system to be sized. Suppose a system is sized for a bigger stack. In that case, all other components can reduce their size, because with a bigger stack, a lower current can be used to provide the same power, and its efficiency increases, reducing the size of all other systems. Therefore, the highest stack size is taken, and the other two points to which that size of stack does not belong are optimised again, with a fixed stack size. This results in lighter systems than what would be the result of the independent optimisation of each point. In this way, the optimisation of all 3 points is coupled. When this happens, the DPF is no longer a design variable and becomes a result of the calculations since the fuel cell model will calculate the lowest DPF to supply the desired power, since the stack size is fixed. An XDSM of this slightly changed optimisation problem is shown in Figure 3.13, where it can be seen that the DPF is no longer a design variable and that the number of cells becomes an external input to the fuel cell block.

Once this second optimisation is finished, the worst case scenario for each system is taken as the solution.

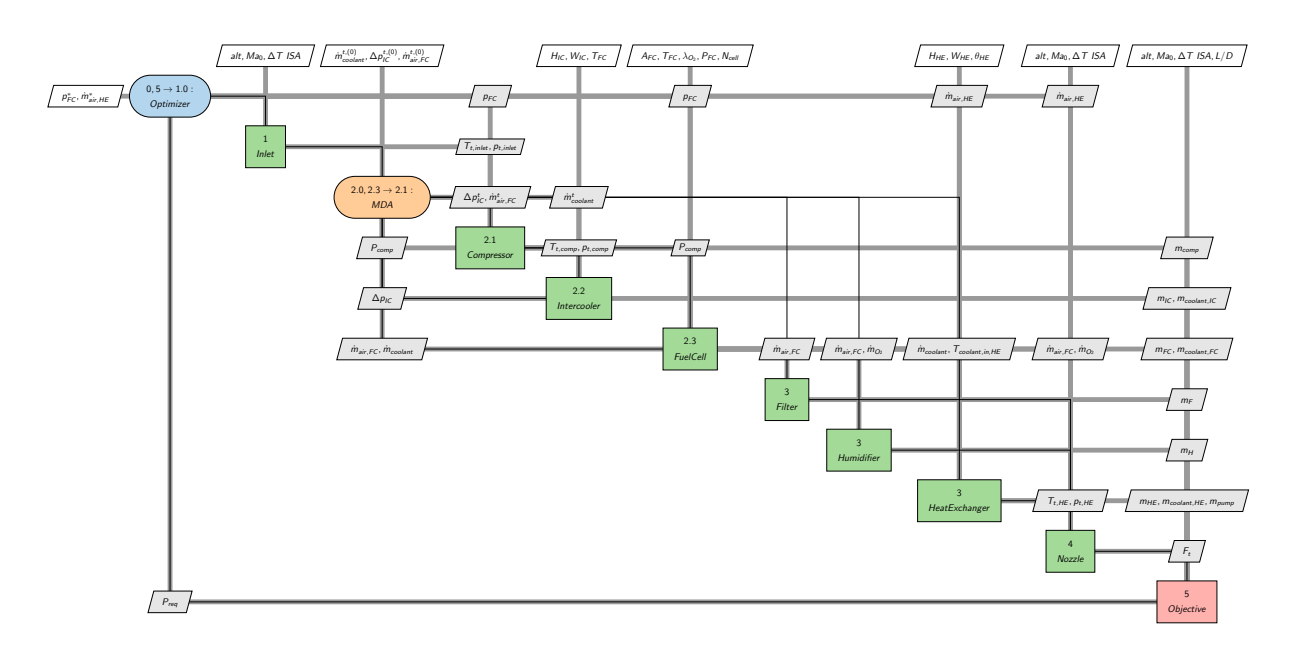


Figure 3.13: XDSM of second optimisation where stack size is fixed by the worst case of the first optimisation

3.3.1. Validation

Even though the fuel cell and heat exchanger modelling were validated, it is also necessary to evaluate how the complete system sizing compares to other studies on fuel cell propulsion in aircraft. For that, four different studies were used. Figure 3.14 shows a bar chart of the systems mass for the present study and the ones used for comparison. To obtain the results under the present study, the required values to run such a sizing procedure were taken when possible. Some values were not retrievable, either because they were not used in the modelling of that study or because they were not given, even though they were part of the modelling requirements. When this was the case, reasonable assumptions were made on the value to use. In this comparison, the heat exchanger part of the system includes the coolant, coolant pump, and pipe mass, since most studies did not consider them or distinguish them from the heat exchanger.

In Figure 3.14a, it is clear that the sizing of all systems is not similar. Starting with the heat exchanger, the predicted mass by Massaro et al. [56] is over 3 times higher than the one obtained in the present study. Such a value seems to be quite an exaggeration of the heat exchanger mass, as any aircraft implementation would be put in question if the heat exchanger had to be that heavy. The fuel cell mass is also much lower due to an assumed power density of the fuel cell higher than the one used in the present study. The compressor modelling follows a similar approach as the one used in the present study, but with a much lower power density of 1.03kW/kg compared to the one obtained in the present work of around 2.03kW/kg, which results in a higher compressor mass. The humidifier, filter, and intercooler are not modelled by Massaro et al. [56] and therefore cannot be compared.

In the study by Vroom [113] the fuel cell mass is comparable to the one obtained by the presented model, and the heat exchange components, be it the main heat exchanger or the intercooler, are predicted to have a higher mass. This is likely because the heat exchanger used has a simpler and less efficient fin design, with just straight fins and no offset. Both the humidifier and compressor are extremely lightweight, and their models follow assumptions that do not seem feasible. For example, the mass of the compressor is assumed to be slightly higher than that of a compressor rated for 200g/s and 32kW, about 1.5 times higher. In comparison, the analysis results provide a mass flow of 2kg/s and a power of 438kW.

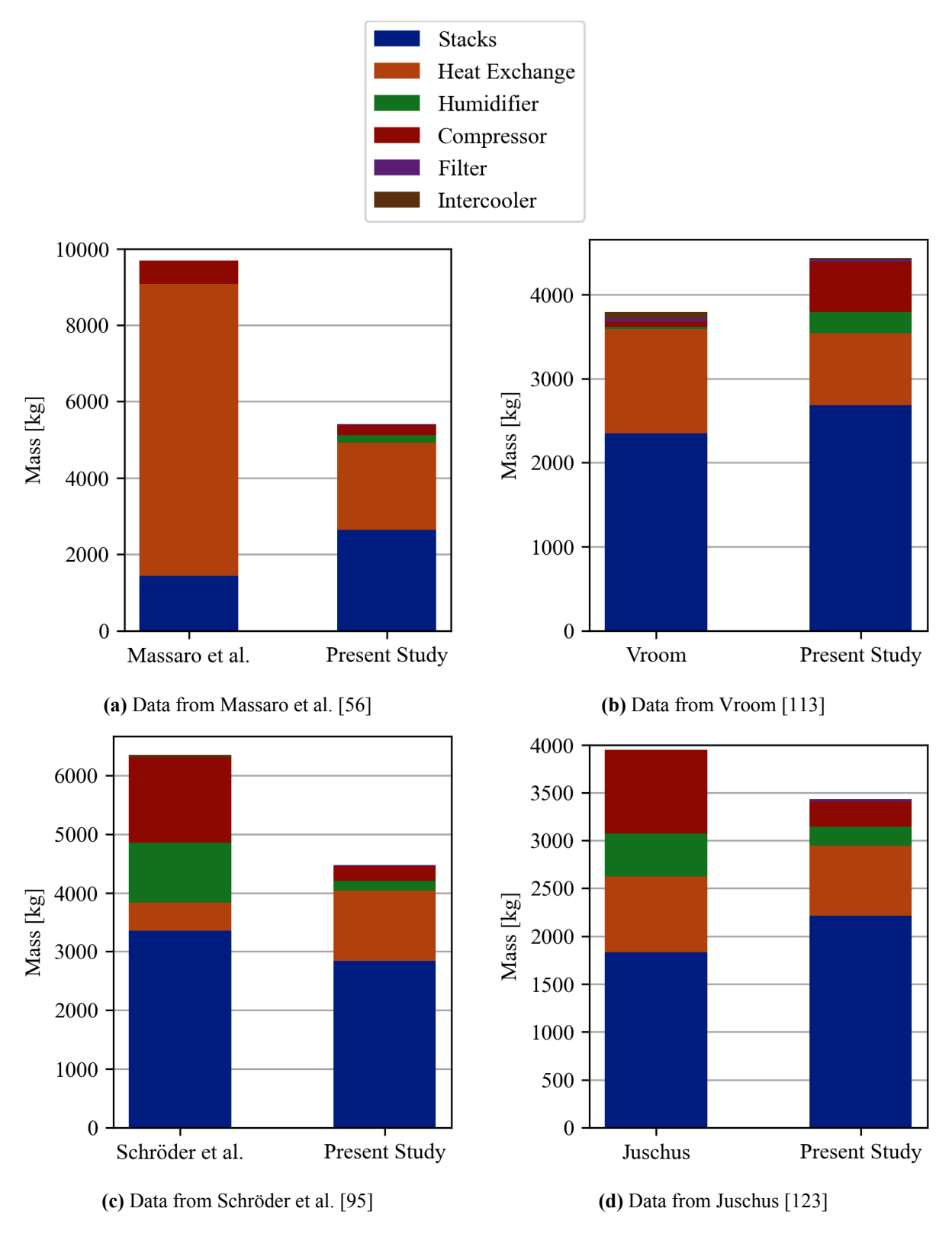


Figure 3.14: System sizing results comparison

The comparison with the study from Schröder et al. [95] gives, once again, a similar fuel cell mass, but a much lower heat exchanger weight, which is likely due to not considering the coolant mass, as it is more than half of the heat exchanger mass. The intercooler mass, even though not noticeable in the graph, is much higher due to using an air-to-air heat exchanger instead of the air-to-liquid one used in the present study. Both the compressor and humidifier

masses are much higher. From personal communications with Matthias, the study's author, the humidifier mass is expected to be much higher since the humidifier is sized to obtain much higher humidity values in that study. The compressor mass being much higher is mainly due to the compressor motor, with the value used for its mass resulting in a much lower power density. The same company that provides the values used in [95], now provides compressors with much higher power densities.

Lastly, the study from Juschus [123] results in similar values for the fuel cell and heat exchanger, with the humidifier and compressor being much heavier. In this case, this difference likely comes from a wrong equation used to calculate the mass flow of air required by the fuel cell. The equation used is missing a division by four, which, if used, would lower the mass of the humidifier and compressor to values similar to the ones obtained in the present study.

From the comparison with these studies, it was concluded that the sizing of the system procedure was working as intended and providing representative results. Any deviation from other studies had a reasonable cause and explanation.

3.4. System Simulation

Once the system is sized, it is required to simulate its performance for many operating conditions to create the engine map used by the other tools in the workflow. The system is simulated for various altitudes, Mach numbers and power levels. The same models used for the sizing of the components are implemented, but now the design is set, and only the mass flows change.

In the case of the air supply, the compressor power is calculated in the same way as for the sizing, and a verification is made to ensure that the maximum power obtained in sizing is not surpassed. In the case of the filter and humidifier, the pressure drop over them is scaled with respect to the mass flow as per the following equations

$$\Delta p_F = 600 \frac{\dot{m}_{air,FC}^2}{\dot{m}_{air,FC,design}^2} \tag{3.91}$$

$$\Delta p_H = 8000 \frac{(\dot{m}_{air,FC} + \dot{m}_{O_2,tank})^2}{(\dot{m}_{air,FC,design} + \dot{m}_{O_2,tank,design})^2}$$
(3.92)

The intercooler has its geometry fixed; therefore, to obtain the desired operating temperature at its exit, the mass flow of air that goes through the intercooler is adjusted. At its exit, the combination of air mass flow that goes through the intercooler and the one that bypasses it results in the desired temperature. This temperature is calculated with the following equation

$$T_{combined} = \frac{(\dot{m}_{air,bp} T_{t,comp,out} + \dot{m}_{air,IC} T_{t,IC,out})}{\dot{m}_{air,bp} + \dot{m}_{air,IC}}$$
(3.93)

The fuel cell simulation follows the same process used for the second optimisation, where the size is fixed and therefore the minimum DPF required is calculated, since it results in the lowest possible fuel consumption.

In the heat exchanger, since now the geometry is fixed, the amount of air mass flow required to dissipate the waste heat can be calculated with the model previously presented.

Besides going through all of the flight conditions, the engine map creation also goes through different operating pressures, from the minimum required to reach the desired operating temperature to the maximum that the components sized can withstand, to obtain the best case scenario for each flight condition. A relatively big step of 0.1atm is used to reduce computational time.

All of the simulation is checked to ensure no infeasible solutions are reached, where the systems would be operating outside the range of their capabilities.

3.5. Aircraft Design and TLARs

This study will be conducted for a regional aircraft with top level aircraft requirements (TLARs) similar to those of an ATR 72-600. The specific TLARs are shown in Table 3.8. It is important to notice that in this study, the maximum operating altitude will be assumed to be the same as the design mission altitude. This is done since to size the oxygen tanks for a potential higher altitude than the design mission, a whole new sizing procedure would have to

Table 3.8: Aircraft TLARs

TLAR	Unit	Value
Design Range	NM	1000
Design PAX	-	70
Mass per PAX	kg	95
Design Payload	kg	6650
Max. Payload	kg	6650
Cruise Mach Number	-	0.44
Max. Operating Mach Number	-	0.55
Max. Operating Altitude	FL	200
Take-Off Field Length(ISA+0K SL)	m	1385
Climb Time to FL170	min	17.5
Approach Speed(CAS)	kts	120
Wing Span Limit	m	36
Alternate Distance	NM	100
Holding Time	min	30
Contingency	-	5%

be developed. For the current study, this analysis was seen as sufficient to obtain representative results that would answer the research questions.

While the TLARs are similar to those of an ATR 72-600, the aircraft design choices are significantly different. The aircraft used in this study uses a low-wing configuration for several reasons. Firstly, the wing's weight can be directly supported by the landing gear, which reduces the structural loads that the fuselage would have to withstand for a high wing configuration. This is important since the propulsion system is much heavier than that of a conventional aircraft; therefore, this penalty would be much higher. Secondly, with a low wing, the landing gear can be integrated in the wing box, reducing the penalty of extra fairings. And finally, what makes this low-wing configuration possible is the fact that instead of having a singular propeller in each wing, the use of several, in this case three, propellers per wing reduces the diameter of each propeller, making it possible to obtain enough clearance between the propeller and the ground. Another possibility opened by having a low wing is using a conventional tail, which provides a lower mass and complexity of the tail assembly while keeping the tail out of the wing wake.

The final choice in the aircraft design to be mentioned is the diameter of the fuselage, which is significantly higher than that of an ATR 72-600 due to the use of hydrogen as fuel, since small diameters would require a significant extension of the fuselage length to accommodate the tank volume.

Results

In this section, the results obtained with the previously detailed methodology will be presented and discussed. Initially, a baseline will be defined as the comparison point for all the results obtained. Then, the oxygen enrichment study will be performed, followed by several sensitivity analyses on the effects of specific parameters on the results, from the design mission parameters to propulsion system design variations. It is important to note that in any results shown, the operation at cruise is always with ambient air, therefore at an oxygen percentage of 21%. Although some graphs have values for cruise conditions that span several oxygen percentages, only ambient air was used during the cruise. These graphs exist since the oxygen enriched operation at take-off and top-of-climb can affect the cruise operation. The decision not to use any oxygen enrichment in the cruise came from the long design mission range, which would result in a high mass of oxygen being stored in the aircraft. With that added mass, the snowball effect was too strong, and the aircraft design workflow could not converge, reflecting the infeasibility of such a study.

The resulting power supply throughout the design mission is shown in Figure 4.1. The terms ambient air and oxygen enriched refer to a fuel cell power supply with the respective oxidant supply.

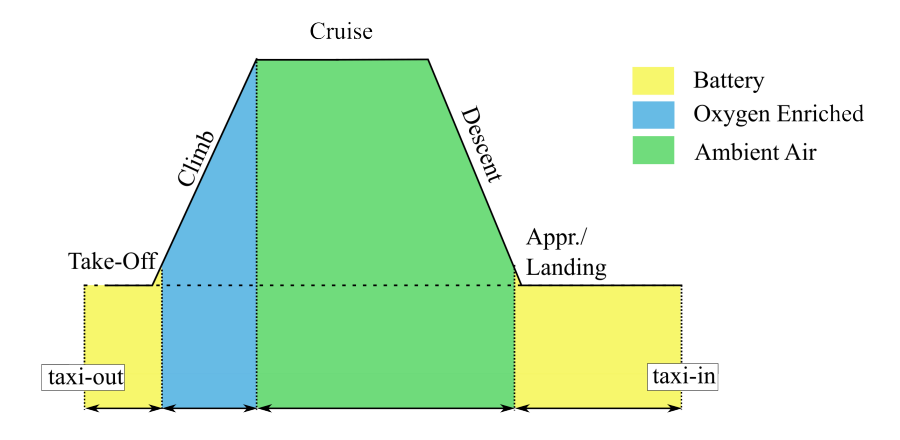


Figure 4.1: Power supply source for the flight mission segments

4.1. Baseline

The first step to reach the desired understanding of oxygen enrichment is defining a baseline result for an aircraft that operates only with ambient air as the fuel cell oxidant.

The converged solution resulted in a maximum take-off mass (MTOM) of 35225kg, which is significantly higher than the MTOM of an ATR 72-600 of 23000kg, representing an increase of 53%. While the different TLARs affect this result, as the higher range used in this study requires more fuel, such an increase is mostly associated with the previously mentioned low power density of the fuel cell system. To understand the changes in mass, its breakdown is shown in Figure 4.2.

From the MTOM breakdown, the significant effect of the fuel cell system is apparent, with its mass almost reaching six tons. This is expected since, as mentioned previously, these systems have significantly lower power densities. In addition, the battery system required for the low speed operation is also a significant part of the total

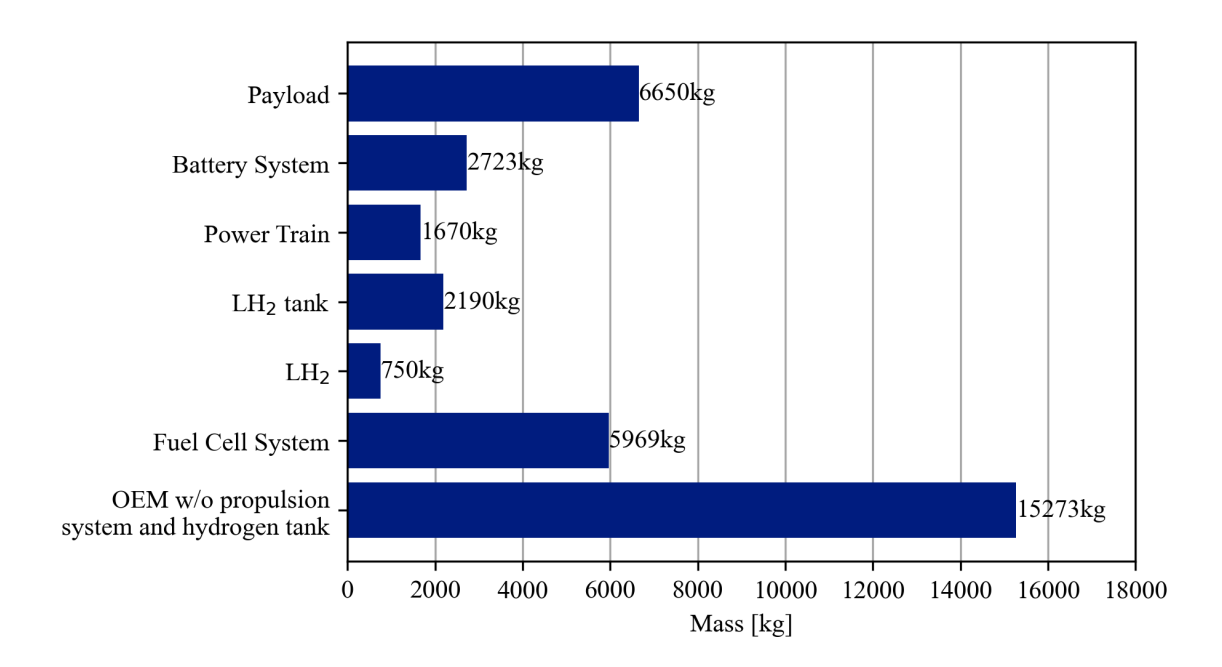


Figure 4.2: MTOM breakdown for ambient air fuel cell operation

mass, even though they are only used for short parts of the flight mission. Lastly, the added mass due to using hydrogen is also seen, where for the required hydrogen mass, the mass of the tanks is almost three times higher, showing that any change in hydrogen consumption creates a much bigger change than the one coming directly from the hydrogen mass variation.

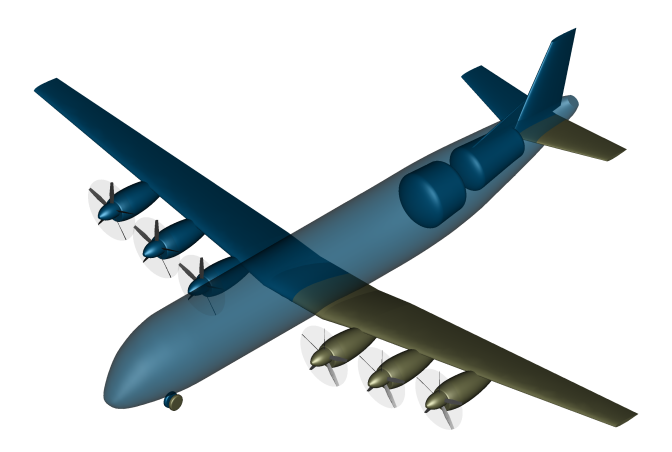


Figure 4.3: Isometric view of 21% oxygen aircraft

In Figure 4.3, the isometric view of the aircraft analysed is shown. In this figure, the configuration described in Section 3.5 can be noticed with the low wing, conventional tail, and the six pod configuration. The hydrogen tanks can be seen in the aircraft's tail, taking advantage of the available space by following the shape of the aircraft. It is also clear that if a narrower fuselage were used, the increased length due to the tanks would be high, since it is already a substantial part of the total length for this wider fuselage. The following analysis of increasing oxygen percentages will include a more detailed analysis of the aircraft and its systems.

4.2. Oxygen Enrichment

The workflow presented previously was used to obtain the aircraft design for several oxygen percentages. The first result to be given is the variation of the MTOM of the aircraft with the oxygen percentage, Figure 4.4.

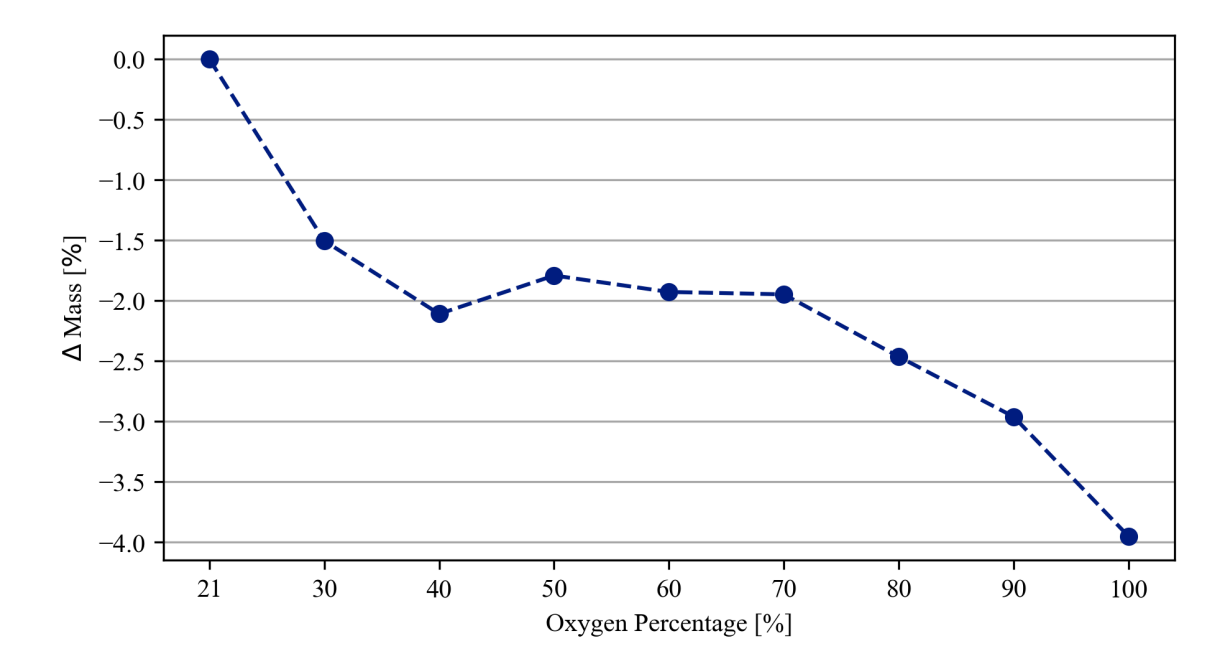


Figure 4.4: Percentage change in MTOM for varying oxygen percentages used in take-off and climb

In Figure 4.4, it is shown that an increase in oxygen percentage reduces MTOM, with two main reductions being observed. One at the initial increase of the oxygen percentage around 30% to 40%, and the other at a value of 70% and higher. These two decreases have two different origins that will be explained with more detailed plots representing the variations of specific aircraft components. The result is a maximum decrease in MTOM of almost 1500kg or around 4%.

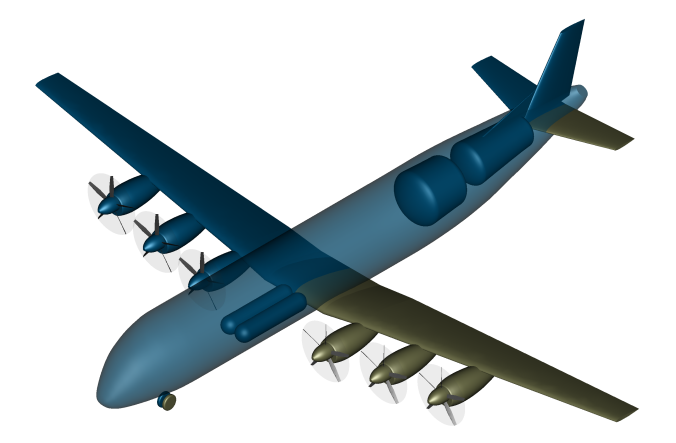


Figure 4.5: Isometric view of 50% oxygen aircraft

In Figure 4.5, the isometric view of the aircraft where an oxygen percentage of 50% is used is shown, where the placement of the oxygen tanks is also evident. They are placed in the cargo bay in front of the wing box. The choice of this configuration was made for several reasons. Firstly, by having the oxygen tanks in front of the wing, reasonable separation is obtained between the oxygen and hydrogen tanks. This is desired due to the increased risk of ignition and explosion created by higher oxygen percentage mixtures with hydrogen. Secondly, this positioning of the oxygen tanks leads to a better weight distribution of the aircraft, which reduces the centre of gravity travel during flight. A known problem for hydrogen aircraft with tanks placed in the rear section of the fuselage. Lastly, this placement prevents any increase in friction drag, since if other positions were adopted, such penalties could exist. An approach similar to that of the hydrogen tanks, where the oxygen tanks occupy the full diameter of the fuselage, would increase the required fuselage length. Lastly, an external pod configuration would also increase the

surface area of the aircraft, and therefore, both of these options would lead to a higher drag. The only downside of this configuration is that it takes up cargo space. Still, since the fuselage diameter is already bigger than that of an ATR 72, more space would be available in the cabin itself for cargo, besides the cargo area under the cabin. Knowing whether the total cargo space would be smaller or larger than the one available in ATR 72 would require a more in depth analysis of the cabin layout, which is beyond the scope of this study.

4.2.1. Fuel Cell System

The main change from an increased oxygen percentage is expected to be at the fuel cell propulsion system level, and therefore, a deeper analysis will now be conducted for this system.

One of the main contributions to the decrease in the mass of the aircraft, which also explains the initial reduction at lower oxygen percentages, comes from the decrease in the mass of the fuel cell propulsion system. In Figure 4.6, the percentage variation of the mass of the fuel cell propulsion system is presented at different oxygen levels.

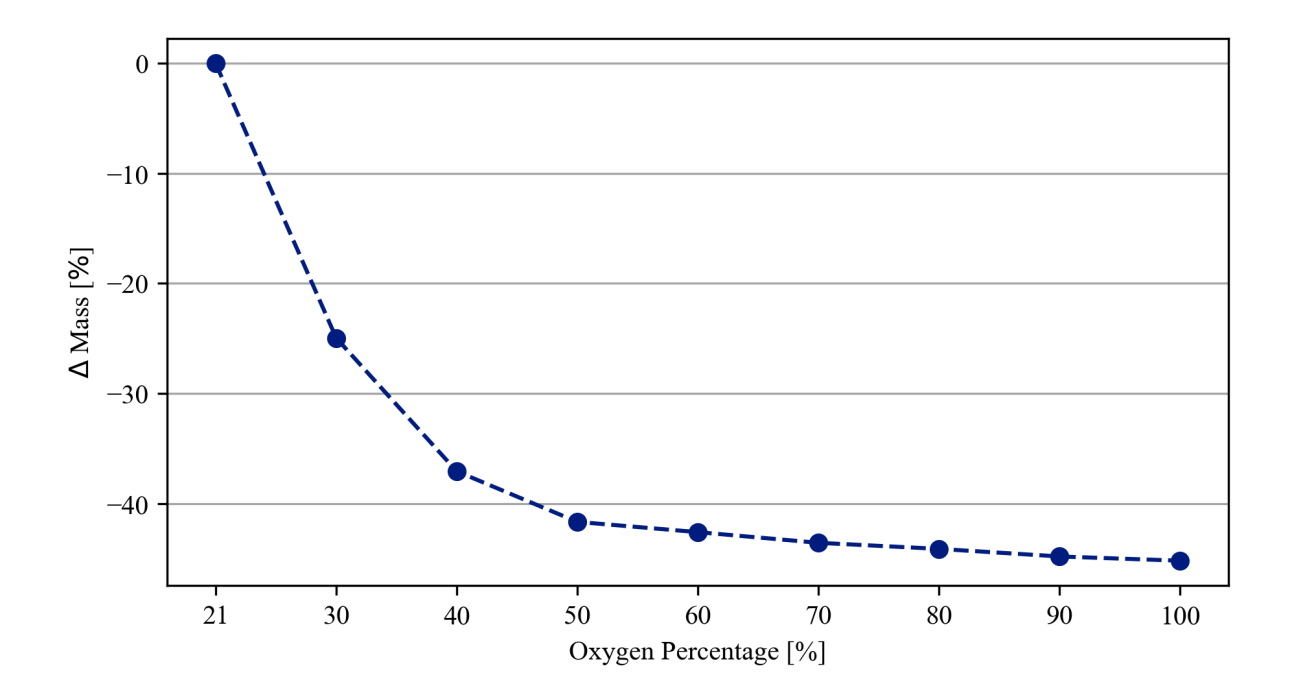


Figure 4.6: Percentage change in fuel cell system mass for varying oxygen percentages used in take-off and climb

There is a clear and substantial decrease in the total mass of the fuel cell system with the initial increases in oxygen percentage. This initial trend is not recurrent once higher oxygen percentage values are reached, where diminishing returns are observed.

To better understand how oxygen enrichment affects each component and what percentage of the total mass each component represents, the masses of the components for each oxygen percentage analysed are given in Table 4.1.

Oxygen Percentage	21%	30%	40%	50%	60%	70%	80%	90%	100%
Stack	665	460	375	333	332	322	324	323	320
Heat Exchanger	89.5	83.8	78.1	76.2	72.4	72.4	68.5	64.7	64.7
Humidifier	42.8	27.0	27.1	28.7	28.8	29.6	29.3	29.3	29.4
Filter	4.58	2.71	2.87	3.04	3.04	3.14	3.10	3.10	3.11
Intercooler	0.12	2.39	1.79	1.43	1.07	0.72	0.36	0.24	0.12
Compressor	53.0	55.4	38.8	40.9	40.9	42.0	41.6	41.6	41.7
Coolant	115	93.3	81.7	76.6	74.1	73.1	71.0	68.6	68.2
Pipe	4.71	4.56	4.40	4.35	4.24	4.24	4.13	4.02	4.02
Coolant Pump	19.6	17.4	16.6	16.0	14.8	14.4	14.2	14.1	14.3
Total	995	747	626	580	571	561	556	549	545
Sizing Point of Stack	TOC	TOC	TOC	TOC	TO	CR	CR	CR	CR

Table 4.1: Mass breakdown of fuel cell system for one pod and sizing point for stack for varying oxygen percentages used in take-off and climb

The main contribution to the mass of the fuel cell system is the fuel cell stack, which, when operating with ambient air, is 67% of the total mass. The coolant mass is the second highest, which shows how important it is to account for it, something that is usually kept out of many studies involving fuel cell systems. On the other hand, the mass of the intercooler is shown to be a very small part of the total system. This result comes from the optimisation performed since the operating pressure of the fuel cell was kept at the minimum required to obtain the desired operating temperature. This result will be examined more thoroughly when analysing the design variables obtained during the optimisation. Therefore, almost no cooling was required for the fuel cell air mass flow.

With the increase in oxygen percentage, the main change comes from a lower stack mass, which at the lowest becomes less than half of that obtained at 21%. This reduction stops after the 60% point, since before this point the stack was sized for top-of-climb or take-off, but for 70% and higher the stack was sized for cruise, a lower power segment. This result shows that the mass reduction due to oxygen enrichment in top-of-climb and take-off became too high, and higher oxygen percentages can no longer bring any benefit related to this component, with the cruise point limiting it.

The air supply components, which are the filter, compressor, intercooler, and humidifier, follow different trends. The intercooler becomes heavier once oxygen enrichment is used, a direct effect of the optimisation performed. That is because at higher oxygen percentages, the same result was not observed regarding operating pressure, as it was kept at the maximum allowed. As a result, the compressor outlet temperature was significantly higher than the temperature required in the fuel cell, increasing the demand for cooling of such a flow. The subsequent reduction with increasing oxygen percentage results from more flow being provided directly by the oxygen tank, reducing the ambient air flow to the fuel cell. Even though the mass flow of air at top-of-climb reduces due to the oxygen enrichment, the compressor initially increases its mass due to the different optimum pressure. After that point, the mass flow of air at top-of-climb reduces significantly, and the compressor sizing is done for cruise. The resulting behaviour of an increase up to 70% followed by a stagnation is directly related to the worsening efficiency at cruise up to that point, which increases the required air mass flow, followed by the stack being sized for cruise, and therefore, maintaining an almost constant efficiency at cruise. This efficiency behaviour at cruise will be looked at in more detail once the fuel consumption is presented. For the humidifier and filter, the behaviour described in the previous line is present from the first oxygen enriched point, since no other parameter besides the air mass flow affects them.

The components related to the main heat exchange are at all oxygen percentages sized for take-off due to the lower temperature differences between the ambient air and the fuel cell. In this case, an increase in oxygen percentage always results in a lower mass since with higher oxygen percentages the system operates at higher efficiencies at take-off.

Inputs Parameters

The inputs provided to the optimisation problem are also of interest, as they define the result. The inputs that change with the aircraft design are the power required in each segment and the aerodynamic efficiency of the aircraft. They are also valuable in understanding how the performance of the aircraft changes with the increase in oxygen percentage.

Starting with the power required, in Figure 4.7, the power for each segment is given, where it can be seen that the power for take-off is significantly lower than the required for climb and from the battery. This behaviour is due to the sizing point used in take-off for the fuel cell. The fuel cell is sized for a Mach of 0.2, and at that point, the aircraft has already completed its ground roll and initial climb up to 35ft; therefore, it has already passed the take-off field length (TOFL). Since the TOFL requirement has already been satisfied by the batteries and the required gradients in the following segments of take-off are less demanding, the fuel cell does not need to provide as much power as the battery. The power required by the battery is quite high, due to the high MTOM of the aircraft and the required TOFL.

The power variation with respect to the oxygen percentage follows a similar trend to the MTOM. Although it is not an unexpected result, the relative reduction is not expected. That is because for all flight segments the relative decrease in power is the same or lower than the relative change in MTOM of 4%, with a relative change of 3.4%, 4.1% and 3.3% between ambient air and 100% oxygen operation, for take-off, top-of-climb and cruise, respectively. At take-off, similar changes to the ones found in MTOM are expected. Still, for the other segments, higher values are expected since the mass reduction is much higher at these points, because oxygen is also used during take-off and climb, which would mean a higher relative mass usage before reaching cruise. This increase in the mass difference between ambient air use and higher levels of oxygen percentage can be seen in Figure 4.8, where the mass of the aircraft is shown throughout the mission. In this graph, it is clear that, while using oxygen from tanks during the climb, the weight of the aircraft reduces substantially more than under ambient air operation, with a relative change of 6% at the beginning of the cruise for 100% oxygen.

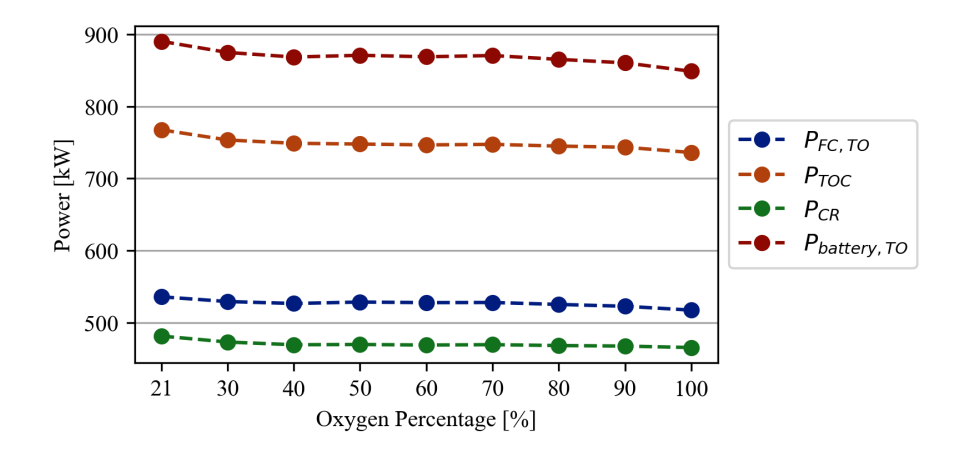


Figure 4.7: Power required at different flight phases for varying oxygen percentages used in take-off and climb

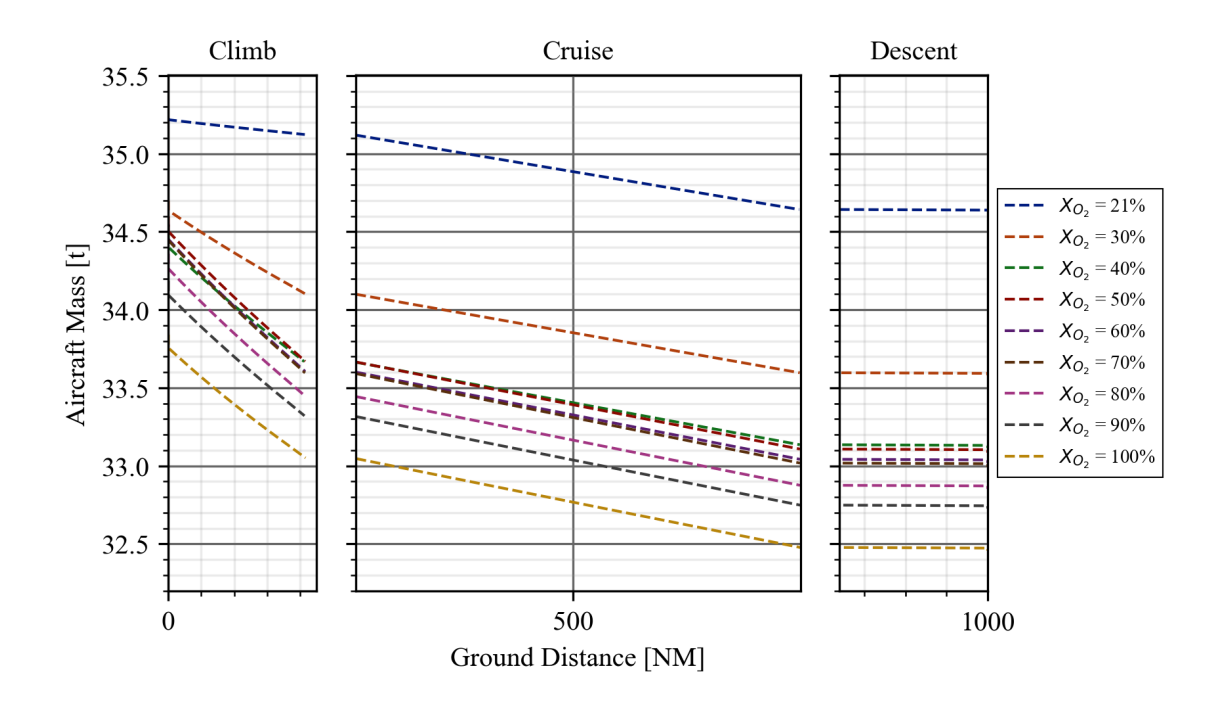


Figure 4.8: Mass of the aircraft during the design mission for varying oxygen percentages used in take-off and climb

To find the answer to why the power reduction is lower than expected, Figure 4.9 is shown, where the aircraft's aerodynamic efficiency is plotted for the different segments. The absolute values of aerodynamic efficiency are of interest since they are relatively high compared to current regional aircraft. This is primarily due to the much higher mass of the aircraft, which requires a much larger wing area, improving aerodynamic efficiency. Nevertheless, in all segments, there is a reduction of the aerodynamic efficiency with the increase in oxygen percentage, which can be attributed to the increase in fuselage length resulting from the higher hydrogen quantity required, which will be looked into at a later point. To confirm this analysis, Table 4.2 shows the constituents of the aircraft drag area, the drag coefficient multiplied by the wing reference area, at cruise.

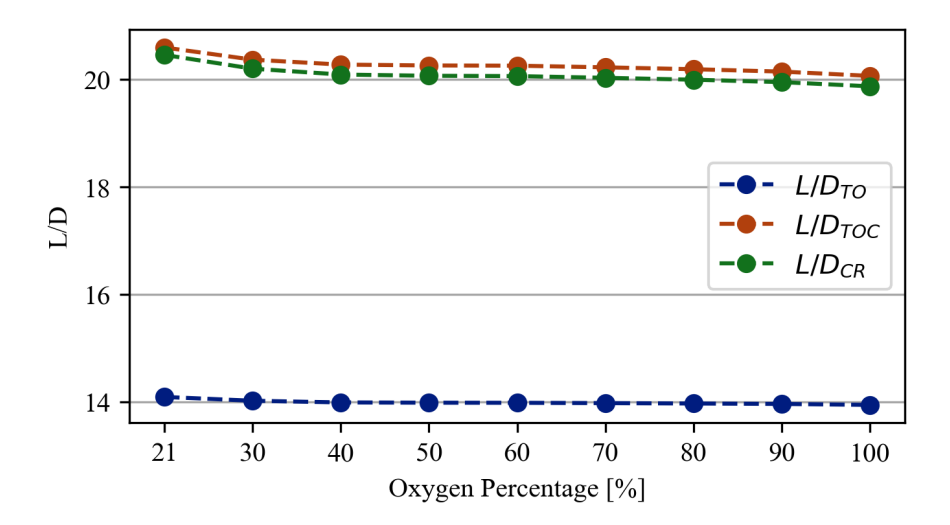


Figure 4.9: Aerodynamic efficiency of the aircraft at the sizing points for varying oxygen percentages used in take-off and climb

The drag area is used since flight conditions are kept the same, while the reference area of the wing changes, so

an analysis of the drag coefficients would not give an accurate depiction of the aircraft's drag. Although the total drag of the aircraft does reduce at higher oxygen percentages, mainly due to a reduction in induced drag, which follows the decrease of mass at cruise, this total reduction is smaller than the percentage reduction of the MTOM and even smaller with respect to the reduction of mass at the top of the climb or cruise. From the values given, it is confirmed that this smaller reduction is mainly due to an increased fuselage drag. The longer fuselage length also has benefits in reducing the horizontal tail plane area and drag due to the longer arm of the tail plane. The longer fuselage length due to the bigger tanks and consequently the longer lever arm between wing and tail plane can be seen in Figure 4.10, where the top fuselage shows the 21% case and the bottom one the 50% case.

Table 4.2: Drag area, in m^2 , at cruise of most relevant components for varying oxygen percentages used in take-off and climb

Oxygen Percentage	21%	30%	40%	50%	60%	70%	80%	90%	100%
Wing	0.585	0.576	0.573	0.575	0.574	0.574	0.571	0.568	0.562
HTP	0.130	0.128	0.125	0.125	0.124	0.125	0.125	0.126	0.127
VTP	0.073	0.071	0.070	0.070	0.070	0.069	0.069	0.069	0.068
Fuselage	0.616	0.622	0.626	0.630	0.630	0.632	0.631	0.630	0.629
Induced	0.936	0.897	0.880	0.876	0.874	0.874	0.871	0.870	0.866
Total	2.577	2.531	2.511	2.513	2.508	2.511	2.504	2.503	2.489
Difference	0%	-1.76%	-2.56%	-2.47%	-2.66%	-2.54%	-2.80%	-2.86%	-3.39%

To better explain the changes in L/D, how the wing is sized was analysed. The constraint that sizes the wing is the stall at landing. In the aircraft design tool used, openAD, the weight that is taken for the landing point can be set with specific inputs. In the case of this study, the landing mass was considered to be the same as MTOM, since for small aircraft with low fuel mass, it is a reasonable and safe approach. As a result, the fact that a larger part of the aircraft mass becomes fuel and is used up during climb is not taken into account, resulting in an oversized wing which, at top-of-climb and cruise, reduces the aircraft's aerodynamic efficiency. This effect was something that penalised the oxygen enriched cases analysed. The representation of this effect can be seen in Table 4.2 in the wing drag area. This value is the zero lift drag of the aircraft and is therefore directly related to its area, opposite to the induced drag, which is associated with the lift generated. An analysis of the behaviour of these two values reveals a reduction that follows the same reduction as the mass at cruise for the induced drag, but a smaller reduction for the wing zero lift drag, which has a similar change to the one observed in MTOM. This confirms that the wing is sized for MTOM and therefore is oversized at cruise, generating extra drag and reducing aerodynamic efficiency.

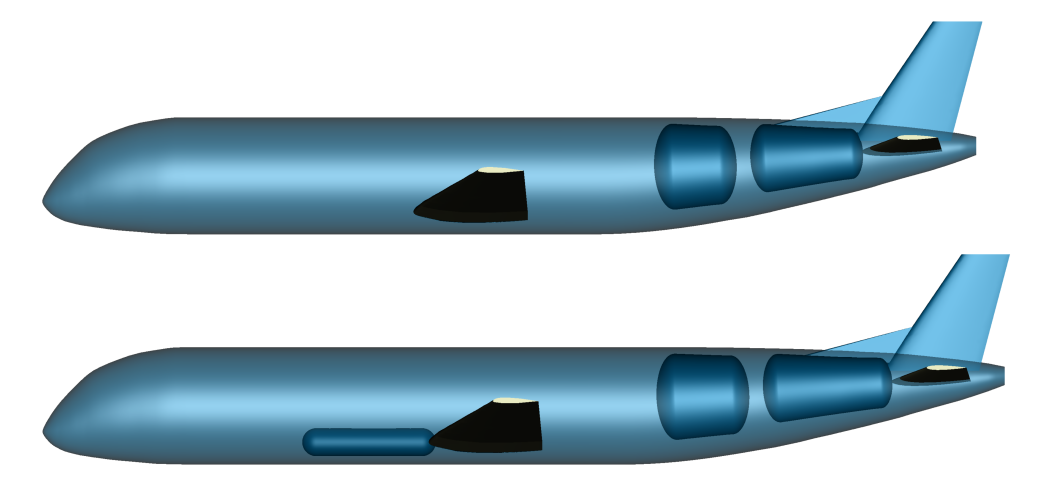


Figure 4.10: Side view of aircraft configurations, 21% oxygen at the top and 50% oxygen at the bottom

With the power data, it is also possible to compute the power density of the fuel cell stack and the complete

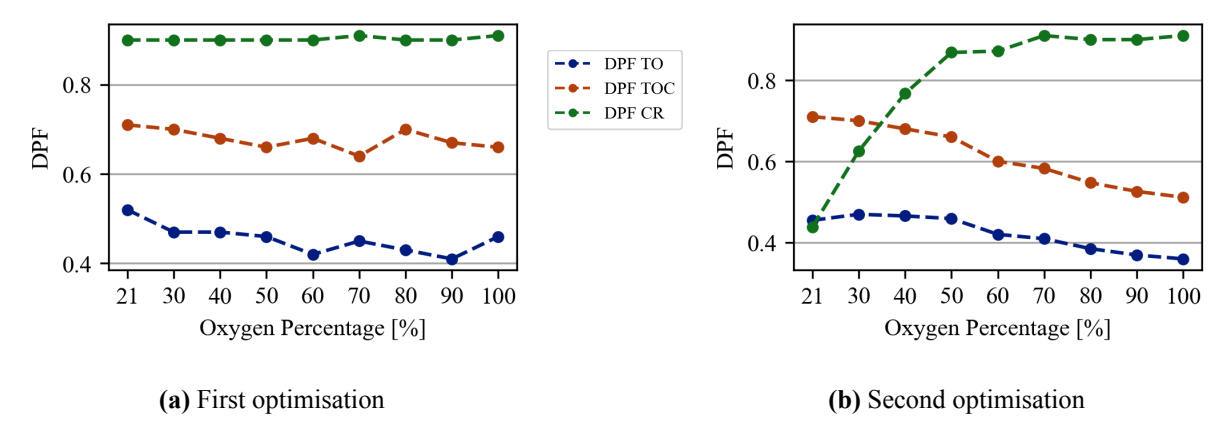


Figure 4.11: Design power factor of the three sizing points for varying oxygen percentages used in take-off and climb

fuel cell and BoP system, shown in Table 4.3. For ambient air, the stack density is lower than the maximum value previously provided of 2kW/kg since the fuel cell does not operate at maximum power. The power density of the stack increases to double its initial value, and once again after 70% since the improvements in stack mass are prevented from the stack being sized by cruise, no increase is observed. When the complete system is accounted for, the power density decreases, and in this case, after 70% minor improvements are still possible due to the heat exchange system mass reduction, as observed before. Nevertheless, it is concluded that the power density of the propulsion system can be significantly improved with oxygen enrichment.

Table 4.3: Power density $\lfloor kW/kg \rfloor$ of fuel cell stack and complete system

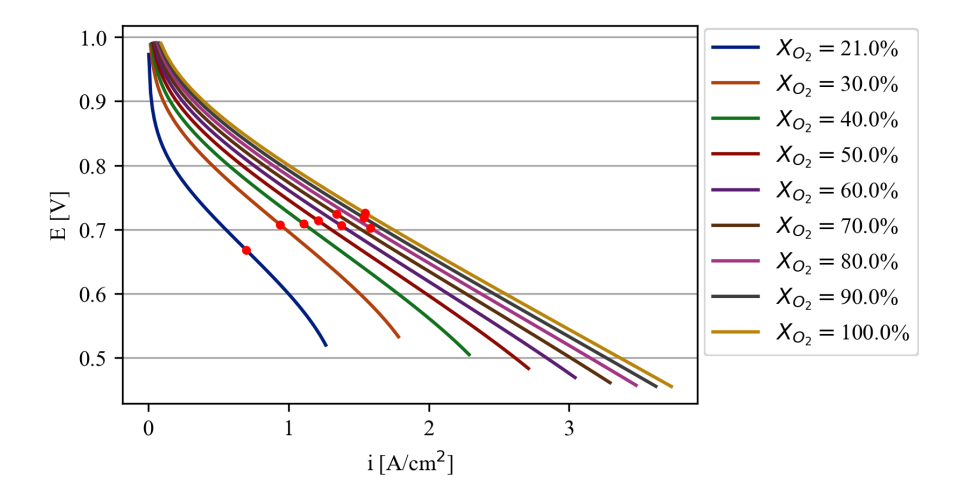
Oxygen Percentage	21%	30%	40%	50%	60%	70%	80%	90%	100%
Stack	1.15	1.64	2.00	2.25	2.25	2.32	2.30	2.30	2.30
Stack and BoP	0.77	1.01	1.20	1.29	1.31	1.33	1.34	1.35	1.35

Design Variables

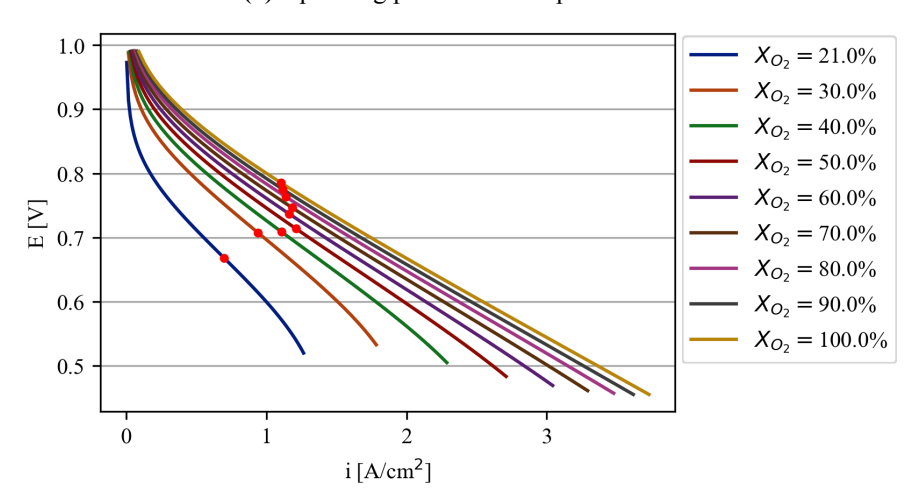
Analysing the results at the fuel cell propulsion system level and the optimisation inputs made it clear that the optimisation variables should be looked into to understand the results better.

In Figure 4.11 the DPF obtained from the initial optimisation, Figure 4.11b, and the second optimisation, Figure 4.11b, are presented. From this figure, the point that determines the stack size can be identified as the one that does not change value from one figure to another. The identified sizing point is the top-of-climb from 21% to 50%, the take-off for 60% and cruise for 70% and higher. When the stack is sized for another flight segment, the DPF reduces from the initial sizing, since a more efficient point can be used when the stack mass is higher. This shows how the DPF and efficiency are related, with a higher DPF being a synonym of a lower efficiency and vice versa. This notion will be relevant for future analysis.

A representation of what these DPF values give in terms of fuel cell operating point is given in Figure 4.12, where the red dots represent the operating point of the fuel cell, in this case for the top-of-climb phase of flight. The effect of the oxygen enrichment on the fuel cell performance is also clearly visible. At higher oxygen percentages for the same current, the voltage obtained is higher, and the maximum current is much higher. Besides that, there are diminishing returns the higher the oxygen percentage; for example, the improvements from 21% to 30% are more significant than those from 90% to 100%. Something that was already confirmed with the mass variation of the fuel cell system previously shown. Another conclusion that can be drawn from Figure 4.12a is that the operating point does not follow a clear trend, with the points being somewhat scattered. This is explained by discontinuities in the mass estimation of the fuel cell stack. Since the stacks are limited to 455 singular fuel cells per stack, the optimisation process results in a number of cells that takes advantage of this characteristic, and prevents the use of more stacks for just a few cells, requiring the weight of another set of endplates to be added.



(a) Operating points of first optimisation



(b) Operating points of second optimisation

Figure 4.12: Polarisation curves for varying oxygen percentages and representation of operating point at top-of-climb

Table 4.4 shows the number of cells, the ratio of number of cells to the maximum allowed per stack of 455 and consequently how many stacks would be required. From these values, the points where the dots in Figure 4.12 start to scatter become clear. At 60% and 70%, the same number of stacks is kept to avoid the penalty of an extra stack. The same happens from 80% to 100%, where six stacks are used. When this occurs, the operating current stays relatively similar, and the system takes advantage of the higher voltages achieved at higher oxygen percentages. In Figure 4.12b it becomes clear that once the stack is sized for a different flight phase, the system operates at higher voltages and consequently higher efficiencies due to a bigger stack than what is required being available, since from 60% the stack is not sized for top-of-climb.

Oxygen Percentage	N_{cells}	$N_{cells}/455$	N_{stacks}
21%	7209	15.84	16
30%	4955	10.98	11
40%	4061	8.93	9
50%	3610	7.93	8
60%	3171	6.97	7
70%	3145	6.91	7
80%	2722	5.98	6
90%	2726	5.99	6
100%	2653	5.83	6

Table 4.4: Number of cells and stacks required at oxygen percentage for top-of-climb initial optimisation

The operating pressure for each flight segment, shown in Figure 4.13, also shows an interesting behaviour with respect to oxygen percentage, already mentioned above. When ambient air is used, the operating pressure is kept lower; in this case, it is kept at the minimum required to reach the fuel cell operating temperature of $80^{\circ}C$. Once higher oxygen percentages are available, the optimal value becomes the maximum allowed. No change is seen at cruise since ambient air is always used, and therefore, the optimum operating pressure is always kept at the minimum.

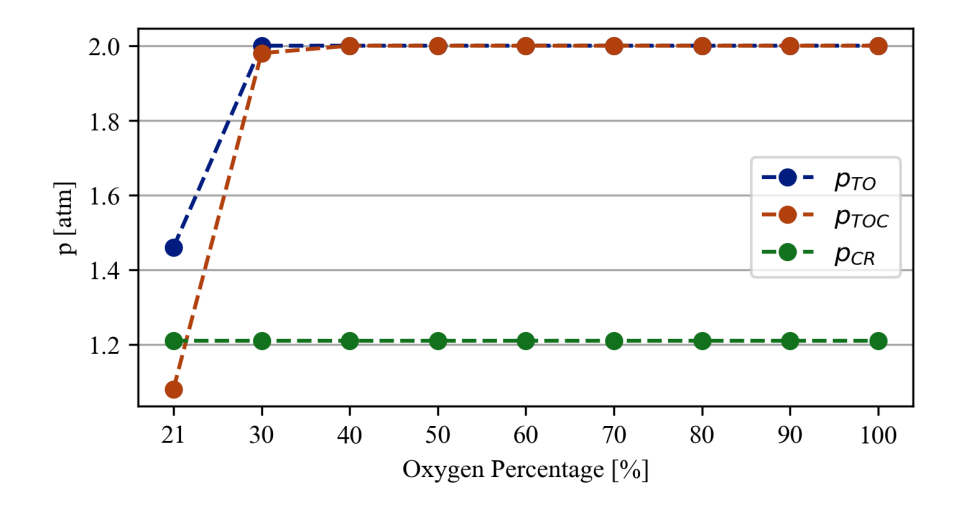


Figure 4.13: Optimum operating pressure for the varying oxygen percentages used in take-off and climb

To better understand why this occurs, the efficiency of the system for different operating pressures and oxygen percentages is shown in Figure 4.14. In these plots, two efficiencies are shown: one where the total power provided by the fuel cells is used and one where only the power used for propulsion, so total power minus compressor power, is considered. Figure 4.14a shows that when ambient air is used, the increase in total efficiency for higher operating pressures is not followed by an increase in the efficiency of the propulsion power. This means that any increase in power produced due to higher operating pressures goes directly to the compressor's power supply, and the amount of required fuel cells does not change. Therefore, a higher compressor and intercooler mass that comes from higher operating pressures is not compensated for and is then not beneficial. Besides that, it is also interesting to notice that the compressor power is around 10% of the total power produced by the fuel cell at the lowest operating pressure and increases to around 15% at the maximum operating pressure. When higher oxygen percentages are used, the same behaviour is not present. In these cases, the fact that some of the flow, the O_2 from the tank, is assumed to be supplied at the desired operating pressure, reduces the compressor power. Once this occurs, the efficiency of the propulsion power also increases with operating pressure, compensating for the increase in the masses mentioned above by reducing the amount of fuel cells required. The reduced compressor power can also be noticed due to the reduction in the difference between the two efficiencies at higher oxygen percentages.

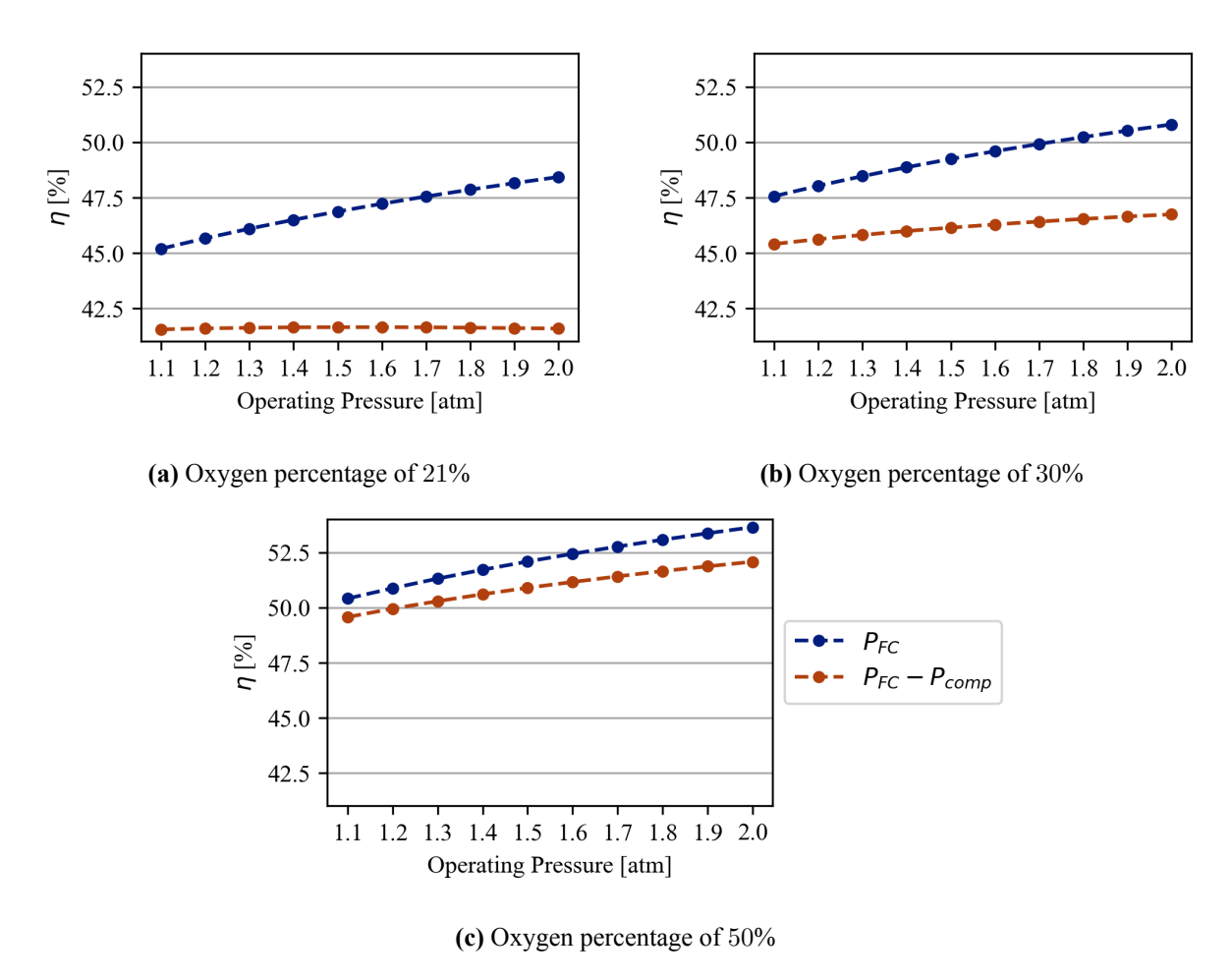


Figure 4.14: Efficiency of system with and without compressor power at a current density of $0.7A/cm^2$ for varying operating pressures

In Figure 4.15, the optimisation results are shown for the three sizing points. These plots show the values of the objective function and the mass and thrust contribution. The drag contribution is the highest at TO, reducing at TOC and is the lowest at CR. This result is expected since heat dissipation is more efficient at higher altitudes due to the larger temperature difference. With respect to the drag contribution at cruise, it is basically non-existent, neither positive nor negative, while for the other two points, it reduces with oxygen percentage as the efficiency at TO and TOC increases. In the case of the top-of-climb, a negative contribution is reached, meaning that thrust is generated instead of drag. Opposite to what happens with the drag contribution, the mass component becomes a bigger part of the total from take-off to cruise, with it following the mass variation observed before in Figure 4.6.

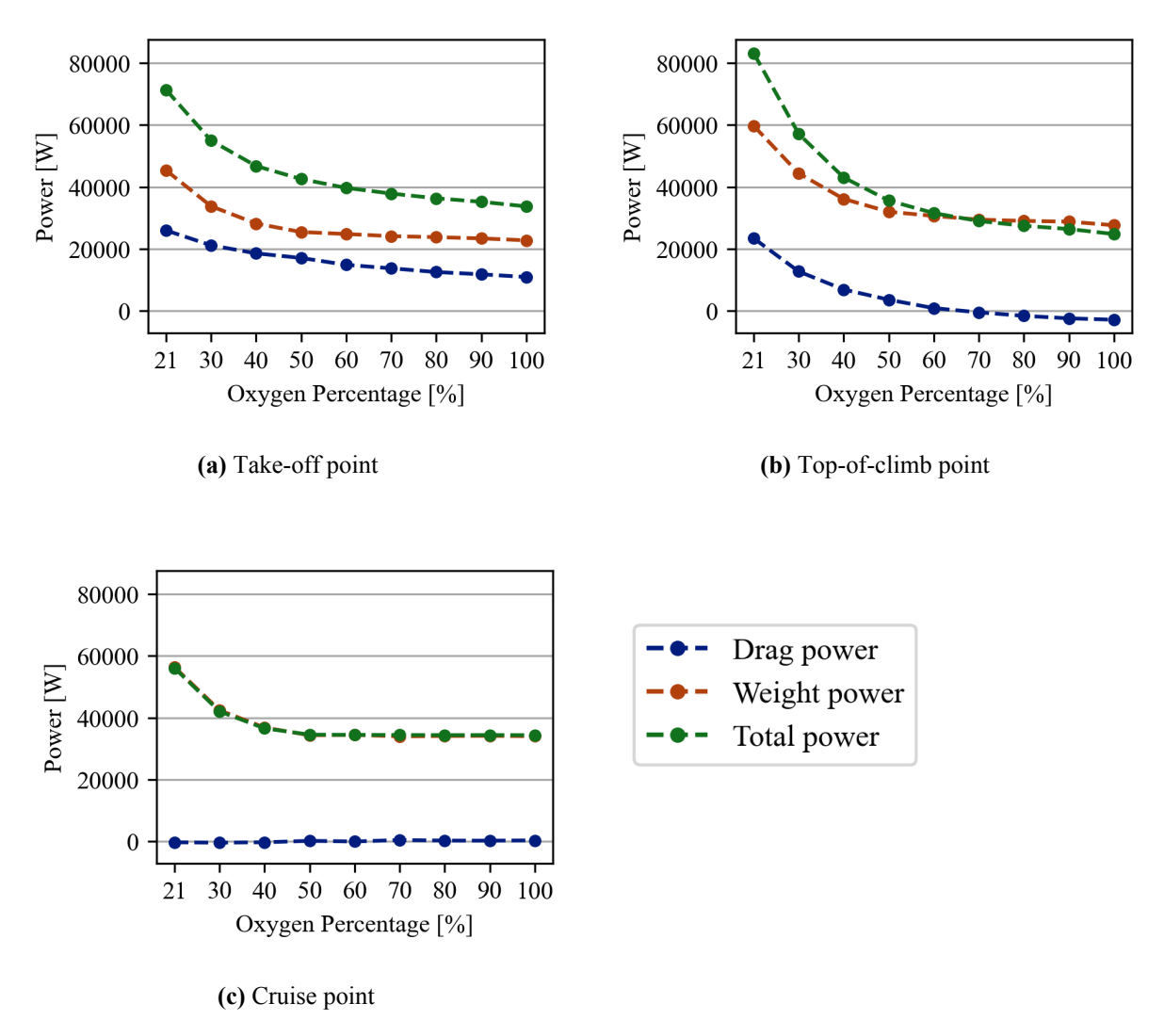


Figure 4.15: Optimisation function and mass and thrust contribution variation with oxygen percentage used in take-off and climb

4.2.2. Hydrogen and Oxygen

With all the optimisation results and inputs analysed, the effects of oxygen enrichment on total fuel consumption were studied. The hydrogen mass variation is shown in Figure 4.16a. Although a reduction in MTOM and power was possible with oxygen enrichment, this plot shows an increase in hydrogen consumption for a given mission. This result comes from the efficiency decrease shown in Figure 4.17, which occurs because the oxygen enrichment allows for smaller stacks. With smaller stacks, the oversizing at cruise is not as significant, and the system has to operate at a higher current, and therefore at a smaller efficiency. Once the system is sized for cruise, above 70% oxygen, there is a slight decrease in hydrogen mass since the efficiency at cruise remains almost constant and the power required reduces.

In Figure 4.16b, the change in the mass of oxygen and its tank is shown. In this case, the absolute values are shown, which will be the case for any other plot of oxygen mass, since no oxygen mass is present in the baseline, and therefore, a percentage change is infinite. The oxygen mass increases with oxygen percentage since to increase the oxygen percentage, more oxygen needs to be supplied by the tank, and this happens despite the increased efficiency during climb shown in Figure 4.17. At higher oxygen percentages, the opposite happens, with the oxygen mass reducing for an increasing oxygen percentage. Once the stack is sized for cruise, the efficiency becomes higher at TO and TOC, resulting in lower oxygen consumption. Another cause for the decrease in the oxygen mass, even though the oxygen percentage increases, is the relation between oxygen percentage and stoichiometric ratio used, which, for higher oxygen percentages, decreases the amount of oxygen required with respect to the stoichiometric values

necessary for the reaction. Lastly, the same power reduction that reduced hydrogen consumption also helps reduce oxygen consumption. This decrease in oxygen and hydrogen mass at high oxygen percentages is the leading cause of the reduction in MTOM, which was previously verified for higher oxygen percentages. Any change in hydrogen mass is made much more significant due to the low gravimetric efficiency of the liquid hydrogen tanks, which make up the majority of the mass associated with hydrogen. These results show that even though the weight of the aircraft, the power, and the hydrogen consumption at take-off and climb reduce, the decreased efficiency at cruise cannot be compensated for, with the hydrogen mass always being higher than in the baseline case.

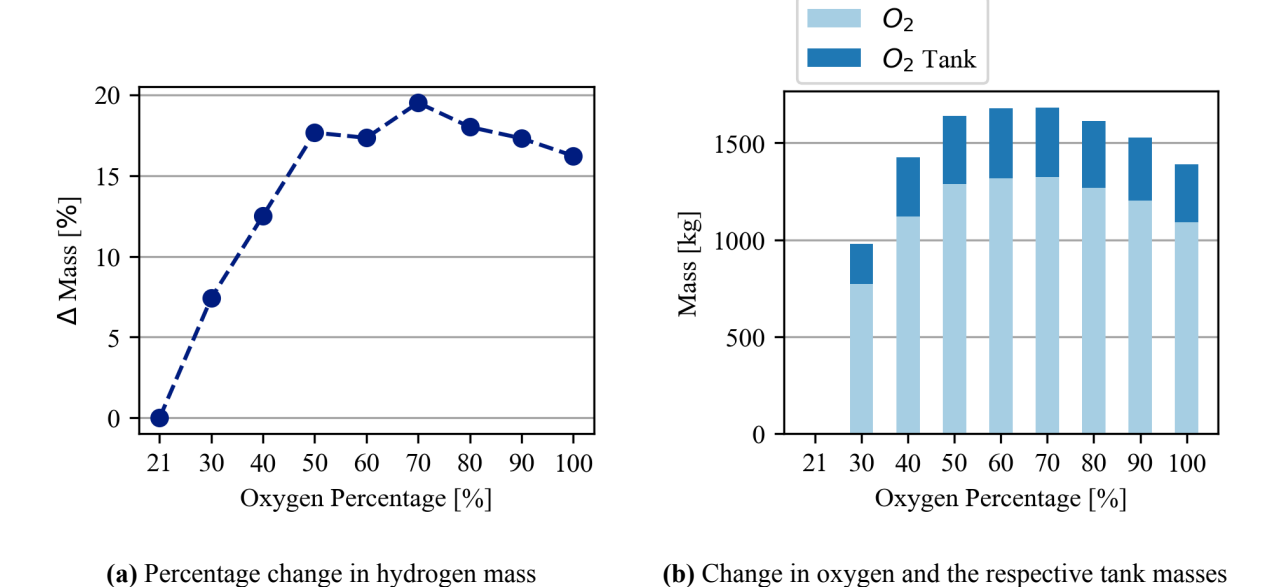


Figure 4.16: Change in hydrogen and oxygen mass for varying oxygen percentages used in take-off and climb

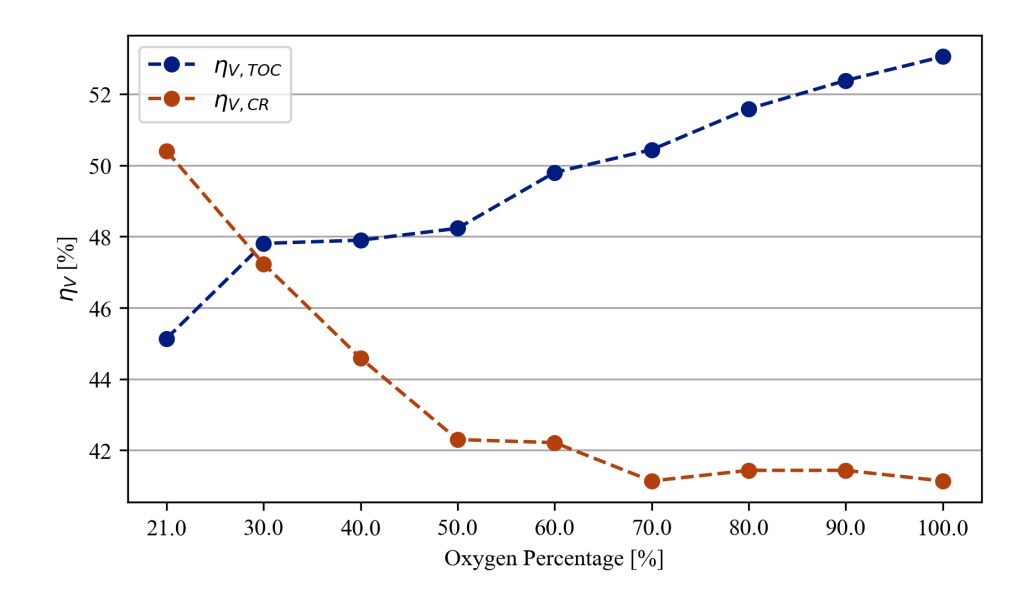


Figure 4.17: Efficiency of fuel cell system at cruise and top-of-climb for varying oxygen percentages used in take-off and climb

4.2.3. Power Train

Finally, while not a fundamental part of the current study, the mass of the power train and battery systems is shown in Figure 4.18. Since the most significant power demand came from the TOFL requirement, and these systems were sized for such a case, their mass follows the same variation observed for the MTOM. The sizing criteria defining the battery mass was the total energy required, not the power demand. It is also shown that the battery and its required cooling system have a significant effect on the mass of the aircraft, and that a fuel cell system heat exchanger capable of operating at low speeds could be beneficial to reduce the aircraft mass.

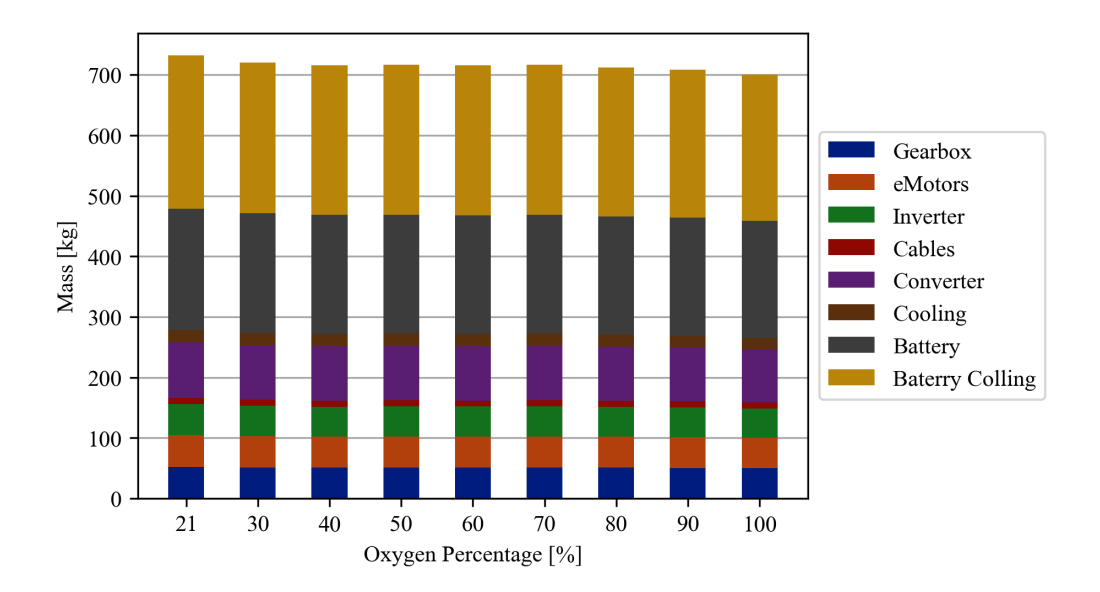


Figure 4.18: Power train and battery assembly mass breakdown per pod for varying oxygen percentages used in take-off and climb

4.3. Sensitivity Analysis

4.3.1. Cell Area

One of the main drawbacks of fuel cell propulsion systems in aviation is their low power density. As a result, efforts to improve it may increase the power density by means of, for example, increasing the fuel cell active area without any increase in its mass. Therefore, to understand how such improvements change the application of oxygen enrichment, a sensitivity analysis, where the fuel cell area is increased, is performed.

An initial analysis is performed by comparing the results obtained for the operation with ambient air exclusively. Figure 4.19 shows how the increase in fuel cell area has a significant effect in reducing the MTOM. This is expected since the power density of the fuel cells increases and, therefore, a lower mass is required to provide the same power. This reduction will contribute to snowball effects, where every other system becomes lighter. Besides that, there are also changes that result from obtaining different optimisation points, as it will be explained with the use of the values in Table 4.5.

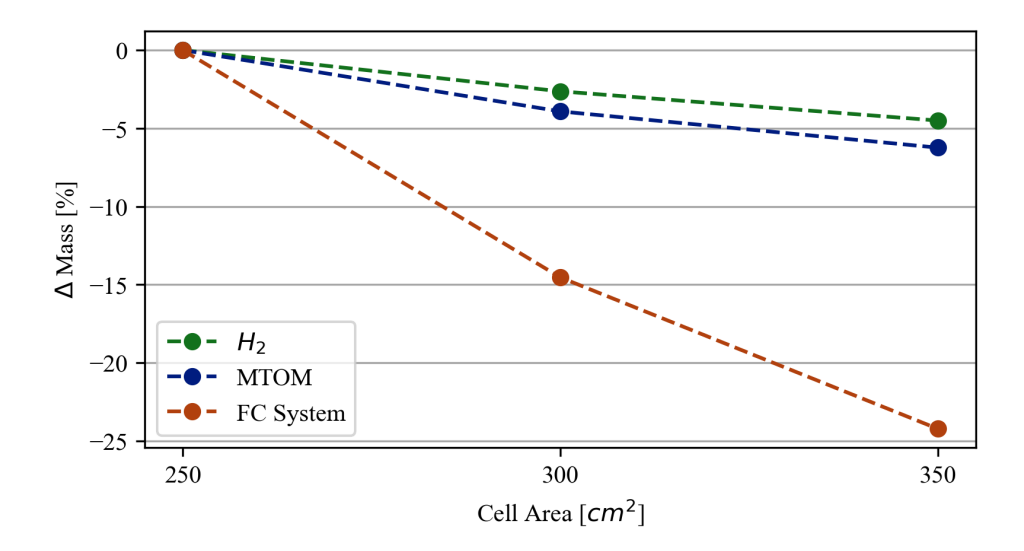


Figure 4.19: Percentage change in MTOM, fuel cell system mass and hydrogen mass for varying fuel cell areas at an oxygen percentage of 21% at take-off and climb

In Figure 4.19 the change in fuel cell system mass for the studied fuel cell areas is also shown, where it can be seen that there is a significant reduction in the total mass of the system. Knowing that the most relevant component for the fuel cell system mass is the fuel cell stacks themselves, it is expected to obtain such a substantial reduction due to the increase in their power density.

While the primary reduction comes from a decrease in the fuel cell mass, the optimisation results also change slightly. In Table 4.5, the mass of each component and the DPF in each flight point are shown. The main reduction in mass stemming from the fuel cell stack is confirmed, but all other systems also follow the same trend of a lower mass for a higher fuel cell area. This can be attributed to two factors. Firstly, the mass of the aircraft is reduced, and consequently, its power requirement is also smaller. If the power required reduces, the systems become lighter at the same operating point or DPF. Secondly, the DPF changes for different cell areas, representing a change in the optimum operating point. Once the cell area, or power density, increases, operating at a higher DPF is less of a penalty to the optimum point in terms of mass, and therefore a new optimum is found at slightly higher DPFs with a lower drag.

Table 4.5: Mass breakdown for one pod and DPFs of fuel cell system for varying fuel cell areas at an oxygen percentage of 21% at take-off and climb

Cell Area	$250cm^2$	$300cm^{2}$	$350cm^2$
Stack	665	543	460
Heat Exchanger	89.5	85.7	83.8
Humidifier	42.8	41.2	40.1
Filter	4.58	4.40	4.28
Intercooler	0.119	0.119	0.119
Compressor	53.0	51.1	49.8
Coolant	115	102	92.8
Pipe	4.71	4.61	4.56
Coolant Pump	19.6	18.8	18.2
Total	995	850	754
DPF TO	0.451	0.446	0.440
DPF TOC	0.710	0.700	0.690
DPF CR	0.438	0.437	0.434

The more efficient operating points, together with the reduction in required power, amount to a decrease in hydrogen mass for higher fuel cell areas, as shown in Figure 4.19.

The analysis performed for the ambient air operation applies to any oxygen percentage. However, changes arise at the aircraft level due to the importance of the fuel cell mass reduction in the initial decrease of MTOM.

In Figure 4.20a, the MTOM change is shown for the different fuel cell areas and several oxygen percentages. The same order in terms of MTOM is kept throughout the different oxygen percentages, with the higher cell area always resulting in a lower MTOM. What is interesting to note is that the variation with respect to oxygen percentage changes significantly. The main difference comes from the initial increase in oxygen percentage, where the lower fuel cell system mass, mainly from the fuel cell stack reduction, could compensate for the addition of oxygen and its tank mass and the higher hydrogen mass. Once the fuel cell mass becomes a smaller portion of the total mass, there is not enough reduction from the increased oxygen percentage to compensate for the oxygen, hydrogen and tank mass. For a fuel cell area of $300cm^2$ there is still a slight reduction in MTOM, but for a fuel cell area of $350cm^2$ the increased oxygen percentage results in a higher MTOM. At the mid range percentages, instead of a stabilisation of MTOM, there is an increase for the higher fuel cell areas. This is a result of the increasing oxygen and hydrogen mass, which is not compensated for by the reduction of fuel cell mass, as was the case for the lower fuel cell area. Although these trends did change, the subsequent variation at oxygen percentages higher than 70% remained. MTOM decreased due to the lower oxygen and hydrogen masses at higher percentages, which comes from the reduction in the stoichiometric ratio and the power required. In the case where the cell area is $350cm^2$ even this final reduction is not enough to reach a reduction in MTOM with respect to the ambient air case for the studied percentages. If a percentage of 100%, it is expected that MTOM would be lower than the ambient air case.

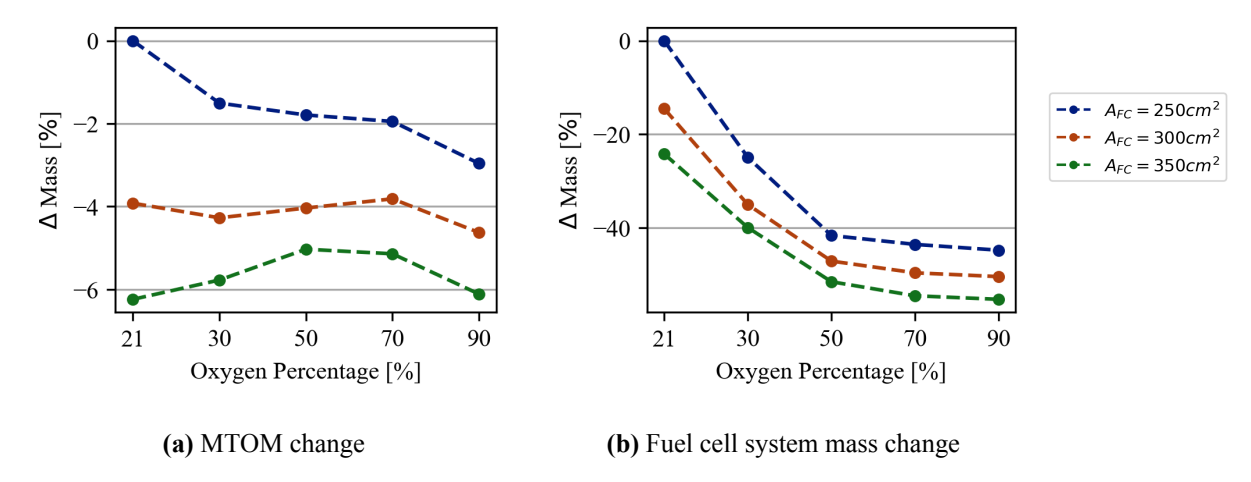


Figure 4.20: Percentage change in MTOM and fuel cell system mass for varying fuel cell areas and oxygen percentages used at take-off and climb

The fuel cell system mass change is shown in Figure 4.20b, where the same behaviour with respect to oxygen percentage is seen for any fuel cell area. The difference between the different cell areas of the fuel cell system mass reduces with higher oxygen percentages as the mass of the fuel cell stack becomes a smaller part of the total mass. Therefore, the difference generated by the higher fuel cell areas, and consequently higher power densities, becomes less significant.

Lastly, the mass of hydrogen and oxygen is shown in Figure 4.21a and Figure 4.21b, respectively. The results show the same reduction in mass from $250cm^2$ to $350cm^2$ due to the reasons previously mentioned of mass reduction and increased efficiency. The same variation with respect to the oxygen percentage observed previously is present, since the slight changes in MTOM variation with oxygen percentage observed in Figure 4.20a were not significant enough to change this behaviour.

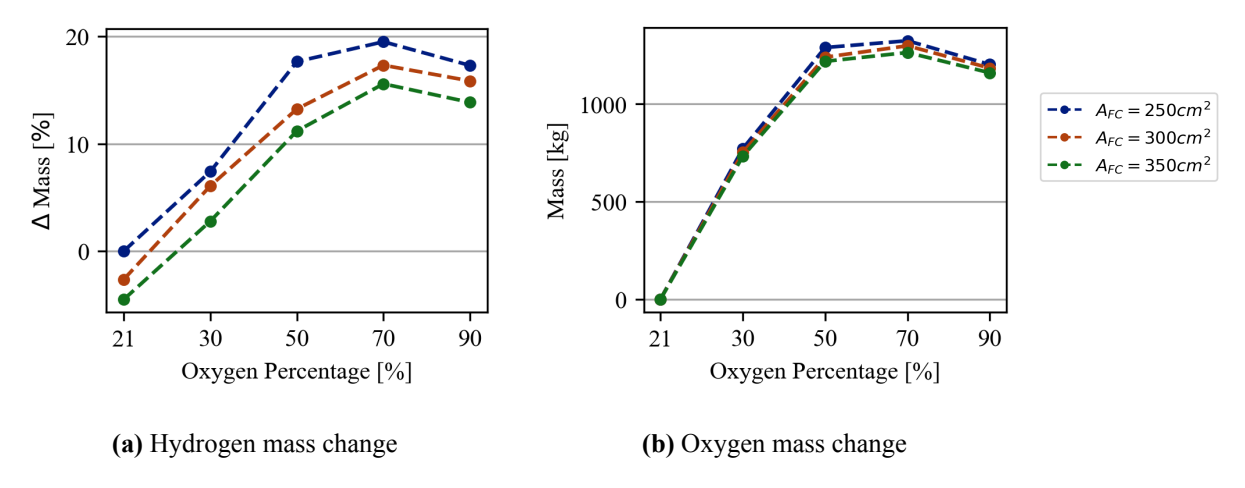


Figure 4.21: Percentage change in hydrogen mass and change in oxygen mass for varying fuel cell areas and oxygen percentages used at take-off and climb

4.3.2. Heat Exchanger Area

The heat exchanger was initially defined with a set of height and width such that it would fit inside the nacelles and would be able to dissipate the generated waste heat. Since it influences the optimisation results and the aircraft design, it is necessary to evaluate how changing its value affects the results. To do this, it was decided that the width of the heat exchanger would be changed. This is because changing the height of the duct where the heat exchanger is placed leads to an increase in the length it occupies, due to the tilt angle. Because no detailed analysis is done with respect to the placement of the heat exchanger, the more straightforward approach was chosen, where the width is changed, and, together with it, the diameter of the nacelle is also adjusted, instead of altering the length of the nacelle.

To understand the effects of changing the heat exchanger area, two values are used, a width of 0.9m and a width of 1.1m which represent a decrease and an increase of 10%, respectively, in relation to the 1m previously used.

In Figure 4.22 the MTOM is shown for each heat exchanger width. There is a clear relation between the heat exchanger width and MTOM, with an increase in the heat exchanger area resulting in a lower MTOM.

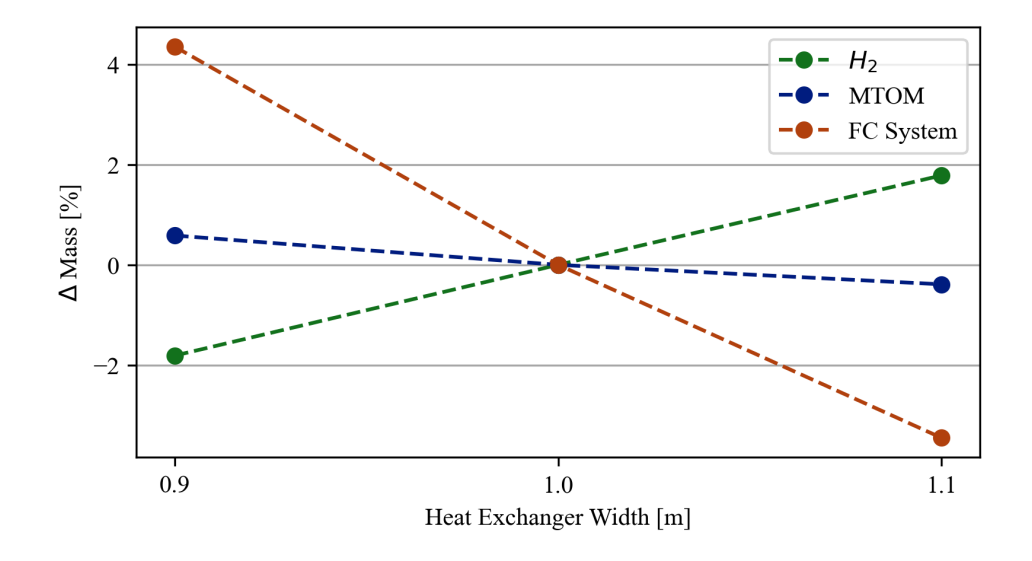


Figure 4.22: Percentage change in MTOM, fuel cell system mass and hydrogen mass for varying heat exchanger widths at an oxygen percentage of 21% at take-off and climb

The reduction in MTOM is partially explained by the lower values obtained for the mass of the fuel cell system, shown in Figure 4.22. The lower mass of the system is a direct effect of a larger heat exchanger area, which shifts

the optimum point to a higher DPF, since a lower drag is obtained for the same waste heat and mass flow of air. The reason for a lower drag is the reduced velocity of the flow in the heat exchanger. A lower velocity at the heat exchanger also decreases the efficiency of the heat exchange, potentially leading to heavier heat exchangers.

The mass breakdown and DPF are shown in Table 4.6, where increasing DPF for larger widths results in a reduction of the stack mass and the increase of all other systems mass, due to lower efficiency. The only exception is the coolant mass, which also decreases, since a significant portion of it is associated with the stack volume. In this case, the heat exchanger mass and volume increase was not greater than the decrease in stack volume, resulting in a lower coolant mass.

Table 4.6: Mass breakdown for one pod and DPFs of fuel cell system for varying heat exchanger widths at an oxygen percentage of 21% at take-off and climb

HE Width	0.9m	1m	1.1m
Stack	711	665	628
Heat Exchanger	85.6	89.5	92.1
Humidifier	41.8	42.8	43.6
Filter	4.46	4.58	4.66
Intercooler	0.239	0.119	0.477
Compressor	51.77	53.0	55.1
Coolant	120	115	112
Pipe	4.85	4.71	4.56
Coolant Pump	18.8	19.6	20.2
Total	1038	995	961
DPF TO	0.425	0.455	0.480
DPF TOC	0.660	0.710	0.750
DPF CR	0.406	0.438	0.467

As already concluded previously, an increase in DPF leads to lower efficiency and therefore a higher hydrogen consumption, which is verified in Figure 4.22. Even though this is the case, the increase in hydrogen and tank mass is not enough to counter the decrease in fuel cell system mass, and therefore, the MTOM does reduce for higher heat exchange areas.

In Figure 4.23a the MTOM variation with oxygen percentage is shown for the different heat exchanger areas. In this case, a completely different behaviour is observed, where the MTOM shows significantly larger reductions for the smaller area. This is attributed to an effect already seen in the studies presented above, where the most significant reduction in mass comes from the fuel cell stack. Therefore, for a heavier stack, the absolute reduction in mass is greater. Due to this greater reduction, the balance between the reduced fuel cell system mass and the added oxygen mass change, and a constant decrease in MTOM is achieved. The opposite effect is present for the larger width, where the stack mass is lower, and consequently, a less significant reduction is possible, leading to a lower reduction in MTOM. Due to these changes, the order found with ambient air operation inverts at the higher oxygen percentages, where the lower the width, the lower the MTOM. Figure 4.23b shows this more significant reduction in mass at lower oxygen percentages. At higher values, the total mass of the fuel cell system is similar in any heat exchanger area, which is a result of the snowball coming from the lower MTOM, since the power required for a width of 0.9m is significantly reduced. This power reduction negates the difference in operating point seen before, which resulted in a heavier system for the lower area.

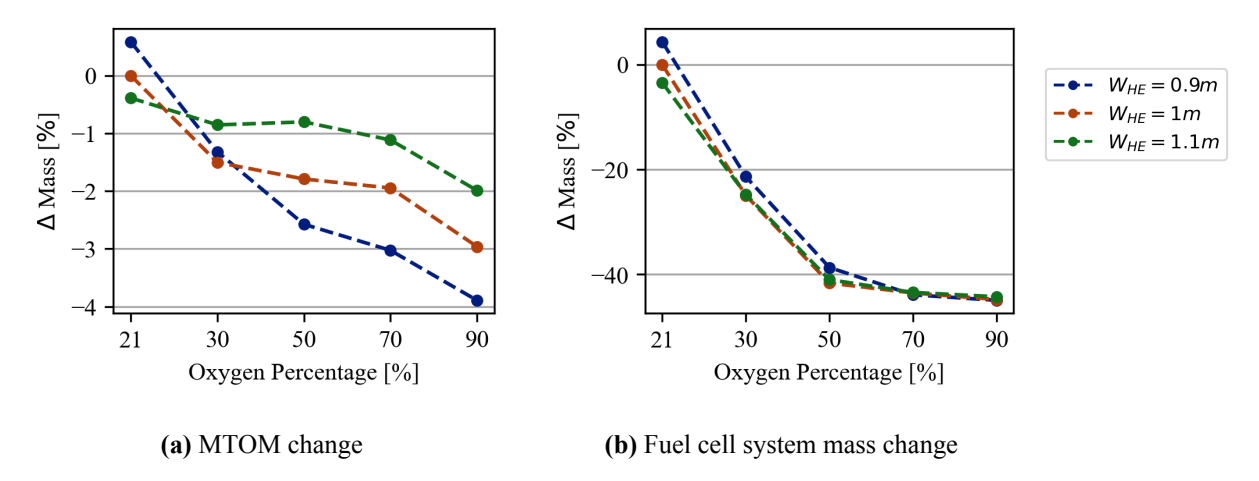


Figure 4.23: Percentage change in MTOM and fuel cell system mass for varying heat exchanger widths and oxygen percentages used at take-off and climb

In terms of oxygen and hydrogen mass, no change in behaviour is seen for the different widths. With Figure 4.24a and Figure 4.24b showing the same trends seen before, where the increase in oxygen percentage results in more hydrogen and oxygen being consumed with a slight reduction in the higher percentages. Nevertheless, the mass of hydrogen remains higher than that obtained for ambient air operation. The order of highest mass to lowest is also kept throughout the different oxygen percentages, with the lower width being more efficient and the higher width less efficient.

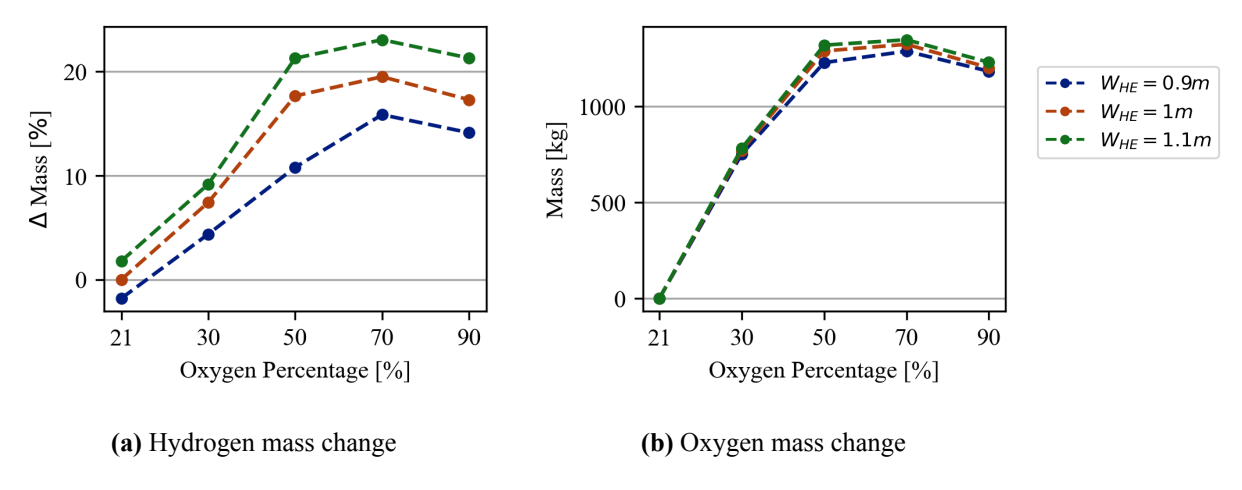


Figure 4.24: Percentage change in hydrogen mass and change in oxygen mass for varying heat exchanger widths and oxygen percentages used at take-off and climb

4.3.3. Flight Level

The use of oxygen enrichment during climb creates a dependence on the added mass due to oxygen storage with respect to the altitude of the design mission. A higher flight level results in a longer climb time, increasing the total oxygen required, and vice versa. Besides that, different flight levels also affect the aircraft performance and also change the propulsion system sizing, which is why the effect of changing the flight level of the design mission will be looked at in this section.

At lower flight levels, the MTOM of the aircraft increases, shown in Figure 4.25, indicating that the expected lower oxygen mass does not translate to a lower MTOM. The resulting reduction in mass for higher flight levels comes from a lower fuel cell system and hydrogen mass.

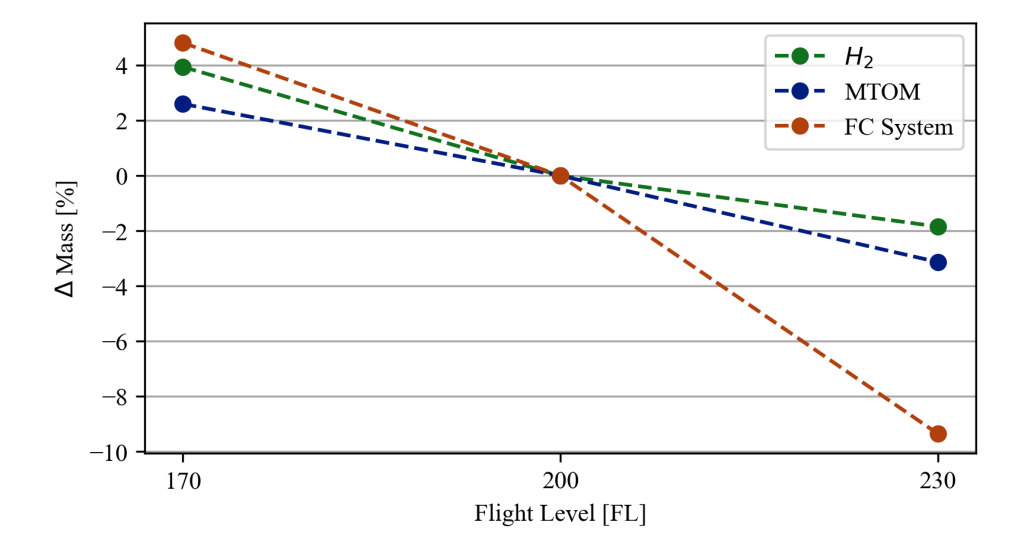


Figure 4.25: Percentage change in MTOM, fuel cell system mass and hydrogen mass for varying cruise altitudes at an oxygen percentage of 21% at take-off and climb

In Figure 4.25 for higher altitudes, a lower mass of the fuel cell system is shown. This behaviour follows the same reasoning as that provided for the variation with heat exchanger width, since the optimisation provides a lower DPF for a lower flight level, resulting in a higher mass but a more efficient system. In this case, the shift of the optimum point is due to the variations in temperature with altitude. At lower altitudes, the ambient temperature is higher and the heat exchange is less efficient; therefore, a more efficient point is beneficial. The trend observed for the balance of plant systems differs from the previously shown trend in the heat exchanger width case, where the lower DPF and higher efficiency resulted in lower masses, with only the compressor following this trend. This suggests that some other major change is occurring in the aircraft sizing, because this trend is inconsistent with previously observed cases. The major change causing this shift is in the power requirements. For a higher MTOM, the power requirement of the aircraft increases. Still, for the previous sensitivity analysis of the heat exchanger area, the higher efficiency of the system could compensate for the extra power. In this case, besides the increased MTOM, at lower altitudes, the aircraft's aerodynamic efficiency is significantly reduced, increasing the power required even more. With a decrease of 3.38% in aerodynamic efficiency, which, together with the MTOM increase, results in an increase of 11.27% in power required, from FL230 to FL170. Even though the system is more efficient, the increase in power requires larger components, explaining the observed change. The compressors are an outlier since, at higher altitudes, more compression is needed for the lower pressure ambient air.

170	200	230
707	665	583
91.4	89.5	89.5
44.0	42.8	40.3
4.70	4.58	4.30
0.239	0.119	0.119
50.9	53.0	53.0
120	115	108
4.76	4.71	4.71
19.8	20.0	18.8
1043	995	902
0.447	0.455	0.494
0.690	0.710	0.750
0.434	0.438	0.483
	707 91.4 44.0 4.70 0.239 50.9 120 4.76 19.8 1043 0.447 0.690	707 665 91.4 89.5 44.0 42.8 4.70 4.58 0.239 0.119 50.9 53.0 120 115 4.76 4.71 19.8 20.0 1043 995 0.447 0.455 0.690 0.710

Table 4.7: Mass breakdown for one pod and DPFs of fuel cell system for varying flight levels at an oxygen percentage of 21% at take-off and climb

The increased power also increases hydrogen consumption, where for the more efficient system, at flight level 170, the mass of hydrogen actually increases.

The variation with the oxygen percentage of the aircraft MTOM and fuel cell system mass, shown in Figure 4.26a and Figure 4.26b, respectively, depicts the same results previously encountered. The heavier the fuel cell system, the more significant the MTOM variation and the relative decrease in the fuel cell system mass.

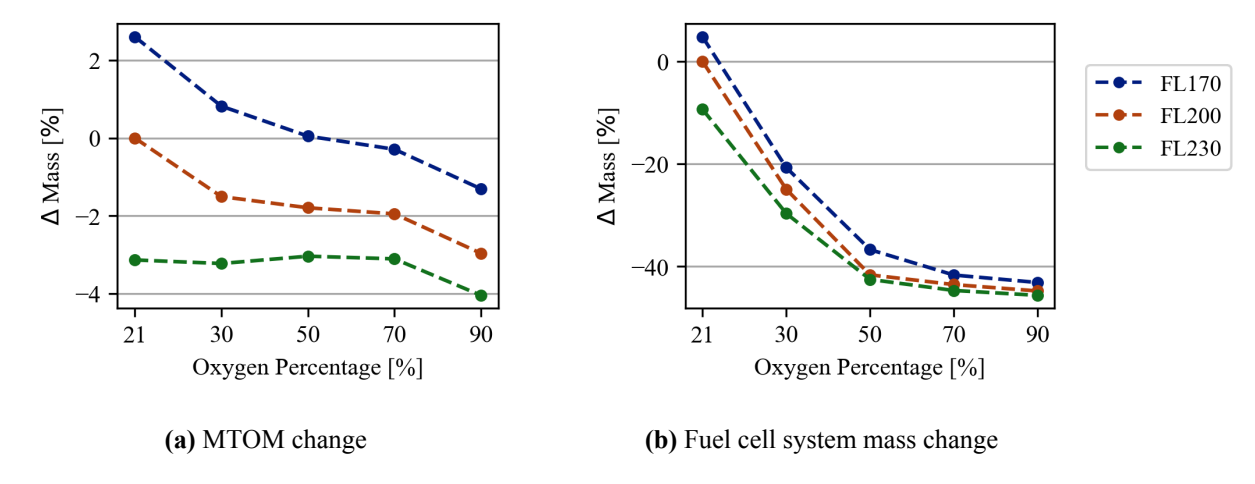


Figure 4.26: Percentage change in MTOM and fuel cell system mass for varying cruise altitudes and oxygen percentages used at take-off and climb

The mass of oxygen required for climb and take-off is reduced with lower flight levels, as seen in Figure 4.27b. However, this reduction was not significant enough to create an overall positive effect on the aircraft MTOM. The mass of hydrogen required for the mission also remains lower for the higher flight level, as shown in Figure 4.27a, since the oxygen percentage does not significantly change the comparative results between flight levels.

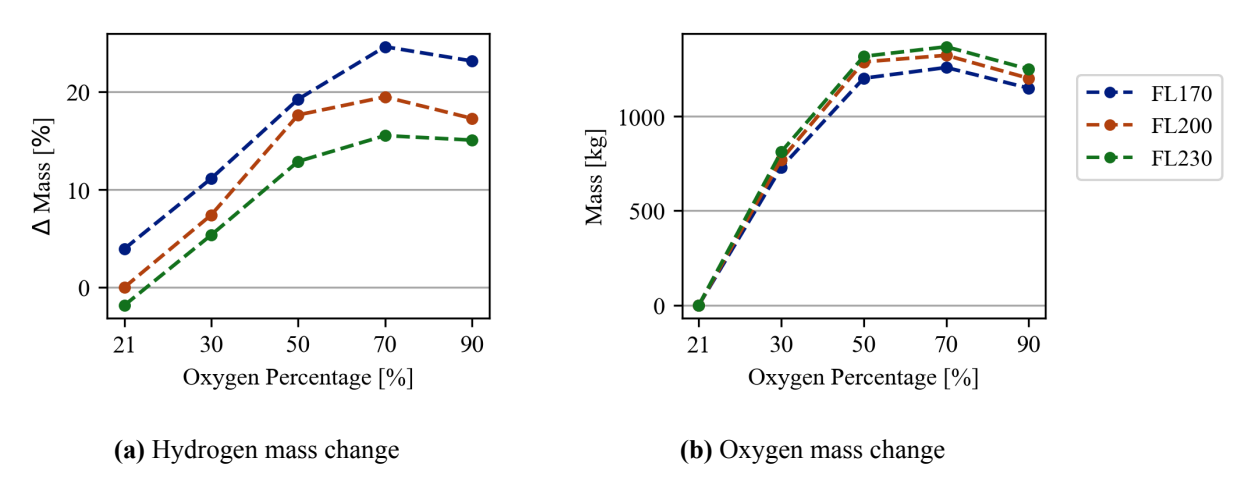


Figure 4.27: Percentage change in hydrogen mass and change in oxygen mass for varying cruise altitudes and oxygen percentages used at take-off and climb

Conclusion and Recommendations

In this chapter, a summary of the results obtained and the answers to the research question are discussed. Followed by recommendations on what could improve the present study by solving some of its limitations.

5.1. Conclusion

This study achieved the objective of creating a sizing procedure for a fuel cell propulsion system by developing and validating a methodology that could consider the effect of different operating conditions on the performance of the fuel cell and the size of the required balance of plant components. The developed methodology achieved a more detailed and accurate sizing of the fuel cell propulsion system. In addition to the system sizing, its simulation was conducted under different flight conditions and power requirements to enable the integration of the developed methods into a preliminary aircraft design workflow. As a result, not only was the sizing of the propulsion system achieved, but its effect at the aircraft design level could also be studied.

With the developed procedure, the evaluation of oxygen enriched fuel cell operation could be carried out, providing the results required to answer the proposed research questions.

The research question "What are the effects of oxygen enrichment on the mass and power requirements of each subsystem?" was addressed through a detailed analysis of the fuel cell system for the different oxygen percentages. From these results, it was concluded that oxygen enrichment can be understood to result in two different improvements. Once higher oxygen percentages are used, there is both an increase in current density for the same voltage and an increase in voltage for the same current density. In the former, efficiency of the system remains the same, and significant reductions in the fuel cell stack mass are achieved, while in the latter, both efficiency and fuel cell stack mass are improved. The results also show that the most significant improvement in terms of mass reduction stems from the mass reduction of the fuel cell stack. In terms of the balance of plant, the increase in oxygen efficiency leads to a general reduction in mass of the multiple subsystems due to combining both scenarios described, increased efficiency and reduced mass. With increased efficiency, the mass flow of air required by the fuel cell decreases, and for lower masses, the power required to fulfil the flight requirements reduces, resulting in the same reduction of air mass flow. In addition to that, oxygen enrichment significantly reduces the amount of air to be taken from the ambient around the aircraft, since a substantial amount of oxygen is provided by the tanks. The lower air mass flow that flows through the air supply path demands lighter components. Although this analysis applies to most situations, some components have slightly different changes with an increase in oxygen percentage. In the case of the compressor and intercooler, the initial increase of oxygen percentage resulted in a more demanding sizing. This was due to a change in optimum operating point, which is another effect of increasing oxygen percentage, since once a lower amount of air needs to be compressed, the improvements in fuel cell performance due to higher operating pressures can be used to provide propulsion power more efficiently, which was not the case when only using ambient air. Therefore, higher operating pressures are used, and more compressor power and heat exchange in the intercooler are required, even if the air mass flow is lower. This answer is sufficient when operating the fuel cell system solely with oxygen enriched flow, which in this study is not the case. Since at cruise no additional oxygen is supplied, the improvements obtained from oxygen enrichment are not sustained. The smaller stacks result in a less efficient operation at cruise. Therefore, the opposite happens to the subsystem's mass once they are sized for cruise; their mass increases with higher oxygen percentages used for take-off and climb. At some point, even the reduction in stack mass is no longer achieved, with the stack being sized for cruise, regardless of the lower power requirements at cruise.

The research question "What is the best position of the H_2 and O_2 tanks taking into account the safety concerns

5.2. Recommendations 80

and performance of the aircraft?" was not fully covered, as different oxygen tank placements were not evaluated. However, a qualitative evaluation of the possible options for the placement of the oxygen tanks was done. From these, the placement of the oxygen tanks in the cargo bay volume in front of the wings resulted in no changes being required in terms of aircraft design and, therefore, no penalty in its performance. This configuration also provides sufficient separation between the hydrogen and oxygen tanks. The use of the cargo volume to accommodate the tanks was not fully evaluated and could potentially be a downside of this configuration.

The research question "What are the effects of flight altitude on an aircraft with oxygen enrichment?" was addressed with an evaluation of the aircraft and its fuel cell system for different design mission flight levels. This evaluation showed that even though the amount of oxygen required increases with flight level, due to spending a longer time using oxygen from the tanks, the total aircraft mass and hydrogen consumption increase for lower flight levels. At lower flight levels, a more efficient propulsion system is required due to the more restrictive heat exchange, as the ambient temperature is higher, which increases the fuel cell system mass. Nevertheless, the more efficient system uses more hydrogen since the aerodynamic efficiency of the aircraft is reduced at lower altitudes, and more power is required. The reduction in MTOM due to oxygen enrichment is affected by altitude, with a higher altitude resulting in a less significant reduction in MTOM due to oxygen enrichment.

The research question "What is the most efficient oxygen enrichment scenario, pure oxygen operation or partial oxygen enrichment?" was answered through all the different evaluations performed in this study. All results showed that in terms of MTOM reduction, the best solution of all oxygen percentages evaluated is obtained using pure oxygen in the fuel cell or an oxygen percentage of 90% when the pure oxygen case was not displayed. Even though this is the case, in terms of reducing hydrogen consumption, any case other than ambient air utilisation results in a higher hydrogen consumption. The lowest hydrogen mass out of all oxygen enriched scenarios is obtained for the lowest oxygen percentage evaluated, 30%.

To conclude the main research question, "What are the effects of a propulsion system based on oxygen enriched fuel cells on the design and performance of the overall aircraft and subsystems, including their masses and power requirements?" can be answered. Three major factors played a role in the results obtained:

- To provide the fuel cell system with oxygen contents higher than those available in the ambient air, tanks are required. The presence of these tanks increases system complexity and adds a weight penalty.
- The mass and power requirements of the balance of plant components are reduced with the use of oxygen enrichment, where the higher the oxygen percentage, the lower the mass. The most significant mass reduction is that of the fuel cell stack, with the possibility of reducing its mass by 50%. No further improvements are possible since it was found that oxygen enrichment at cruise is not feasible due to the amount of stored oxygen required. Therefore, after initial improvements, the cruise point limits the benefits of oxygen enrichment.
- Any reduction in the fuel cell stack mass resulted in a lower efficiency at cruise. This lower efficiency increases the hydrogen consumption and the fuselage length required to accommodate the longer tanks.

From these factors, the resulting aircraft designs showed that a reduction in MTOM is possible with oxygen enrichment, reaching a maximum of 4% for the base case studied. Even though MTOM reduces the aircraft's aerodynamic efficiency worsens with increasing oxygen enrichment, due to both an increase in fuselage length and an oversized wing. The latter is a result of a conservative approach to wing sizing. With the reduction in MTOM, the power required by the aircraft was also reduced. The sensitivity analysis showed that the reduction in MTOM is mostly related to the mass of the fuel cell stack and that future design choices and improvements can affect it.

To conclude, the study conducted showed that oxygen enrichment can bring benefits in terms of MTOM reduction, but always at the cost of increased hydrogen consumption. In addition, future fuel cell power density improvements may even nullify the reduction in MTOM.

5.2. Recommendations

While this study made it possible to answer the proposed research questions and understand how oxygen enrichment can affect aircraft design and performance, there are limitations to the proposed models and methods that should be recognised. Therefore, the following recommendations are made, which would improve the accuracy of future studies.

First of all, it is recommended that a more detailed design and sizing of the inlet and nozzle be done. The current study was carried out assuming that a variable nozzle would be used and that the losses at the inlet and nozzle were constant. With this simple loss calculation, spillage drag and other drag sources created by varying mass flows at

5.2. Recommendations 81

the inlet are not considered. The mass estimation of varying nozzle systems could also be introduced to improve accuracy.

One of the main problems encountered with the sizing of the heat exchange system was that such a passive system would not work at low speeds. This occurred because the effect of the propeller on the incoming flow was not considered. As a result, a battery was required. An improvement in the prediction of the propeller wake at the inlet of the air duct would be beneficial and create a more realistic scenario of the air flow through the air duct. Related to the same subject is the introduction of a fan in the ram air duct that would allow heat dissipation at low speeds. Evaluating whether a fan is required would only be possible with an accurate prediction of the propeller wake.

The model used for the fuel cell does not provide any transient analysis; therefore, no assessment of the influence of oxygen enrichment on fuel cell performance could be carried out. Another improvement that could be made to the fuel cell modelling is the prediction of the reactant flow pressure loss throughout the fuel cell to obtain the outlet conditions of the flow and consequently the drag or thrust generated by this flow. Concerning the fuel cell mass modelling, improvements could be made, since it was verified that the method used created significant discontinuities, altering the results. If such a system were to be applied, the fuel cell manufacturing would probably be adjusted to avoid such penalties.

Another improvement that could be made is introducing the supply system to the sizing procedure. This would include the pipes that transport hydrogen and oxygen from the tanks to the fuel cell. Sizing these components would improve the accuracy of the results, and together with a simulation of the distribution, could lead to different design choices due to the distribution of the reactants.

Lastly, an improvement could be made in the methodology created to take into account the effects of the sized system on hydrogen consumption. In this study, the optimisation of the propulsion system did not consider its impact on the resulting hydrogen mass. This was done to keep the methods simple since a mission analysis would have to be done internally or an outside of the tool method would have to be developed to provide the information to the tool. In addition, the decision on whether the hydrogen or system mass is more influential on the desired optimum would have to be made.

With respect to the future of oxygen enrichment studies, it was made clear that with current and possible future technology levels, in long cruise durations, the oxygen mass becomes detrimental and oxygen enrichment is limited to shorter flight segments. Therefore, developments of other systems that can increase the oxygen percentage without needing oxygen tanks to be transported in the aircraft should be studied. Currently, such systems would be too heavy and require too much power to supply the necessary mass flows. Still, if smaller systems are available in the future, oxygen enrichment would become a much more viable solution that could be used during any flight phase. Reaching the same benefits observed in this study for climb and take-off for the whole flight mission.

- [1] D. S. Lee et al. "The contribution of global aviation to anthropogenic climate forcing for 2000 to 2018". In: *Atmospheric environment (Oxford, England : 1994)* 244 (2021), p. 117834. DOI: 10.1016/j.atmosenv. 2020.117834.
- [2] M. Gauss, I. Isaksen, D. Lee, and A. Haslerud. "Impact of aircraft NOx emissions on the atmosphere Tradeoffs to reduce the impact". In: *Atmospheric Chemistry & Physics Discussions* 5 (2005). DOI: 10.5194/acp-6-1529-2006
- [3] L. Chapman. "Transport and climate change: a review". In: *Journal of Transport Geography* 15.5 (2007), pp. 354–367. DOI: 10.1016/j.jtrangeo.2006.11.008.
- [4] A. Anger. "Including aviation in the European emissions trading scheme: Impacts on the industry, CO2 emissions and macroeconomic activity in the EU". In: *Journal of Air Transport Management* 16.2 (2010), pp. 100–105. DOI: 10.1016/j.jairtraman.2009.10.009.
- [5] Federal Aviation Administration. *Hydrogen-Fueled Aircraft Safety and Certification Roadmap*. Tech. rep. Federal Aviation Administration (FAA), 2024. URL: https://www.faa.gov/aircraft/air_cert/step/disciplines/propulsion_systems/hydrogen-fueled_aircraft_roadmap.
- [6] S. Matthes, L. Lim, U. Burkhardt, K. Dahlmann, S. Dietmüller, G. Volker, A. Haslerud, J. Hendricks, B. Owen, G. Pitari, M. Righi, and A. Skowron. "Mitigation of Non-CO2 Aviation's Climate Impact by Changing Cruise Altitudes". In: *Aerospace* 8 (2021), p. 36. DOI: 10.3390/aerospace8020036.
- [7] Air Transport Action Group. Waypoint 2050. 2021. URL: https://aviationbenefits.org/media/167417/w2050_v2021_27sept_full.pdf.
- [8] Fuel Cells and Hydrogen 2 Joint Undertaking. *Hydrogen-powered aviation A fact-based study of hydrogen technology, economics, and climate impact by 2050.* Luxembourg, 2020. DOI: 10.2843/471510.
- [9] European Technology and Innovation Platform on Batteries Batteries Europe. Strategic Research Agenda for Batteries 2020. 2020. URL: https://batterieseurope.eu/results/strategic-research-innovation-agenda/.
- [10] E. J. Adler and J. R. Martins. "Hydrogen-powered aircraft: Fundamental concepts, key technologies, and environmental impacts". In: *Progress in Aerospace Sciences* 141 (2023), p. 100922. DOI: 10.1016/j.paerosci.2023.100922.
- [11] T. Hoff, F. Becker, A. Dadashi, K. Wicke, and G. Wende. "Implementation of Fuel Cells in Aviation from a Maintenance, Repair and Overhaul Perspective". In: *Aerospace* 10 (2022), p. 23. DOI: 10.3390/aerospace10010023.
- [12] C. Koroneos, A. Dompros, G. Roumbas, and N. Moussiopoulos. "Advantages of the use of hydrogen fuel as compared to kerosene". In: *Resources, Conservation and Recycling* 44.2 (2005), pp. 99–113. DOI: 10.1016/j.resconrec.2004.09.004.
- [13] G. Dannet. "Integration of cryogenic tanks and fuel cells for future hydrogen-powered aircraft". MA thesis. Linkoping university, 2021. URL: https://www.diva-portal.org/smash/record.jsf?pid=diva2% 3A1570277&dswid=4790.
- [14] C. Svensson, A. A. Oliveira, and T. Grönstedt. "Hydrogen fuel cell aircraft for the Nordic market". In: *International Journal of Hydrogen Energy* 61 (2024), pp. 650–663. DOI: 10.1016/j.ijhydene.2024.02.382.
- [15] P. Schumann, C. Graf, J. Kallo, and K. A. Friedrich. "Architecture Analysis, Modelling and Simulation of PEM Fuel Cell Systems for Aircraft Applications". In: *ECS Transactions* 17.1 (2009), pp. 285–293. DOI: 10.1149/1.3142758.

[16] G. A. Clark, M. J. Rowan, Aeronautical, Maritime Research Laboratory, Defence Science, and Technology Organisation. A feasibility study of using oxygen enrichment for fuel cell air independent propulsion. Vol. DSTO-TR-0397. Technical report / DSTO. Melbourne: DSTO Aeronautical and Maritime Research Laboratory, 1996.

- [17] J. St-Pierre. "Perspective—Oxygen-Based Fuel Cell and Reversible Systems for Heavy-Duty Motive and Stationary Applications". In: *Journal of The Electrochemical Society* 169.4 (2022), p. 044506. DOI: 10.1149/1945-7111/ac6093.
- [18] H. Ye, F. Chen, T. Li, W. Shen, S. Xu, and S. Zhou. "Effects on the Performance of Low Temperature Proton Exchange Membrane Fuel Cell (LT-PEMFC) Using Oxygen Enrichment Air". In: *Proceedings of the 10th Hydrogen Technology Convention, Volume 2*. Ed. by H. Sun, W. Pei, Y. Dong, H. Yu, and S. You. Singapore: Springer Nature Singapore, 2024, pp. 134–139. DOI: 10.1007/978-981-99-8585-2_14.
- [19] K. M. Spencer and C. A. Martin. *Investigation of Potential Fuel Cell Use in Aircraft*. URL: https://www.ida.org/research-and-publications/publications/all/i/in/investigation-of-potential-fuel-cell-use-in-aircraft.
- [20] L. L. Kohout and P. C. Schmitz. *An Analysis of Fuel Cell Options for an All-Electric Unmanned Aerial Vehicle*. URL: https://ntrs.nasa.gov/citations/20070022837.
- [21] M. Schmelcher and J. Häßy. "Hydrogen fuel cells for aviation? A potential analysis comparing different thrust categories". In: *International Society of Air Breathing Engines, Proceedings*, 2022. Sept. 2022. URL: https://elib.dlr.de/188835/.
- [22] R. P. O'Hayre, S.-W. Cha, W. G. Colella, and F. B. Prinz. *Fuel cell fundamentals*. Third edition. Hoboken New Jersey: Wiley, 2016.
- [23] Z. Pu, G. Zhang, A. Hassanpour, D. Zheng, S. Wang, S. Liao, Z. Chen, and S. Sun. "Regenerative fuel cells: Recent progress, challenges, perspectives and their applications for space energy system". In: *Applied Energy* 283 (2021), p. 116376. DOI: 10.1016/j.apenergy.2020.116376.
- [24] J. Luo, W. Jiang, C. Deng, Q. Wan, Y. Zhang, J. He, Y. Liu, G. Li, J. Hou, X. Zhuang, J. Zhang, and C. Ke. "Boosting the power density of the H3PO4/polybenzimidazole high-temperature proton exchange membrane fuel cell to >1.2 W cm—2 via the deposition of acid-based polymer layers on the catalyst layers". In: *Journal of Power Sources* 589 (2024), p. 233756. DOI: 10.1016/j.jpowsour.2023.233756.
- [25] R. E. Rosli, A. B. Sulong, W. Daud, M. A. Zulkifley, T. Husaini, M. I. Rosli, E. H. Majlan, and M. A. Haque. "A review of high-temperature proton exchange membrane fuel cell (HT-PEMFC) system". In: *International Journal of Hydrogen Energy* 42.14 (2017), pp. 9293–9314. DOI: 10.1016/j.ijhydene.2016.06.211.
- [26] Wasim Bhatti, Wei Wu, Finn Doyle, Jorge Llambrich, Helen Webber, and Nigel Town. Fuel Cells Roadmap Report. Tech. rep. Aerospace Technology Institute, 2022. URL: https://www.ati.org.uk/wp-content/uploads/2022/03/FZO-PPN-COM-0033-Fuel-Cells-Roadmap-Report.pdf.
- [27] Fuel Cell Technologies Office. *Fuel Cells*. Tech. rep. U.S Department of Energy, 2015. URL: https://www.energy.gov/sites/prod/files/2015/11/f27/fcto_fuel_cells_fact_sheet.pdf.
- [28] M. A. Azizi and J. Brouwer. "Progress in solid oxide fuel cell-gas turbine hybrid power systems: System design and analysis, transient operation, controls and optimization". In: *Applied Energy* 215 (2018), pp. 237–289. DOI: 10.1016/j.apenergy.2018.01.098.
- [29] Y. Li, W. Shao, Z. Ma, M. Zheng, and H. Song. "Performance Analysis of a HT-PEMFC System with 6FPBI Membranes Doped with Cross-Linkable Polymeric Ionic Liquid". In: *International journal of molecular sciences* 23.17 (2022). DOI: 10.3390/ijms23179618.
- [30] J. W. Pratt, J. Brouwer, and G. S. Samuelsen. "Performance of Proton Exchange Membrane Fuel Cell at High-Altitude Conditions". In: *Journal of Propulsion and Power* 23.2 (2007), pp. 437–444. DOI: 10.2514/ 1.20535.
- [31] M. Schröder, F. Becker, J. Kallo, and C. Gentner. "Optimal operating conditions of PEM fuel cells in commercial aircraft". In: *International Journal of Hydrogen Energy* 46.66 (2021), pp. 33218–33240. DOI: 10.1016/j.ijhydene.2021.07.099.

[32] Z. Abdin, C. J. Webb, and E. Gray. "PEM fuel cell model and simulation in Matlab-Simulink based on physical parameters". In: *Energy* 116 (2016), pp. 1131–1144. DOI: 10.1016/j.energy.2016.10.033.

- [33] Y. Zhang, Z. Hu, L. Xu, H. Liu, K. Ye, J. Li, and M. Ouyang. "Fuel cell system for aviation applications: Modeling, parameter sensitivity, and control". In: *Energy Conversion and Management* 312 (2024), p. 118555. DOI: 10.1016/j.enconman.2024.118555.
- [34] J. Hoeflinger and P. Hofmann. "Air mass flow and pressure optimisation of a PEM fuel cell range extender system". In: *International Journal of Hydrogen Energy* 45.53 (2020), pp. 29246–29258. DOI: 10.1016/j.ijhydene.2020.07.176.
- [35] W. Ng and A. Datta. "Development of Propulsion System Models for Electric-VTOL Aircraft". In: *2018 AIAA Aerospace Sciences Meeting*. Reston, Virginia: American Institute of Aeronautics and Astronautics, 2018. DOI: 10.2514/6.2018–1750.
- [36] Q. Yan, H. Toghiani, and H. Causey. "Steady state and dynamic performance of proton exchange membrane fuel cells (PEMFCs) under various operating conditions and load changes". In: *Journal of Power Sources* 161.1 (2006), pp. 492–502. DOI: 10.1016/j.jpowsour.2006.03.077.
- [37] Jacky Jiang, Sarjeel Zaman, Abdulhazeez Adeniji, and Hillary Wong. "Optimization of Operating Parameters on Proton Exchange Membrane Fuel Cells for Efficiency". In: *Journal of Undergraduate Chemical Engineering Research* (2021), pp. 63–71. URL: https://cpb-us-e1.wpmucdn.com/you.stonybrook.edu/dist/f/2071/files/2021/05/pgs-63-71.pdf.
- [38] B. Blunier and A. Miraoui. "Air management in PEM fuel cells: State-of-the-art and prospectives". In: 2007 International Aegean Conference on Electrical Machines and Power Electronics. 2007, pp. 245–254. DOI: 10.1109/ACEMP.2007.4510510.
- [39] F. Barbir. "Chapter Three Fuel Cell Electrochemistry". In: PEM Fuel Cells (Second Edition). Ed. by F. Barbir. Boston: Academic Press, 2013, pp. 33–72. DOI: 10.1016/B978-0-12-387710-9.00003-5. URL: https://www.sciencedirect.com/science/article/pii/B9780123877109000035.
- [40] V. Palladino, N. Bartoli, V. Pommier-Budinger, E. Benard, P. Schmollgruber, and A. Jordan. "Optimization of a hydrogen-based hybrid propulsion system under aircraft performance constraints". In: *Chinese Journal of Aeronautics* 36.5 (2023), pp. 41–56. DOI: 10.1016/j.cja.2023.02.019.
- [41] Z. Xia, B. Wang, Z. Yang, K. Wu, Q. Du, and K. Jiao. "Effect of operating conditions on performance of proton exchange membrane fuel cell with anode recirculation". In: *Energy Procedia* 158 (2019), pp. 1829–1834. DOI: 10.1016/j.egypro.2019.01.428.
- [42] M. C. Massaro, R. Biga, A. Kolisnichenko, P. Marocco, A. H. A. Monteverde, and M. Santarelli. "Potential and technical challenges of on-board hydrogen storage technologies coupled with fuel cell systems for aircraft electrification". In: *Journal of Power Sources* 555 (2023), p. 232397. DOI: 10.1016/j.jpowsour.2022. 232397.
- [43] J. Moreno-Blanco, G. Petitpas, F. Espinosa-Loza, F. Elizalde-Blancas, J. Martinez-Frias, and S. M. Aceves. "The storage performance of automotive cryo-compressed hydrogen vessels". In: *International Journal of Hydrogen Energy* 44.31 (2019), pp. 16841–16851. DOI: 10.1016/j.ijhydene.2019.04.189.
- [44] R. K. Ahluwalia, J. K. Peng, H. S. Roh, T. Q. Hua, C. Houchins, and B. D. James. "Supercritical cryocompressed hydrogen storage for fuel cell electric buses". In: *International Journal of Hydrogen Energy* 43.22 (2018), pp. 10215–10231. DOI: 10.1016/j.ijhydene.2018.04.113.
- [45] M. Sielemann, A. Renuke, K. O'Donovan, D. Andersson, and A. Nguyen. "On Tank and Dormancy Design Spaces for Hydrogen Powered Aircraft". In: AIAA SCITECH 2025 Forum. Reston, Virginia: American Institute of Aeronautics and Astronautics, 2025. DOI: 10.2514/6.2025-0504.
- [46] G. Onorato, P. Proesmans, and M. F. M. Hoogreef. "Assessment of hydrogen transport aircraft: Effects of fuel tank integration". In: CEAS aeronautical journal 13.4 (2022), pp. 813–845. DOI: 10.1007/s13272– 022-00601-6.
- [47] P. C. d. Boer, A. d. Wit, and R. C. van Benthem. "Development of a Liquid Hydrogen-based Fuel Cell System for the HYDRA-2 Drone". In: *AIAA SCITECH 2022 Forum*. American Institute of Aeronautics and Astronautics, 2022. DOI: 10.2514/6.2022-0443.

[48] F. Michel, H. Fieseler, G. Meyer, and F. Theiben. "On-board equipment for liquid hydrogen vehicles". In: International Journal of Hydrogen Energy 23.3 (1998), pp. 191-199. DOI: 10.1016/S0360-3199(97) 00044-X. URL: https://www.sciencedirect.com/science/article/pii/S036031999700044X.

- [49] D. Silberhorn, G. Atanasov, J.-N. Walther, and T. Zill. "Assessment of Hydrogen Fuel Tank Integration at Aircraft Level". In: *Deutscher Luft- und Raumfahrtkongress 2019*. 2019.
- [50] Federal Aviation Administration. Airworthiness Standards: Transport Category Airplanes, 14 C.F.R. Part 25. URL: https://www.ecfr.gov/current/title-14/chapter-I/subchapter-C/part-25?toc=1.
- [51] European Union Aviation Safety Agency. Certification Specifications and Acceptable Means of Compliance for Large Aeroplanes (CS-25). URL: https://www.easa.europa.eu/en/document-library/easy-access-rules/easy-access-rules-large-aeroplanes-cs-25.
- [52] E. J. Choi, J. Y. Park, and M. S. Kim. "Two-phase cooling using HFE-7100 for polymer electrolyte membrane fuel cell application". In: *Applied Thermal Engineering* 148 (2019), pp. 868-877. DOI: 10.1016/j.applthermaleng.2018.11.103.
- [53] S. A. Atyabi, E. Afshari, and C. Udemu. "Comparison of active and passive cooling of proton exchange membrane fuel cell using a multiphase model". In: *Energy Conversion and Management* 268 (2022), p. 115970. DOI: 10.1016/j.enconman.2022.115970.
- [54] A. Fly and R. H. Thring. "A comparison of evaporative and liquid cooling methods for fuel cell vehicles". In: *International Journal of Hydrogen Energy* 41.32 (2016), pp. 14217–14229. DOI: 10.1016/j.ijhydene. 2016.06.089.
- [55] A. Scoccimarro. "Preliminary Design Methods for the Thermal Management of Fuel Cell Powered Aeroengines". MA thesis. Delft: Delft University of Technology, 2023. URL: https://resolver.tudelft.nl/uuid:9a16e0f8-722d-4a17-9f79-96cea2de6906.
- [56] M. C. Massaro, S. Pramotton, P. Marocco, A. H. A. Monteverde, and M. Santarelli. "Optimal design of a hydrogen-powered fuel cell system for aircraft applications". In: *Energy Conversion and Management* 306 (2024), p. 118266. DOI: 10.1016/j.enconman.2024.118266. URL: https://www.sciencedirect. com/science/article/pii/S0196890424002073.
- [57] Q. Chen, G. Zhang, X. Zhang, C. Sun, K. Jiao, and Y. Wang. "Thermal management of polymer electrolyte membrane fuel cells: A review of cooling methods, material properties, and durability". In: *Applied Energy* 286 (2021), p. 116496. DOI: 10.1016/j.apenergy.2021.116496.
- [58] H. Kellermann, M. Lüdemann, M. Pohl, and M. Hornung. "Design and Optimization of Ram Air-Based Thermal Management Systems for Hybrid-Electric Aircraft". In: Aerospace 8.1 (2021), p. 3. DOI: 10.3390/ aerospace8010003.
- [59] T. L. Kösters, X. Liu, D. Kožulović, S. Wang, J. Friedrichs, and X. Gao. "Comparison of phase-change-heat-pump cooling and liquid cooling for PEM fuel cells for MW-level aviation propulsion". In: *International Journal of Hydrogen Energy* 47.68 (2022), pp. 29399–29412. DOI: 10.1016/j.ijhydene.2022.06.235.
- [60] G. Zhang and S. G. Kandlikar. "A critical review of cooling techniques in proton exchange membrane fuel cell stacks". In: *International Journal of Hydrogen Energy* 37.3 (2012), pp. 2412–2429. DOI: 10.1016/j.ijhydene.2011.11.010.
- [61] R. W. Morse, T. A. Moreira, J. Chan, K. M. Dressler, G. Ribatski, E. T. Hurlburt, L. L. McCarroll, G. F. Nellis, and A. Berson. "Critical heat flux and the dryout of liquid film in vertical two-phase annular flow". In: *International Journal of Heat and Mass Transfer* 177 (2021), p. 121487. DOI: 10.1016/j.ijheatmasstransfer. 2021.121487.
- [62] F. Beltrame, L. Dongen, P. Colonna, and C. de Servi. "Optimal design of a ram air cooling duct housing the condenser of an airborne ORC WHR unit". In: Global Power and Propulsion Society, 2024. DOI: 10.33737/gpps24-tc-107.
- [63] L. Piancastelli, L. Frizziero, and G. Donnici. "The meredith ramjet: An efficient way to recover the heat wasted in piston engine cooling". In: *ARPN Journal of Engineering and Applied Sciences* 10 (2015), pp. 5327–5333. URL: https://www.arpnjournals.com/jeas/research_papers/rp_2015/jeas_0715_2249.pdf.

[64] S. Bhapkar and S. Kazula. "Development of a predictive model for the preliminary design of Heat Exchangers in Electric Aviation". In: *Deutscher Luft- und Raumfahrtkongress 2023*. 2023. DOI: 10.25967/610378.

- [65] C. K. Sain, J. Hänsel, and S. Kazula. "Conceptual Design of Air and Thermal Management in a Nacelle-Integrated Fuel Cell System for an Electric Regional Aircraft". In: *AIAA AVIATION 2023 Forum*. Reston, Virginia: American Institute of Aeronautics and Astronautics, 2023. DOI: 10.2514/6.2023-3875.
- [66] M. Nichols. *Investigation of flow through an intercooler set at various angles to the supply duct.* 1942. URL: https://ntrs.nasa.gov/citations/%2019930093676.
- [67] S. Kazula and D. Hintermayr. "Conceptual Design and Evaluation of Air Inlets of Fuel Cell-Powered Electric Aero Engines for Regional Aircraft". In: *Journal of Physics: Conference Series* 2716.1 (2024), p. 012016. DOI: 10.1088/1742-6596/2716/1/012016.
- [68] J. Schröter. "Fuel cell air supply for hydrogen electric propulsion systems in aircraft applications". PhD thesis. Ulm University, 2023. DOI: 10.18725/0PARU-49048.
- [69] M. Brebenel. "An analytical method for simulation of centrifugal compressors". In: *INCAS BULLETIN* 12.1 (2020), pp. 35–49. DOI: 10.13111/2066-8201.2020.12.1.4.
- [70] L. L. Phuong, M. Schröder, M. Schorr, and C. Gentner. D4.10: Fuel Cells Feasibility Study. Tech. rep. IMOTHEP (Horizon 2020 Project), 2024. URL: https://www.imothep-project.eu/files/D4.10-Fuel-cells-feasibility-study.pdf.
- [71] T. Reynolds, D. Bailey, D. Lewinski, C. Roseburg, and B. Palaszewski. *Onboard Inert Gas Generation System/Onboard Oxygen Gas Generation System (OBIGGS/OBOGS) Study*. 2013. URL: https://ntrs.nasa.gov/api/citations/20010092198/downloads/20010092198.pdf.
- [72] L. Shao, J. Tan, W. Liu, J. Yang, B. Hei, and J. Qu. "System performance comparison of oxygen consumption and air separation for aircraft fuel tank inerting". In: *Case Studies in Thermal Engineering* 60 (2024), p. 104749. DOI: 10.1016/j.csite.2024.104749.
- [73] G. Li, W. Kujawski, R. Válek, and S. Koter. "A review The development of hollow fibre membranes for gas separation processes". In: *International Journal of Greenhouse Gas Control* 104 (2021), p. 103195. DOI: 10.1016/j.ijggc.2020.103195.
- [74] S. S. Hashim, A. R. Mohamed, and S. Bhatia. "Oxygen separation from air using ceramic-based membrane technology for sustainable fuel production and power generation". In: *Renewable and Sustainable Energy Reviews* 15.2 (2011), pp. 1284–1293. DOI: 10.1016/j.rser.2010.10.002.
- [75] Y. Zhang, J. R. G. Evans, and S. Yang. "Corrected Values for Boiling Points and Enthalpies of Vaporization of Elements in Handbooks". In: *Journal of Chemical & Engineering Data* 56.2 (2011), pp. 328–337. DOI: 10.1021/je1011086.
- [76] Q. Cai, D. Brett, D. Browning, and N. P. Brandon. "A sizing-design methodology for hybrid fuel cell power systems and its application to an unmanned underwater vehicle". In: *Journal of Power Sources* 195.19 (2010), pp. 6559–6569. DOI: 10.1016/j.jpowsour.2010.04.078.
- [77] Asia Industrial Gases Association (AIGA). Liquid Oxygen, Nitrogen and Argon Cryogenic Tanker Loading Systems (AIGA 085/13). Tech. rep. Based on CGA P-31 2013, 3rd edition. Asia Industrial Gases Association, 2013. URL: https://asiaiga.org/uploaded_docs/AIGA%20085_13%20Liquid%20oxygen, %20nitrogen%20and%20argon%20cryogenic%20tanker%20loading%20system%20guide.pdf.
- [78] E. Industries. *Liquid Oxygen Equipment*. 2025. URL: https://essexindustries.com/products-home/liquid-oxygen-equipment/.
- [79] R. Ring, J. Stott, and C. Hales. "Modeling the Risk of Fire/Explosion due to Oxidizer/Fuel Leaks in the AresI Interstage". In: 3rd IAASS Conference. 2008. URL: https://ntrs.nasa.gov/citations/20110004369.
- [80] World Health Organization and International Labour Organization. ICSC 0001 HYDROGEN. International Peer Reviewed Chemical Safety Information (INCHEM), 2014. URL: https://inchem.org/documents/icsc/icsc/eics0001.htm?utm_source=chatgpt.com.

[81] World Health Organization and International Labour Organization. ICSC 0663 - KEROSENE. International Peer Reviewed Chemical Safety Information (INCHEM), 2018. URL: https://www.inchem.org/documents/icsc/eics0663.htm.

- [82] N. I. for Occupational Safety and H. (NIOSH). NIOSH Pocket Guide to Chemical Hazards: Kerosene (CAS No. 8008-20-6). https://www.cdc.gov/niosh/npg/npgd0366.html. Accessed: 6 October 2025. 2024.
- [83] M. S. B. Rietdijk. "Architecture Design For a Commercially Viable Hydrogen-Electric Powered Retrofitted Regional Aircraft". In: Congress of the International Council of the Aeronautical Sciences. 2024. URL: https://www.icas.org/icas_archive/icas2024/data/papers/icas2024_1090_paper.pdf.
- [84] A. Polak, G. Grzeczka, and T. Piłat. "Influence of cathode stoichiometry on operation of PEM fuel cells' stack supplied with pure oxygen". In: *Journal of Marine Engineering & Technology* 16.4 (2017), pp. 283–290. DOI: 10.1080/20464177.2017.1381061.
- [85] Clean Aviation. TheMa4HERA: Thermal Management for the Hybrid Electric Regional Aircraft. URL: https://www.clean-aviation.eu/research-and-innovation/clean-aviation/clean-aviation-projects/thema4hera.
- [86] B. M. Fröhler, M. Iwanizki, S. Woehler, and T. Zill. "Increasing Fuel Efficiency for Short to Medium Range Market: A Conceptual Aircraft Design Study on Unconventional Configuration". In: AIAA Aviation Forum and ASCEND 2024. DOI: 10.2514/6.2024-4325.
- [87] S. Woehler, G. Atanasov, D. Silberhorn, B. Fröhler, and T. Zill. "Preliminary Aircraft Design within a Multidisciplinary and Multifidelity Design Environment". In: *Aerospace Europe Conference 2020*. 2020. URL: https://elib.dlr.de/185515/.
- [88] S. Woehler, T. Burschyk, J. Häßy, and M. Iwanizki. "Design and Assessment of Long Range Aircraft Concepts with focus on Fossil Kerosene, Sustainable Aviation Fuel and Liquid Hydrogen as Energy Carriers". In: *AIAA AVIATION 2023 Forum*. Reston, Virginia: American Institute of Aeronautics and Astronautics, 2023. DOI: 10.2514/6.2023-3229.
- [89] T. Burschyk, D. Silberhorn, J. Wehrspohn, M. Kühlen, and T. Zill. "Scenario-based implications of liquid hydrogen storage tank insulation quality for a short-range aircraft concept". In: *AIAA AVIATION 2023 Forum*. Reston, Virginia: American Institute of Aeronautics and Astronautics, 2023. DOI: 10.2514/6.2023-3522.
- [90] B. Fröhler, C. Hesse, G. Atanasov, and P. Wassink. *Disciplinary Sub-Processes to Assess Low-Speed Performance and Noise Characteristics within an Aircraft Design Environment*. Deutsche Gesellschaft für Luft- und Raumfahrt Lilienthal-Oberth e.V, 2021. DOI: 10.25967/530201.
- [91] S. A. Vilekar and R. Datta. "The effect of hydrogen crossover on open-circuit voltage in polymer electrolyte membrane fuel cells". In: *Journal of Power Sources* 195.8 (2010), pp. 2241–2247. DOI: 10.1016/j.jpowsour.2009.10.023.
- [92] L. Mao and C.-Y. Wang. "Analysis of Cold Start in Polymer Electrolyte Fuel Cells". In: *Journal of The Electrochemical Society* 154.2 (2006), B139. DOI: 10.1149/1.2402123.
- [93] A. Z. Weber and J. Newman. "Transport in Polymer-Electrolyte Membranes: I. Physical Model". In: *Journal of The Electrochemical Society* 150.7 (2003), A1008. DOI: 10.1149/1.1580822.
- [94] Roman Vetter and Jürgen O. Schumacher. "Free open reference implementation of a two-phase PEM fuel cell model". In: *Computer Physics Communications* 234 (2019), pp. 223-234. DOI: 10.1016/j.cpc.2018. 07.023. URL: https://www.sciencedirect.com/science/article/pii/S0010465518302807.
- [95] M. Schröder, F. Becker, and C. Gentner. "Optimal design of proton exchange membrane fuel cell systems for regional aircraft". In: *Energy Conversion and Management* 308 (2024), p. 118338. DOI: 10.1016/j.enconman.2024.118338.
- [96] P. Virtanen et al. "SciPy 1.0: Fundamental Algorithms for Scientific Computing in Python". In: *Nature Methods* 17 (2020), pp. 261–272. DOI: 10.1038/s41592-019-0686-2.
- [97] Anubhav Datta. PEM Fuel Cell MODEL for Conceptual Design of Hydrogen eVTOL Aircraft. 2021. URL: https://ntrs.nasa.gov/citations/20210000284.

[98] F. Si, Y. Zhang, L. Yan, J. Zhu, M. Xiao, C. Liu, W. Xing, and J. Zhang. "Electrochemical Oxygen Reduction Reaction". In: *Rotating Electrode Methods and Oxygen Reduction Electrocatalysts*. Elsevier, 2014, pp. 133–170. DOI: 10.1016/B978-0-444-63278-4.00004-5.

- [99] S. Authayanun, M. Mamlouk, K. Scott, and A. Arpornwichanop. "Comparison of high-temperature and low-temperature polymer electrolyte membrane fuel cell systems with glycerol reforming process for stationary applications". In: *Applied Energy* 109 (2013), pp. 192–201. DOI: 10.1016/j.apenergy.2013.04.009.
- [100] K. C. Neyerlin, W. Gu, J. Jorne, and H. A. Gasteiger. "Determination of Catalyst Unique Parameters for the Oxygen Reduction Reaction in a PEMFC". In: *Journal of The Electrochemical Society* 153.10 (2006), A1955. DOI: 10.1149/1.2266294.
- [101] F. Jiang, W. Fang, and C.-Y. Wang. "Non-isothermal cold start of polymer electrolyte fuel cells". In: *Electrochimica Acta* 53.2 (2007), pp. 610–621. DOI: 10.1016/j.electacta.2007.07.032.
- [102] R. K. Shah and D. P. Sekulić. *FUNDAMENTALS OF HEAT EXCHANGER DESIGN*. John Wiley & Sons, Ltd, 2003. DOI: 10.1002/9780470172605.
- [103] Raj M. Manglik and Arthur E. Bergles. "Heat transfer and pressure drop correlations for the rectangular offset strip fin compact heat exchanger". In: *Experimental Thermal and Fluid Science* 10.2 (1995), pp. 171–180. DOI: 10.1016/0894-1777 (94) 00096-Q.
- [104] D. G. Goodwin, H. K. Moffat, I. Schoegl, R. L. Speth, and B. W. Weber. *Cantera: An Object-oriented Software Toolkit for Chemical Kinetics, Thermodynamics, and Transport Processes*. Version 3.1.0. 2024. DOI: 10.5281/zenodo.14455267.
- [105] I. H. Bell, J. Wronski, S. Quoilin, and V. Lemort. "Pure and Pseudo-pure Fluid Thermophysical Property Evaluation and the Open-Source Thermophysical Property Library CoolProp". In: *Industrial & Engineering Chemistry Research* 53.6 (2014), pp. 2498–2508. DOI: 10.1021/ie4033999.
- [106] *VDI heat atlas*. 2nd ed. VDI-buch. Berlin and New York: Springer, 2010. DOI: 10.1007/978-3-540-77877-6.
- [107] Fabio Beltrame, Dabo Krempus, Piero Colonna, and Carlo De Servi. "Reduced Order Modelling of Optimized Heat Exchangers for Maximum Mass-Specific Performance of Airborne ORC Waste Heat Recovery Units". In: *Proceedings of the 7th International Seminar on ORC Power System (ORC 2023)*. Ed. by D. T. Sánchez Martínez. Editorial Universidad de Sevilla, 2024, pp. 563–573. DOI: 10.12795/9788447227457{\textunderscore}93.
- [108] J.-H. Hao, Q. Chen, J.-X. Ren, M.-Q. Zhang, and J. Ai. "An experimental study on the offset-strip fin geometry optimization of a plate-fin heat exchanger based on the heat current model". In: *Applied Thermal Engineering* 154 (2019), pp. 111–119. DOI: 10.1016/j.applthermaleng.2019.03.072.
- [109] Celeroton. Turbo compressors. 2025. URL: https://www.celeroton.com/en/products/compressors/.
- [110] Fischer. Compressors- Our Portfolio. 2025. URL: https://www.fischer-fuelcell-compressor.com/en/products.
- [111] ROTREX. Fuel Cell Compressors. 2025. URL: https://rotrex-fuel-cell-compressor.com/contact/.
- [112] Sprintex. Fuel Cells Compressors. 2024. URL: https://sprintex.com.au/products/fuelcell-ecompressor/.
- [113] M. Vroom. "Preliminary Sizing of Balance-of-Plant Systems for Liquid Hydrogen Fuel Cell-Electric Propulsion in Regional Retrofitted Aircraft". MA thesis. Delft: Delft University of Technology, 2025. URL: https://repository.tudelft.nl/record/uuid:9a938412-d806-4235-b297-62c4250f1318.
- [114] Freudenberg. micronAir fuel cell filter. 2025. URL: https://www.freudenberg-filter.com/en/products/automotive/fuel-cell-solutions/#c34034.
- [115] fumatech. Humidifier Modules Ecomate. 2025. URL: https://www.fumatech.com/en/fumatech/.
- [116] S. Farokhi. *Aircraft Propulsion*. Newark, United Kingdom: John Wiley & Sons, Incorporated, 2014. URL: http://ebookcentral.proquest.com/lib/delft/detail.action?docID=7104095.

[117] C. Viguier. D5.14: Synthesis on Electric Components. Tech. rep. IMOTHEP (Horizon 2020 Project), 2024. URL: https://www.imothep-project.eu/files/D5.14_SYNTHESIS-ON-ELECTRIC-COMPONENTS.pdf.

- [118] W. Affonso et al. "System architectures for thermal management of hybrid-electric aircraft FutPrInt50". In: *IOP Conference Series: Materials Science and Engineering* 1226.1 (2022), p. 012062. DOI: 10.1088/1757-899X/1226/1/012062.
- [119] R. Storn and K. Price. "Differential Evolution A Simple and Efficient Heuristic for global Optimization over Continuous Spaces". In: *Journal of Global Optimization* 11.4 (1997), pp. 341–359. DOI: 10.1023/A: 1008202821328.
- [120] J. Qiang and C. Mitchell. "A Unified Differential Evolution Algorithm for Global Optimization". In: *IEEE Transactions on Evolutionary Computation*. (2014). URL: https://www.osti.gov/biblio/1163659.
- [121] M. Wormington, C. Panaccione, K. M. Matney, and D. K. Bowen. "Characterization of Structures from X-Ray Scattering Data Using Genetic Algorithms". In: *Philosophical Transactions: Mathematical, Physical and Engineering Sciences* 357.1761 (1999), pp. 2827–2848. URL: http://www.jstor.org/stable/55273.
- [122] J. Lampinen. "A constraint handling approach for the differential evolution algorithm". In: *Proceedings of the 2002 Congress on Evolutionary Computation (CEC'02)*. Vol. 2. IEEE, 2002, pp. 1468–1473. DOI: 10.1109/CEC.2002.1004498.
- [123] D. Juschus. "Preliminary Propulsion System Sizing Methods for PEM Fuel Cell Aircraft". MA thesis. Delft: Delft University of Technology, 2021. URL: https://repository.tudelft.nl/record/uuid:fdc14875-175e-4a4b-8cde-f2f4b6028194.